

# **INTEGRATION OF PHOTOVOLTAIC SYSTEMS IN COLD REGIONS**

**By**

**Seyedkazem Hosseini**

**Thesis Presented to**

**Département d'informatique et d'ingénierie**

**Université du Québec en Outaouais (UQO)**

**In partial fulfillment of the requirements for the degree of doctor of philosophy  
Ph.D.**

**January 2019**

© Copy Right Reserved by Seyedkazem Hosseini, 2019



## Board of Examiners

This thesis has been evaluated by the following board of examiners:

|                       |                                                                                                             |
|-----------------------|-------------------------------------------------------------------------------------------------------------|
| Thesis Supervisor:    | Prof. Shamsodin Taheri<br>Département d'informatique et d'ingénierie,<br>Université du Québec en Outaouais. |
| Thesis Co-Supervisor: | Prof. Masoud Farzaneh<br>Université du Québec à Chicoutimi.                                                 |
| Committee President:  | Prof. Nadia Baaziz<br>Département d'informatique et d'ingénierie,<br>Université du Québec en Outaouais.     |
| Internal Examiner :   | Prof. Marek Zaremba<br>Département d'informatique et d'ingénierie,<br>Université du Québec en Outaouais.    |
| External Examiner :   | Dr. Branislav Djokic<br>National Research Council Canada                                                    |

This thesis was presented and defended in the presence of the board of examiners and the public on December 18, 2018, at the département d'informatique et d'ingénierie.



# ABSTRACT

Photovoltaic (PV) technologies are promising solutions in addressing climate change and long-term energy supply issues. Majority of the solar energy plants are presently installed in cold geographical locations with a considerable amount of snowfall every year. More PV capacity is expected for the future power grid to be smart and flexible. This expected growth raises concerns about the availability, quality, and reliability of the whole power grid mainly due to changing atmospheric conditions. Moreover, in cold climate regions, snow and ice accumulation could challenge the performance of the PV systems. Achieving high efficiency and reliability is of great importance for PV systems in order to reduce the cost of energy. These objectives can be achieved by appropriate design and control of PV systems and developing an appropriate model.

The goal of this research project is to enhance the knowledge in the applications of PV systems, especially in cold climate regions, and to develop controllers and modeling toolbox for PV systems designers and professionals. This research work was approached from three perspectives: 1) improvement of existing PV models applicable for outdoor operated PV systems to achieve more accurate performance predictions, 2) enabling the research of PV systems in cold regions through a simulation tool capable of characterizing the snow-covered PV panels, and 3) increasing the efficiency of the PV systems under partial shading condition through a novel maximum power point tracking (MPPT) method.

With respect to the first perspective, an improved procedure for modeling of PV modules was presented based on the single-diode model. This improvement allows more accurate energy yield predictions and performance analysis in real field conditions. With the proposed approach, it is possible to update the parameters of the model for given environmental conditions. Moreover, the spectral effects, which influence the output of PV modules, are included in the model. The second perspective led to a novel PV model that determines instantaneous electrical characteristics of PV cells in the presence of snow coverage. The proposed model utilizes the Bouguer-Lambert Law to estimate the level of insolation reaching the surface of snow-covered PV cells. This is achieved by introducing an extinction coefficient that depends on the snow properties. In the third perspective, a

novel high performance shade-tolerant maximum power point tracking (STMPPT) method was proposed for DC-DC converter stage of PV applications. The proposed STMPPT method enables fast and reliable tracking of the global maximum power point, thus maximizing the efficiency of the PV systems. In addition, it stably works under dynamic environmental change without losing correct sense of tracking direction. The proposed STMPPT technique is simple, accurate, and readily adaptable to a variety of PV converters.

This research may be regarded as an important contribution to the development of PV systems and further studies of applications of the PV systems for cold weather regions.

# RÉSUMÉ

Les technologies photovoltaïques (PV) sont des solutions prometteuses pour faire face au changement climatique et aux problèmes d'approvisionnement énergétique à long terme. La majorité des centrales photovoltaïques sont actuellement installées dans des zones géographiques froides avec une quantité considérable de neige chaque année. On s'attend à une plus grande capacité PV pour le futur réseau électrique qui sera intelligent et flexible. Cette croissance prévue soulève des inquiétudes quant à la disponibilité, la qualité et la fiabilité de l'ensemble du réseau électrique, principalement en raison des conditions atmosphériques changeantes. De plus, dans les régions froides, l'accumulation de neige et de glace pourrait nuire à la performance des systèmes PV. Pour les systèmes PV, il est très important d'atteindre un niveau élevé d'efficacité et de fiabilité afin de réduire le coût de l'énergie. Ces objectifs peuvent être atteints par une conception et un contrôle appropriés des systèmes PV et par l'élaboration d'un modèle approprié.

L'objectif de ce projet de recherche est d'améliorer les connaissances sur les applications des systèmes PV, en particulier dans les régions de climat froid, et de développer des contrôleurs et des outils de modélisation pour les concepteurs de systèmes PV et les professionnels. Ce travail de recherche a été abordé sous trois angles : 1) l'amélioration des modèles PV existants applicables aux systèmes PV exploités à l'extérieur afin d'obtenir des prévisions de rendement plus précises, 2) permettre la recherche de systèmes PV dans les régions froides grâce à un outil de simulation capable de caractériser les panneaux PV recouverts de neige, et 3) accroître l'efficacité des systèmes PV dans des conditions de protection partielle par une nouvelle méthode de suivi du point de puissance maximale (MPPT).

En ce qui concerne la première perspective, une procédure améliorée de modélisation des modules PV a été présentée sur la base du modèle à diode unique. Cette amélioration permet des prévisions de rendement énergétique et des analyses de performance plus précises en conditions réelles sur le terrain. L'approche proposée permet de mettre à jour les paramètres du modèle pour des conditions environnementales données. De plus, les effets spectraux, qui influencent le rendement des modules PV, sont inclus dans le modèle. La deuxième perspective a mené à un nouveau modèle PV qui détermine les caractéristiques électriques instantanées des cellules PV en présence de couverture de neige. Le modèle proposé utilise la loi de Bouguer-Lambert pour estimer

le niveau d'ensoleillement atteignant la surface des cellules PV recouvertes de neige. Ceci est obtenu en introduisant un coefficient d'extinction qui dépend des propriétés de la neige. Dans la troisième perspective, une nouvelle méthode de suivi de point de puissance maximale tolérante à l'ombre à haute performance (STMPPT) a été proposée pour l'étage convertisseur DC-DC des applications PV. La méthode STMPPT proposée permet un suivi rapide et fiable du point de puissance maximale globale, maximisant ainsi l'efficacité des systèmes PV. De plus, il fonctionne de façon stable dans des conditions de changement environnemental dynamique sans perdre le sens de l'orientation correcte. La technique STMPPT proposée est simple, précise et facilement adaptable à divers convertisseurs PV.

Cette recherche peut être considérée comme une contribution importante au développement des systèmes PV et à la poursuite des études sur les applications des systèmes PV dans les régions froides.

# ACKNOWLEDGEMENT

This research project was done under the supervision of Prof. Shamsodin Taheri and co-supervision of Prof. Masoud Farzaneh. First and foremost, I would like to express my deepest gratefulness to my supervisors for their professional and patient guidance with their open-mindedness and earnestness. I do believe that the encouragement which I received from them during my Ph.D. study will be of great supportiveness for my career and through my future life.

In particular, many thanks to Dr. Hamed Taheri, Power Electronics Designer at Primax Technologies Inc., for his endless support and technical advice on designing the power electronics circuits and controllers.

Also, I would like to thank to Mr. Antoine Shaneen and Mr. Abdelkrim Chebihi for all their great help in the laboratory which have not ended till now.

It is my pleasure to express my sincere appreciation to Dr. Hamid Soltani for his professional guidance, constructive suggestions, and countless hours of discussions.

And, last but not least, I wish to express my deepest love and gratitude to my mom and dad for their immense love, support, unforgettable inspiration and encouragement, and also to my friends for their help and support throughout the duration of my Ph.D. studies.

## **DEDICATION**

This thesis is dedicated to

*my friends*

# TABLE OF CONTENTS

|                                                                                                                                 |           |
|---------------------------------------------------------------------------------------------------------------------------------|-----------|
| <b>ABSTRACT</b> .....                                                                                                           | v         |
| <b>RÉSUMÉ</b> .....                                                                                                             | vii       |
| <b>ACKNOWLEDGEMENT</b> .....                                                                                                    | ix        |
| <b>DEDICATION</b> .....                                                                                                         | x         |
| <b>List of Figures</b> .....                                                                                                    | xiii      |
| <b>LIST OF TABLES</b> .....                                                                                                     | xvii      |
| <b>LIST OF ABBREVIATIONS</b> .....                                                                                              | XVIII     |
| <b>1</b> <b>CHAPTER 1 INTRODUCTION</b> .....                                                                                    | <b>2</b>  |
| 1.1    Overview.....                                                                                                            | 2         |
| 1.2    Motivation of Research.....                                                                                              | 3         |
| 1.3    Problem Statement.....                                                                                                   | 4         |
| 1.3.1    Problem 1: PV Modeling for Real Field Operation.....                                                                   | 6         |
| 1.3.2    Problem 2: Effect of Snow Coverage on PV Systems.....                                                                  | 8         |
| 1.3.3    Problem 3: MPPT Control under Partial Shading Condition .....                                                          | 9         |
| 1.4    Objectives of Research .....                                                                                             | 10        |
| 1.5    Methodology.....                                                                                                         | 11        |
| 1.6    Statement of the Originality of the Thesis .....                                                                         | 12        |
| 1.7    Thesis Outline.....                                                                                                      | 13        |
| 1.8    List of Publications .....                                                                                               | 14        |
| <b>2</b> <b>CHAPTER 2 LITERATURE REVIEW</b> .....                                                                               | <b>17</b> |
| 2.1    Introduction.....                                                                                                        | 17        |
| 2.2    PV Effect .....                                                                                                          | 17        |
| 2.3    PV Technologies.....                                                                                                     | 18        |
| 2.4    Review of PV Modeling Methods .....                                                                                      | 18        |
| 2.5    Review of Research into Effects of Snow on PV Systems .....                                                              | 22        |
| 2.6    Review of MPPT Techniques under Partial Shading Condition .....                                                          | 23        |
| <b>3</b> <b>CHAPTER 3 AN IMPROVED PROCEDURE IN DETERMINATION OF PV</b><br><b>CHARACTERISTICS IN REAL FIELD CONDITIONS</b> ..... | <b>28</b> |
| 3.1    Introduction.....                                                                                                        | 28        |
| 3.2    Solar Angles.....                                                                                                        | 28        |
| 3.3    Proposed Methodology.....                                                                                                | 31        |
| 3.3.1    Updating $I_{ph}$ and $I_s$ .....                                                                                      | 32        |
| 3.3.2    Updating $R_s$ and $R_{sh}$ .....                                                                                      | 34        |
| 3.3.3    Determining Diode Ideality Factor.....                                                                                 | 35        |
| 3.4    Results and Model Validation .....                                                                                       | 36        |
| 3.4.1    Parameters Variation .....                                                                                             | 37        |
| 3.4.2    Experimental Validation.....                                                                                           | 39        |
| 3.4.2.1    Experimental Setup .....                                                                                             | 39        |
| 3.4.2.2    Experimental Results.....                                                                                            | 40        |
| 3.4.2.3    Comparative Study .....                                                                                              | 41        |
| 3.4.2.4    Discussion .....                                                                                                     | 42        |
| 3.5    Conclusion .....                                                                                                         | 44        |
| <b>4</b> <b>CHAPTER 4 A NOVEL MODELING TECHNIQUE FOR PV MODULES COVERED</b><br><b>WITH SNOW/ICE</b> .....                       | <b>47</b> |
| 4.1    Introduction.....                                                                                                        | 47        |
| 4.2    Proposed Methodology for Modeling of Snow-Covered PV Modules .....                                                       | 47        |
| 4.2.1    Solar Radiation Penetration in Snow.....                                                                               | 48        |
| 4.2.2    Determining the Photocurrent of the PV Module.....                                                                     | 49        |
| 4.2.3    Obtaining the Saturation Current and the Ideality Factor of the Model Diodes .....                                     | 50        |

|         |                                                                                      |     |
|---------|--------------------------------------------------------------------------------------|-----|
| 4.2.4   | Obtaining the Model Resistances .....                                                | 52  |
| 4.3     | Model Evaluation and Results .....                                                   | 53  |
| 4.3.1   | PV Performance under Uniform Snow Accumulation .....                                 | 54  |
| 4.3.1.1 | PV Electrical Characteristics .....                                                  | 55  |
| 4.3.1.2 | Power Loss due to Snow .....                                                         | 57  |
| 4.3.1.3 | Case Study .....                                                                     | 59  |
| 4.3.1.4 | Variation of Photocurrent and Diode Saturation Current .....                         | 61  |
| 4.3.2   | PV Performance under Nonuniform Snow Accretion .....                                 | 62  |
| 4.3.2.1 | PV Electrical Characteristics .....                                                  | 63  |
| 4.3.2.2 | Effect of Bypass Diodes .....                                                        | 66  |
| 4.3.2.3 | Effect of PV Panels Layout .....                                                     | 68  |
| 4.4     | Conclusion .....                                                                     | 72  |
| 5       | CHAPTER 5 A HIGH PERFORMANCE SHADE-TOLERANT MPPT BASED ON CURRENT-MODE CONTROL ..... | 74  |
| 5.1     | Introduction .....                                                                   | 74  |
| 5.2     | Worthwhile $I$ - $V$ Characteristics of Shaded PV Arrays .....                       | 75  |
| 5.3     | Proposed ACMC-Based STMPPT .....                                                     | 77  |
| 5.3.1   | LMPPT Mode .....                                                                     | 79  |
| 5.3.2   | GMPPT Mode .....                                                                     | 79  |
| 5.3.3   | Dynamic Changing Environment .....                                                   | 82  |
| 5.3.4   | Inherent Partial Shading Recognition .....                                           | 84  |
| 5.4     | Simulation Verification .....                                                        | 85  |
| 5.4.1   | Simulation Results under Different Partial Shading Conditions .....                  | 87  |
| 5.4.2   | Dynamic Tracking Performance and Inherent Recognition of Partial Shading .....       | 98  |
| 5.5     | Experimental Verification .....                                                      | 100 |
| 5.5.1   | Experimental Setup and Digital Design Overview .....                                 | 100 |
| 5.5.2   | Experimental Results Using a Real PV Array .....                                     | 102 |
| 5.5.3   | Experimental Results using a PV simulator .....                                      | 107 |
| 5.6     | Conclusion .....                                                                     | 110 |
| 6       | CHAPTER 6 CONCLUSIONS AND FUTURE WORK .....                                          | 112 |
| 6.1     | Concluding Remarks .....                                                             | 112 |
| 6.2     | Research Perspectives .....                                                          | 115 |
|         | <b>APPENDICES</b> .....                                                              | 117 |
|         | Appendix A Interface Circuits .....                                                  | 118 |
| A.1     | Analog to Digital Conversion .....                                                   | 118 |
| A.2     | PWM Signal .....                                                                     | 119 |
|         | Appendix B MPPT Software Development on DSP .....                                    | 121 |
| B.1     | Timing Code .....                                                                    | 121 |
| B.2     | ADC Code .....                                                                       | 122 |
| B.3     | P&O MPPT Algorithm .....                                                             | 124 |
|         | <b>REFERENCES</b> .....                                                              | 126 |

# List of Figures

|                                                                                                                                                                                                                                                                           |    |
|---------------------------------------------------------------------------------------------------------------------------------------------------------------------------------------------------------------------------------------------------------------------------|----|
| Figure 1.1 Cumulative installed capacity of PV in Canada. ....                                                                                                                                                                                                            | 4  |
| Figure 1.2 Schematic of a grid-connected/microgrid system with solar energy and battery storage. ....                                                                                                                                                                     | 5  |
| Figure 1.3 Equivalent circuit model of the PV module. ....                                                                                                                                                                                                                | 6  |
| Figure 1.4 Normalized spectral response of crystalline silicon and amorphous silicon PV technologies. ....                                                                                                                                                                | 7  |
| Figure 1.5 Snow accumulation on PV systems. ....                                                                                                                                                                                                                          | 8  |
| Figure 1.6 Typical $P$ - $V$ graphs of a PV array under (a) uniform irradiance condition and (b) partial shading condition. ....                                                                                                                                          | 10 |
| Figure 2.1 Different PV equivalent circuits ....                                                                                                                                                                                                                          | 19 |
| Figure 3.1 Solar angles: (a) the altitude $\beta$ and declination angle $\delta$ of the sun, (b) position of the sun in terms of azimuth $A$ and altitude angle $\beta$ . ....                                                                                            | 29 |
| Figure 3.2 Single-diode PV circuit model. ....                                                                                                                                                                                                                            | 31 |
| Figure 3.3 Algorithm of the proposed technique. ....                                                                                                                                                                                                                      | 36 |
| Figure 3.4 Variation of series resistance with (a) irradiance, and (b) temperature. ....                                                                                                                                                                                  | 37 |
| Figure 3.5 Variation of shunt resistance with (a) irradiance, and (b) temperature. ....                                                                                                                                                                                   | 38 |
| Figure 3.6 Outdoor experiments of PV modules. ....                                                                                                                                                                                                                        | 39 |
| Figure 3.7 Modeled and experimentally measured $I$ - $V$ curves in different operating conditions for (a) FS-275 (thin film), (b) CS6P-260P (polycrystalline), and (c) ET-M53695 (monocrystalline). ....                                                                  | 40 |
| Figure 3.8 Comparison with respect to manufacturer provided $I$ - $V$ curves between the proposed model and previous models with constant parameters presented (a) in [18] for thin film Na-E125G5 PV module, and (b) in [16] for polycrystalline KC200GT PV module. .... | 42 |
| Figure 3.9 Efficiency of PV modules as a function of irradiance. ....                                                                                                                                                                                                     | 43 |
| Figure 4.1 Two-diode PV module model. ....                                                                                                                                                                                                                                | 48 |
| Figure 4.2 Algorithm of the proposed modeling methodology for snow-covered PV modules. ....                                                                                                                                                                               | 53 |
| Figure 4.3 Experimental measurements of PV modules in cold months. ....                                                                                                                                                                                                   | 54 |
| Figure 4.4 $I$ - $V$ and $P$ - $V$ curves of proposed model and experimental results in different operating conditions and snow depths for (a) CS6P-260P (polycrystalline), (b) ET-M53695 (monocrystalline), and (c) FS-275 (thin film). ....                             | 55 |
| Figure 4.5 Percentage error between the proposed PV model and the experimental measurements. ....                                                                                                                                                                         | 56 |

|                                                                                                                                                                                                                                                |    |
|------------------------------------------------------------------------------------------------------------------------------------------------------------------------------------------------------------------------------------------------|----|
| Figure 4.6 Effect of different snow depths on power production of (a) CS6P-260P, (b) ET-M53695, and (c) FS 275. ....                                                                                                                           | 57 |
| Figure 4.7 Power loss due to snow coverage for different PV technologies.....                                                                                                                                                                  | 58 |
| Figure 4.8 Tilted irradiance, back-surface temperature, and output DC power of a 12-MW grid-connected PV farm from SCADA database, along with estimated output power using the proposed model for day 1 with a snow depth of $h=1.6$ cm. ....  | 60 |
| Figure 4.9 Tilted irradiance, back-surface temperature, and output DC power of a 12-MW grid-connected PV farm from SCADA database, along with estimated output power using the proposed model for day 2 with a snow depth of $h=2.55$ cm. .... | 61 |
| Figure 4.10 Variation of (a) the photocurrent and (b) the diode saturation current of the CS6P-260P PV module for three different days with different snow depths. ....                                                                        | 62 |
| Figure 4.11 Simulated and experimental (a) $I-V$ graph and (b) $P-V$ graph, along with (c) field photo, under nonuniform snow accretion on the CS6P-260P PV panel (two peaks).....                                                             | 64 |
| Figure 4.12 Simulated and experimental (a) $I-V$ graph and (b) $P-V$ graph, along with (c) field photo, under nonuniform snow accretion on the CS6P-260P PV panel (three peaks).....                                                           | 65 |
| Figure 4.13 A PV string of four series-connected panels.....                                                                                                                                                                                   | 66 |
| Figure 4.14 Power loss of a PV string due to different snow depths of (a) 1 cm, (b) 4 cm, and (c) 7.5 cm.....                                                                                                                                  | 67 |
| Figure 4.15 Snow-covered area change on PV panel in (a) landscape position, and (b) portrait position.....                                                                                                                                     | 68 |
| Figure 4.16 Power loss due to different snow-covered areas of a depth of 2 cm for landscape and portrait positioning.....                                                                                                                      | 69 |
| Figure 4.18 Experimental snow loss due to different snow-covered areas for (a) ET-M53695 PV module and (b) FS-275 PV module. ....                                                                                                              | 70 |
| Figure 4.17 Snow-covered area change on PV panel, (a) horizontal change, (b) vertical change. ....                                                                                                                                             | 70 |
| Figure 4.19 A PV array configuration with (a) horizontal layout, and (b) vertical layout.....                                                                                                                                                  | 71 |
| Figure 5.1 Experimental PV characteristics under partial shading condition. (a) $P-V$ graph. (b) $I-V$ graph. ....                                                                                                                             | 75 |
| Figure 5.2 Configuration of the ACMC-based STMPPT with the front-end boost converter... ..                                                                                                                                                     | 77 |
| Figure 5.3 Flowchart of the proposed STMPPT technique.....                                                                                                                                                                                     | 78 |
| Figure 5.4 Tracking principle of the proposed STMPPT for a shaded PV characteristic.....                                                                                                                                                       | 81 |
| Figure 5.5 Tracking behavior of the proposed STMPPT for a uniform irradiance change.....                                                                                                                                                       | 85 |
| Figure 5.6 Simulation schematic of the PV system.....                                                                                                                                                                                          | 86 |
| Figure 5.7 Layout of the PV array with three series-connected ET-M53695 PV module.....                                                                                                                                                         | 87 |

|                                                                                                                                                                                                                                                         |     |
|---------------------------------------------------------------------------------------------------------------------------------------------------------------------------------------------------------------------------------------------------------|-----|
| Figure 5.8 $I-V$ and $P-V$ graphs of different partial shading cases: (a) Case 1, (b) Case 2, and (c) Case 3.....                                                                                                                                       | 88  |
| Figure 5.9 Simulation results of the proposed STMPPT and the PSO GMPPT for Case 1: (a) current waveforms, (b) voltage waveforms, and (c) power waveforms. ....                                                                                          | 90  |
| Figure 5.10 Expanded simulation results of the proposed STMPPT showing GMPPT mode performance for Case 1: (a) current waveform, (b) voltage waveform, and (c) power waveform. ....                                                                      | 91  |
| Figure 5.11 Simulation results of the proposed STMPPT and the PSO GMPPT for Case 2: (a) current waveforms, (b) voltage waveforms, and (c) power waveforms. ....                                                                                         | 92  |
| Figure 5.12 Expanded simulation results of the proposed STMPPT showing GMPPT mode performance for Case 2: (a) current waveform, (b) voltage waveform, and (c) power waveform. ....                                                                      | 93  |
| Figure 5.13 Simulation results of the proposed STMPPT and the PSO GMPPT for Case 3: (a) current waveforms, (b) voltage waveforms, and (c) power waveforms. ....                                                                                         | 94  |
| Figure 5.14 Expanded simulation results of the proposed STMPPT showing GMPPT mode performance for Case 3: (a) current waveform, (b) voltage waveform, and (c) power waveform. ....                                                                      | 95  |
| Figure 5.15 PV graphs of different partial shading patterns verified in [113]: (a) Pattern 1, (b) Pattern 2, and (c) Pattern 3.....                                                                                                                     | 96  |
| Figure 5.16 Simulation results of proposed STMPPT for Pattern 2: (a) current waveform, (b) voltage waveform, and (c) power waveform. ....                                                                                                               | 97  |
| Figure 5.17 Test conditions for a dynamic test. (a) Changing irradiance condition on SS1, SS2, SS3, and SS4. (b) Changing irradiance condition on SS5 and SS6. (c) Resulting $P-V$ curves. ....                                                         | 99  |
| Figure 5.18 Power waveform of dynamic test results .....                                                                                                                                                                                                | 100 |
| Figure 5.19 Experimental setup, PV array, and PV simulator .....                                                                                                                                                                                        | 101 |
| Figure 5.20 PWM generation and ADC sampling in DSP .....                                                                                                                                                                                                | 102 |
| Figure 5.21 Experimental results under partial shading condition: (a) $P-V$ curve and (b) experimental waveforms during GMPPT mode of the proposed technique (Scale time: 20 ms/div, $V_{pv}$ : 55 V/div, $I_{pv}$ : 3 A/div, $P_{pv}$ : 40 W/div)..... | 104 |
| Figure 5.22 Experimental results under partial shading condition: (a) $P-V$ curve and (b) experimental waveforms during GMPPT mode of the proposed technique (Scale time: 20 ms/div, $V_{pv}$ : 55 V/div, $I_{pv}$ : 3 A/div, $P_{pv}$ : 40 W/div)..... | 105 |
| Figure 5.23 Experimental results under partial shading condition: (a) $P-V$ curve and (b) experimental waveforms during GMPPT mode of the proposed technique (Scale time: 20 ms/div, $V_{pv}$ : 55 V/div, $I_{pv}$ : 3 A/div, $P_{pv}$ : 40 W/div)..... | 106 |

|                                                                                                                                                                                               |     |
|-----------------------------------------------------------------------------------------------------------------------------------------------------------------------------------------------|-----|
| Figure 5.24 A moving shadow test. (a) the resulting $P$ - $V$ graphs. (b) Experimental waveforms<br>(Scale time: 7 s/div, $V_{pv}$ : 45 V/div, $I_{pv}$ : 5 A/div, $P_{pv}$ : 110 W/div)..... | 108 |
| Figure 5.25 Dynamic test results as per EN50530 (Scale time: 5 s/div, $V_{pv}$ : 45 V/div, $I_{pv}$ : 6<br>A/div, $P_{pv}$ : 180 W/div). .....                                                | 109 |
| Figure A.1 Analog interface circuit for DSP ADC. ....                                                                                                                                         | 119 |
| Figure A.2 IGBT driver circuit. ....                                                                                                                                                          | 120 |

# LIST OF TABLES

|                                                                                                     |     |
|-----------------------------------------------------------------------------------------------------|-----|
| Table 3.1 Annual energy yield of a 12-MW grid-connected PV farm.....                                | 44  |
| Table 4.1 Energy production of a 12-MW PV farm for two typical days with uniform snow coverage..... | 61  |
| Table 4.2 Power loss for two PV array layouts.....                                                  | 71  |
| Table 5.1 Parameters of the PV system.....                                                          | 86  |
| Table 5.2 Electrical parameters of the ET-M53695 PV module at STC.....                              | 87  |
| Table 5.3 Different partial shading cases.....                                                      | 87  |
| Table 5.4 Comparison of the simulation results for three patterns in Figure 5.15.....               | 98  |
| Table 5.5 Averaged dynamic MPPT efficiency (%).....                                                 | 109 |

# LIST OF ABBREVIATIONS

|         |                                             |
|---------|---------------------------------------------|
| AC      | Alternating Current                         |
| ACMC    | Average Current-Mode Control                |
| ADC     | Analog to Digital Converter                 |
| AM      | Air mass                                    |
| AOI     | Angle of Incidence                          |
| DC      | Direct Current                              |
| GMPP    | Global Maximum Power Point                  |
| GMPPT   | Global Maximum Power Point Tracking         |
| IGBT    | Insulated Gate Bipolar Transistor           |
| I-V     | Current-Voltage                             |
| LHS-MPP | Left-Hand Side of Maximum Power Point       |
| LMPP    | Local Maximum Power Point                   |
| LMPPT   | Local Maximum Power Point Tracking          |
| MPP     | Maximum Power Point                         |
| MPPT    | Maximum Power Point Tracking                |
| P&O     | Perturb and Observe                         |
| PSO     | Particle Swarm Optimization                 |
| PV      | Photovoltaic                                |
| P-V     | Power-Voltage                               |
| PWM     | Pulse Width Modulation                      |
| RHS-MPP | Right-Hand Side of Maximum Power Point      |
| SS      | Sub-Strings                                 |
| STC     | Standard Test Condition                     |
| STMPPT  | Shade-Tolerant Maximum Power Point Tracking |



# CHAPTER 1

---

## INTRODUCTION

### 1.1 Overview

The electric power network around the world is experiencing long-term technical, economic, and market transformations. Main part of these transformations is the challenge of integrating high shares of renewable energy sources. A number of factors are contributing to the increase in renewable energy production worldwide. These factors include rapidly declining costs of electricity produced from renewable energy sources, regulatory and policy measures and incentives, and efforts to reduce pollution from fossil fuel-based power generation, including greenhouse gas emissions. In recent years, photovoltaic (PV) energy has been one of the fastest-growing renewable energy generating technologies because of its beneficial features, including very little maintenance cost, high reliability, long lifetime, and being environmentally friendly.

The PV system with its intermittent generation provide the output power which is affected by weather conditions. Therefore, the integration of the PV plants into the power systems through power convertors represents challenges which impose unwanted impacts on the power system operation. The uncertainty and variability of solar generation are commonly caused by passing clouds which can significantly affect voltage control, power quality, and system operation. In cold climate regions, two additional factors, ice and snow, increase the uncertainty and variability of PV generation. Since PV systems are frequently installed in countries that experience unpredictable snow and ice conditions, attention to the behavior of PV plants and their control becomes essential.

The aim of this research is to extend the knowledge in modeling and control of PV systems in cold climate regions. This thesis (i) states the problems of integration of PV plants, (ii) gives a literature review on PV modeling, effects of snow on PV systems, and maximum power point tracking (MPPT) techniques under partial shading condition, (iii) presents an improved procedure in the modeling of PV modules which gives more accurate energy yield predictions and performance analysis in real field conditions, (iv)

proposes an improved electrical model for PV modules that can predict their performance under cold weather conditions where output and efficiency of PV systems are influenced by the accumulation of snow, (v) proposes a high performance shade-tolerant MPPT (STMPPT) method based on current-mode control of DC-DC power electronic converters, and (vi) finally discusses the results using simulation in Matlab/Simulink, outdoor measurements on real PV panels, and experimentation in laboratory for validation purposes.

This research project is useful for the analysis and proper selection of PV systems integrated in power grids and microgrids under changing environmental conditions. It is also a contribution to the development of PV models and a practical tool for the design and selection of PV systems subjected to snowfall.

## **1.2 Motivation of Research**

Solar PV energy is of increasing competitiveness and utilization in electric power generation as an alternative to fossil energy resources. PV technology is a proper solution to the energy demand in suburb and remote areas where power networks are not available. Moreover, grid-connected PV systems are widely known electricity resources as an integral part of the power network. The total installed PV capacity at the end of 2017 globally amounted to 402.5 GW as compared to around 40 GW at the end of 2010 [1]. Even so, driven by advantageous supporting policies and substantial cost reductions, electricity generation from PV systems will take a major share in the future. Recent reports show that many countries have set ambitious goals for the next few decades to accept high penetration of PV systems as a part of their renewable energy systems. For instance, the European Commission has set a “2020” renewable energy target, in which it is stated that 12% of European electricity demand will be supplied by PV systems by 2020 [2]. Thus, it can be seen that world-wide expectations are increasing for energy production by means of PV energy systems.

The majority of PV systems are installed in regions of the world which experience cold winter and snow such as Germany, Czech Republic, Japan, the USA, and Canada [3]. For instance in Canada, during 2009-2016, as shown in Figure 1.1, the installed capacity of solar PV grew from 95 MW to more than 2500 MW [4]. It is also estimated that the capacity of solar electricity will increase to 6300 MW by 2020 [5]. Furthermore,

Japan has set a national goal of 60 GW of PV capacity by 2030 [6], and the total installed PV capacity in the U.S. is now around 51 GW [1]. Thus, solar energy industry is growing rapidly in these countries.

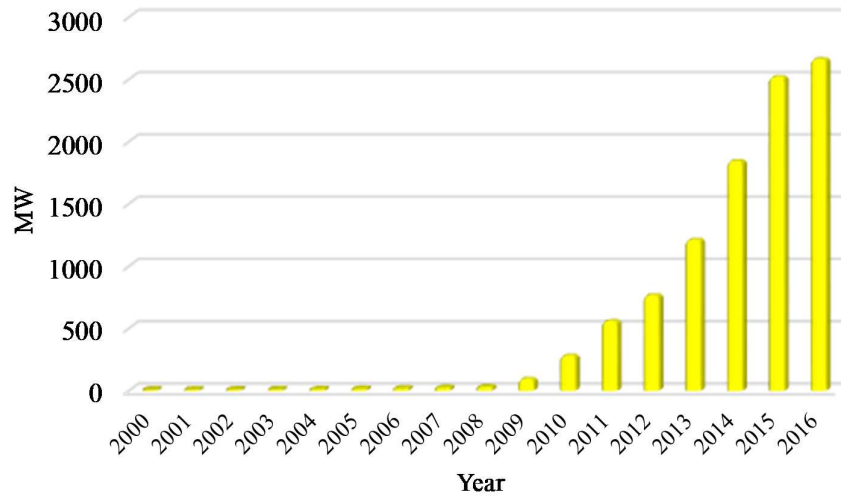


Figure 1.1 Cumulative installed capacity of PV in Canada.

PV developers are always seeking ways to achieve better efficiency and consequently more power from PV installations. Due to the increasing deployment of PV systems, there is a significant interest in optimal utilization of PV potential in cold climate regions. PV system researchers are contributing to the achievement of this goal by endeavoring to increase the overall efficiency through proper design and control of PV systems. Investigation of various aspects of PV systems operations can be greatly facilitated through the enhancement of existing PV models and simulation tools.

### 1.3 Problem Statement

Figure 1.2 shows a typical application of the PV generation in a grid-connected or microgrid system. The energy storage is a necessity to balance supply with demand and enable deep penetration of renewables. With storage, the solar resource is easily time-shifted to better align with consumption, offsetting demand at point of use, as well as lowering stress on transmission and generation infrastructure. The power electronic

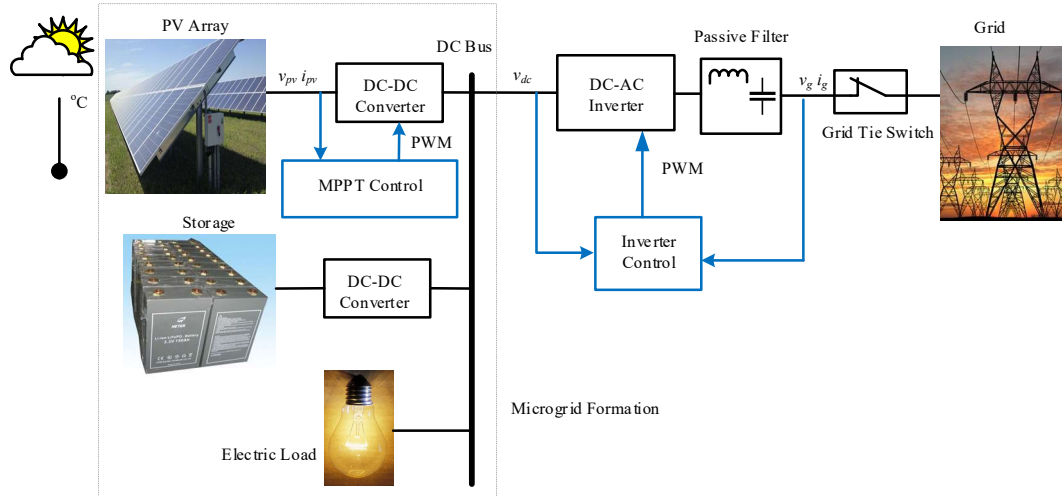


Figure 1.2 Schematic of a grid-connected/microgrid system with solar energy and battery storage.

converters integrate solar PV with batteries to deliver stable and reliable energy for both off-grid and grid-interactive applications, keeping the power on when the grid goes down. The PV cells are combined in series to form the PV module, which may incorporate bypass diodes to alleviate the effects of partial shading. PV modules are assembled in a parallel-series configuration to form a PV array, in order to provide the power at the expected voltage and current. The PV array is normally connected to a DC-DC boost converter to step up the PV voltage  $v_{pv}$  to reach the required DC-link voltage  $v_{dc}$ . The boost converter also performs the MPPT control to extract the maximum energy from the PV array. Then, a DC-AC inverter injects the power to the grid by regulating the DC-link voltage.

To develop comprehensive and sustainable energy plans, the use of PV energy offers flexible and promising solutions, as substantial investments are being increasingly made on PV generation technologies. However, it is still challenging to properly integrate them into power grids. Primary limitations on PV generation integration are their intermittent operation and uncertainty. PV generation fluctuates randomly with the atmospheric changes influencing the grid stability and security, especially when integrating in large-scale. Hence, an accurate prediction of PV energy generation through an effective model of PV modules under various environmental conditions is needed for coordination and operation of power system [7]. With an increasing penetration level of PV systems, more advanced control functionalities are also needed.

### 1.3.1 Problem 1: PV Modeling for Real Field Operation

Effective use of PV panels requires reliable modeling methods, targeting to predict the behavior of a PV system at conditions different from those characterized by the manufacturer datasheet. The PV model can be used for simulating the electrical characteristics and dynamics of PV power plants under various meteorological conditions or for estimating the energy production and efficiency of a solar plant in a specific location [8]. In addition, PV models help designers optimize the design and sizing of PV power plants and are also used to verify and test the performance of MPPT algorithms, control schemes, and design of PV power electronic converters [9-11]. Furthermore, PV models are useful in stability studies for understanding the effect of PV generation penetration on the stability of a system and for guaranteeing a system power quality and reliability [12].

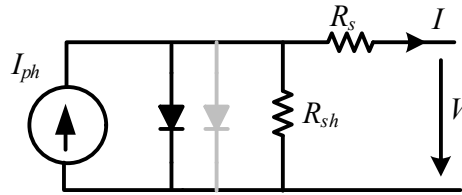


Figure 1.3 Equivalent circuit model of the PV module.

In order to simulate a PV module, an electrical equivalent circuit, as shown in Figure 1.3, is often employed mainly based on single-diode [13, 14] or two-diode [15], model. Many techniques have been proposed in literature to determine the parameters of the PV model [16-19]. The accuracy of the PV modeling in a given condition depends on the accuracy of the extracted parameters. Parameter extraction methods normally yield the parameters of the PV model for standard test condition (STC) provided by manufacturer datasheets. Although this approach simplifies the modeling, it may cause significant errors in PV characteristics for different environmental conditions. As a matter of fact, the parameters of the PV module model, and consequently the PV characteristics, are dependent on the surrounding conditions such as temperature and insolation.

PV panels respond only to a limited range of wavelengths. Different PV technologies feature different spectral responses. The spectral response of typical crystalline silicon and amorphous silicon PV technologies are shown in Figure 1.4 [20]. The crystalline silicon technologies have a better response in wavelengths of around 700 nm – 1100 nm (red and near infrared portions), whereas the amorphous silicon responds well to shorter wavelengths of around 350 nm – 550 nm (blue and green portions). Moreover, the efficiency of the PV cells varies nonlinearly as the insolation level changes, which is not characterized by manufacturer datasheets. It has been shown in [21] that neglecting the variation of efficiency versus irradiance can cause errors in annual yield as high as 4.5%.

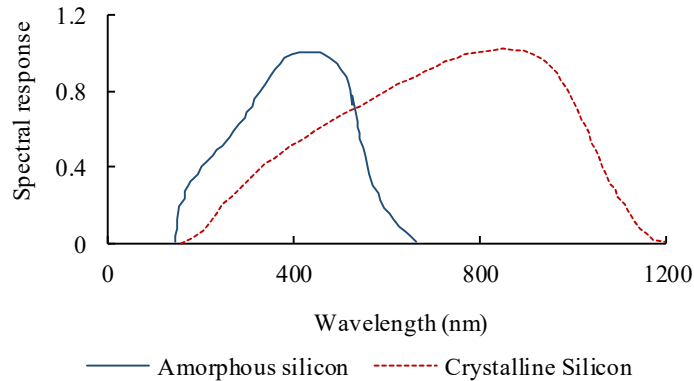


Figure 1.4 Normalized spectral response of crystalline silicon and amorphous silicon PV technologies.

The air mass ( $AM$ ), which continuously changes over time, has the major impact on the solar spectrum. Furthermore, the spectral distribution of solar irradiance changes depending on the atmosphere and the position of the sun with respect to PV modules. As sun rays travel through more atmosphere, for instance, which corresponds to a higher  $AM$ , the solar spectrum shifts towards longer wavelengths. As a result of different spectral responses, some PV technologies could benefit but it might be disadvantageous for others. Nevertheless, the influence of variation of  $AM$  and spectral response on the performance of PV devices has been largely neglected in PV module modeling.

### 1.3.2 Problem 2: Effect of Snow Coverage on PV Systems

PV systems have found different applications in cold areas for long such as remote research facilities in the South and North Pole, and space travelling. Many solar energy plants are presently installed in cold geographical locations with a considerable measure of snowfall every year. PV panels efficiency is not only influenced by the PV technology, but environmental conditions can result in variation in solar energy production. Solar energy potential is greater in cold regions as the PV cells produce electricity more efficiently at cold temperatures [22]. Temperature primarily influences the output voltage of the PV module. As the temperature decreases, the output voltage increases while the output current decreases slightly and vice versa. As a result, the maximum power point (MPP) of the PV module rises as the temperature declines. PV technologies are anticipated to have a longer lifespan in cold climates [23, 24]. Furthermore, the tilted PV panels can benefit from greater reflected sunlight since the albedo of snow-covered ground is considerably higher than the bare ground. However, snowfall during cold months challenges the behavior of the PV systems in snowy climates [25]. The accumulation of snow on PV modules weakens the intensity of incoming solar radiation, and hence, limits their ability to generate electricity during cold months. Figure 1.5 shows typical snow accumulation on PV systems after a snowfall.



Figure 1.5 Snow accumulation on PV systems. (Ref: <https://solarbuildermag.com/>)

However, the true extent of such impact on the energy production of PV modules cannot be specified in a straightforward way since it is not proportional to the snow-covered area. In some instances, snow covering only one cell can reduce the efficiency

of a whole module by a noticeable amount. Snow is a complex phenomenon, and a quantitative characterization of radiation transmittance through snow coverage requires knowledge of physical properties of snow.

Accurate modeling of the electric behavior of PV modules and systems is a key element in improving system operation and efficiency. For instance, proper modeling of the operation of PV generators under varying environmental conditions improves their performance control and assists the design of PV converters and their MPPT controller. As the application of PV systems is increasing in cold areas, it is also vitally important to address this issue through an appropriate method capable of estimating PV performance due to snow effect.

### **1.3.3 Problem 3: MPPT Control under Partial Shading Condition**

PV developers are always seeking ways to achieve better efficiency and more power from solar installations. A capability to harvest the maximum amount of energy is crucial which would help optimize return on a PV system investment. The maximum available power of a PV system changes over time as a result of ambient condition variation. In response to this challenge, power electronic conversion systems featuring MPPT control have been developed to optimize power production by operating at the MPP of the nonlinear PV characteristics.

Partial shading often occurs due to shadows created by passing clouds, presence of snow, neighboring buildings, towers, trees and telephone poles which has detrimental effects on performance of PV systems. As a result, the most heavily shaded cells limit the current and power that can be extracted from the system. The shaded cells can also be forced to support current levels exceeding their characteristic short-circuit current. This may push the shaded cells into reverse voltage regimes where they start behaving as a load [26]. Thermal power dissipation by these cells may cause excessive power losses, the formation of localized “hot spots”, and permanent cell damage.

The PV manufacturers and installers normally use bypass diodes to prevent hot-spot problem and to stop unproductive cells from disrupting the production of active cells. However, the resultant PV characteristics of the shaded PV array become more complicated showing multiple peaks in the  $P-V$  graph. This introduces a new challenge

for the control of power electronic interface to optimize energy harvesting. Figure 1.6(a) shows a typical  $P$ - $V$  graph when a PV array is uniformly irradiated exhibiting a singular power peak. A traditional dynamic MPPT could track the singular power peak and attain a suitable PV harvest performance. Figure 1.6(b) shows a typical multi-peak  $P$ - $V$  graph under partial shading condition. The traditional MPPT algorithms are unable to find the global MPP (GMPP) and track the right-most local MPP (LMPP), leading to a considerable loss of energy. Tracking the true peak of a PV system under partial shading condition has clear advantages and optimizes the power production. However, implementing a working global MPPT (GMPPT) for real operating condition is not a simple task.

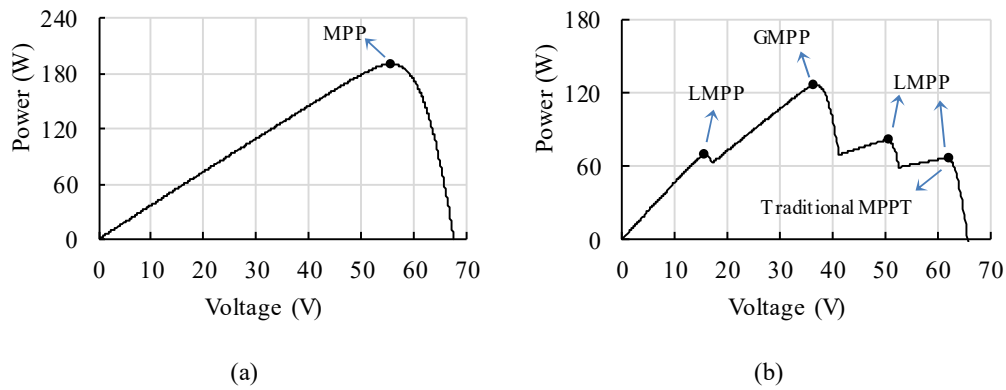


Figure 1.6 Typical  $P$ - $V$  graphs of a PV array under (a) uniform irradiance condition and (b) partial shading condition.

## 1.4 Objectives of Research

It is expected that PV systems will play a prominent role in providing both developing and developed countries with clean and renewable energy. Issues such as snow accumulation on PV panels need to be addressed to properly utilize the solar energy in cold climate conditions. Modeling of performance and expected output energy is an important factor influencing the design and operation of the PV systems. In addition, controller design is essential for the effective integration of the PV power plants. With these challenges as motivation, the goal of the research presented in this thesis is to contribute to the expansion of the utilization of PV systems, especially in cold climate

regions, and to develop controllers and modeling toolbox available for PV system designers and professionals. To this end, the following specific objectives are presented:

- **Objective 1:** An improved procedure for determination of PV characteristics in real field Conditions
- **Objective 2:** A novel modeling technique for PV modules covered with snow/ice
- **Objective 3:** A high performance shade-tolerant MPPT (STMPPT) technique for PV systems under partial shading condition

## 1.5 Methodology

To achieve the objectives stated in previous section, this study is accomplished based on modeling, control design, and validation using both simulation and experimental investigation. The proposed methodologies are briefly described below:

First, an accurate PV modeling method is presented to predict the behavior of a PV system at conditions different from those characterized by the manufacturer datasheet. The proposed model is capable of translating the parameters of the PV equivalent circuit to a given environmental condition. The analytical expressions of the single-diode model along with the standard Newton-Raphson iterative technique are used to support the modeling approach. Moreover, the spectral effects are taken into account in the model such that the characteristics of the PV modules in real outdoor operating conditions could be precisely predicted. The validity of the proposed procedure was tested against experimental measurements taken in a PV installation with different commercially available PV modules as well as real data collected by SCADA system of a 12 MW PV farm.

Next, a novel PV modeling technique is proposed to determine the electrical characteristics of snow-covered PV cells. The Bouger-Lambert Law is used in the model to estimate the amount of insolation reaching the surface of a snow-covered PV module. An extinction coefficient based on snow properties is incorporated to determine the attenuation of radiation for a given snow depth. Then, the true impact of uniform/nonuniform snow accumulation on PV system performance is investigated. Outdoor measurements of a PV panel during cold months are used to evaluate the PV model. Different simulations for verifying the effect of bypass diodes and different

layouts are carried out. This model is helpful for PV system performance assessment, MPPT development and testing, power generation prediction, and proper arrangement of panels in cold regions.

Finally, a high performance STMPPT technique is proposed to track the GMPP of a PV array with multipeak characteristic under partial shading condition. The basic idea of the proposed technique is to benefit from the simple features of the  $I-V$  profile. This enables significant reduction of the search space, independency of the algorithm from shading conditions and PV array configuration, and inherent recognition of the occurrence of partial shading conditions. The proposed STMPPT technique operates in two modes. The average current-mode control (ACMC) with the perturb and observe (P&O) MPPT algorithm functions in a local MPPT (LMPPT) mode under normal irradiance condition. When the PV array is likely to be partially shaded, a global MPPT (GMPPT) subroutine effectively scans the PV profile to optimize the PV system operation. This is achieved by implementing innovations to the ACMC-based P&O algorithm using the observations from  $I-V$  profiles. The performance improvement with the proposed technique for different partial shading conditions and environmental changes is assessed by both simulation and experimental results.

## **1.6 Statement of the Originality of the Thesis**

The necessity for an accurate PV model, which can predict the real behavior of PV modules under changing atmospheric conditions, has motivated the first objective of this thesis. In order to make precise estimations of performance of outdoor operated PV modules, an extended investigation of PV characteristics rather than STC parameters is needed. An improved procedure in the modeling of PV modules based on the single-diode model is presented (the first contribution) [R1, R5]. This improvement allows more accurate energy yield predictions and performance analysis. The novelties of the model are updating the parameters and including the spectral effects.

There is still no available electrical model of PV modules that can be implemented for online applications, such as integration to power electronic converters and MPPT algorithms, under snow coverage. Hence, there is an obvious need for a PV model which can effectively characterize the PV modules in the presence of snow. Addressing this shortage was the second objective of this research project (the second contribution),

aiming at the development of a novel model for PV modules [R2, R4] that can be used for cold weather conditions in which the accumulation of snow reduces the output power and efficiency of the PV systems. This research may be regarded as a basis for the development of PV models and a practical tool for the design and selection of PV modules subjected to snowfall.

The third objective of this thesis was motivated by performance degradation of PV systems under partial shading conditions. A novel STMPPT strategy based on the ACMC of the DC-DC converter is proposed (the third contribution) [R3]. Useful features from the  $I-V$  curves of PV array are derived to track the GMPP at high speed. This is an important contribution presented in this research project. It states that instead of scanning the voltage in  $P-V$  curve under partial shading condition, it is better to use the  $I-V$  characteristics. A simple solution is also proposed to overcome the issue of dynamic irradiance variation. This is another key idea presented in this thesis. The proposed STMPPT strategy is simple yet effective and independent from the PV array parameters similar to the P&O method. Its inherent feature is to recognize the occurrence of partial shading condition. Moreover, no additional hardware than that of the P&O method is required.

## 1.7 Thesis Outline

The individual chapters are organized as follows.

**Chapter 2** is mainly a literature review. It entails the physical operation of PV cells, different PV technologies, and PV modeling techniques. The effect of snow on the performance of PV systems is also studied in this chapter. It further reviews the negative effects of partial shading condition and MPPT techniques to track the GMPP.

**Chapter 3** presents an improved PV modeling method for precise characterization of PV modules in real field conditions. Outdoor experimental measurements are used to evaluate the PV model.

**Chapter 4** proposes a novel PV modeling method capable of representing the electrical characteristics of snow-covered PV modules. The proposed model is validated experimentally by outdoor measurements during cold months when PV modules are uniformly/nonuniformly covered with snow. Effect of employing bypass diodes on a PV

string power generation is also verified. Different PV array layouts are studied to improve the PV harvest efficiency in cold climate regions.

**Chapter 5** discloses a novel high performance STMPPT algorithm for PV systems which enables a fast and reliable GMPPT under different partial shading conditions. Simulation and experimental performance assessments are presented under different operating conditions that could happen in outdoor PV installations.

**Chapter 6** summarizes the work presented in this thesis, highlights the research contributions, and outlines the topics for future investigation.

## 1.8 List of Publications

A list of the papers and reports derived from this project, which are published so far or have been submitted, is given as follows:

### *Journal Papers:*

- [R1] **Seyedkazem Hosseini**, Shamsodin Taheri, Masoud Farzaneh, Hamed Taheri, and Mehdi Narimani, "Determination of Photovoltaic Characteristics in Real Field Conditions", *IEEE Journal of Photovoltaics*, vol. 8, no. 2, pp. 572-580, Mar. 2018.
- [R2] **Seyedkazem Hosseini**, Shamsodin Taheri, Masoud Farzaneh, and Hamed Taheri, "Modeling of Snow-Covered Photovoltaic Modules" *IEEE Transactions on Industrial Electronics*, vol. 65, no. 10, pp. 7975-7983, Oct. 2018.
- [R3] **Seyedkazem Hosseini**, Shamsodin Taheri, Masoud Farzaneh, and Hamed Taheri, "A High Performance Shade-Tolerant MPPT Based on Current-Mode Control" Accepted at *IEEE Transactions on Power Electronics*.
- [R4] **Seyedkazem Hosseini**, Shamsodin Taheri, Masoud Farzaneh, and Hamed Taheri, "Impact of Nonuniform Snow Accretion on PV Array" Under review at *IET Energy Systems Integration*.

### *Conference Papers:*

- [R5] **S.K. Hosseini**, S. Taheri, M. Farzaneh, H. Taheri, "An Approach to Precise Modeling of Photovoltaic Modules under Changing Environmental Conditions", *IEEE Electrical Power and Energy Conference (EPEC)*, 2016, Ottawa, Canada.

### *Research Report:*

- [R6] **Seyedkazem Hosseini**, Shamsodin Taheri, "Analytical calculation of technical losses of Arnprior photovoltaic Systems" *A collaboration between UQO and EDF Energies Nouvelles*.

- [R7] **Seyedkazem Hosseini**, Shamsodin Taheri, “An improved shade-tolerant MPPT for a PV DC Optimizer platform” *in collaboration with Solantro Semiconductor Corp.*.

*Co-Authored Publications:*

- [R8] Mohammad Khenar Malek Kheili, **Seyedkazem Hosseini**, Shamsodin Taheri, Ana-Maria Cretu, Hamed Taheri, and Edris Pouresmail “PSO-based Model of Uniformly Snow-Covered Photovoltaic Modules” Under revision at *IET Renewable Power Generation*.



## CHAPTER 2

---

### LITERATURE REVIEW

#### 2.1 Introduction

This chapter starts with a description of PV effect and PV technologies. Then, a literature review pertinent to the objectives of the research project is presented, including strengths, weaknesses, and existing challenges of state-of-the-art methods. In this regard, different PV modeling methods are first verified. Then, a review of research studies dealing with the issue of snowfall and PV systems is given in this chapter. Finally, performance of the traditional MPPT techniques in the presence of partial shading condition and relevant solutions in literature are presented.

#### 2.2 PV Effect

A PV cell is an electronic device that converts sunlight into DC electricity through the PV effect. In order for this energy conversion to be possible, silicon-based semiconductors are widely used to form a  $p$ - $n$  junction in the PV cell. This junction is created by connecting  $n$ -type and  $p$ -type semiconductors, which are usually produced through ‘doping’, which is a technique used to vary the number of electrons and holes in semiconductors so as to modify their electrical properties through the addition of impurities [27]. Through the connection, excess electrons diffuse to the  $p$ -type semiconductor from the  $n$ -type semiconductor, and conversely excess holes diffuse to the  $n$ -type semiconductor from the  $p$ -type semiconductor. These movements create a positively charged area at the  $n$ -type side and a negatively charged area at the  $p$ -type side, forming an electric field at the junction [28]. When the PV cell is illuminated, electrons in the semiconductor material will be knocked loose from their atoms, assuming that the energy of the photons is greater than the energy band gap of the material. Hence, multiple electron-hole pairs will be formed and electrons will start to flow through the material and the external circuit in the direction dictated by the electric field at the junction. After completing all the traveling, the electrons will return and recombine with the holes back in the semiconductor to close the circuit, generating a DC electricity.

## 2.3 PV Technologies

Silicon, a type IV semiconductor, is the most popular material in PV technologies. Solar PV silicon would be either crystalline or amorphous. In the crystalline technology, the constituent silicon is a crystal with the thickness of around 0.1-0.2 mm. The amorphous technology is utilized as a thin film of around 1  $\mu\text{m}$  thick deposited on a backing [20]. Other semiconductors, which are used in solar PV, are of types III-V such as gallium arsenide and thin films including cadmium telluride (CdTe) and copper indium selenide (CIS). Hence, there are two main groups of PV technologies: crystalline silicon (c-Si) materials which constitute 85-90% of the global market, and thin films which represent 10-15% of global PV panel sales [29]. The crystalline silicon cells are further divided into monocrystalline silicon and polycrystalline silicon (also called multicrystalline) depending on whether they are made up of a single crystal or of several assembled crystals.

## 2.4 Review of PV Modeling Methods

PV simulation models are essential in conducting PV studies since the information acquired from manufacturing datasheets is usually limited. It is widely recognized that a user-defined simulation model is beneficial for creating more accurate and reliable designs under different operating conditions [30, 31]. As shown in Figure 2.1, a PV cell can generally be described by two major types of equivalent circuits: a single-diode model and a double-diode model, which can be distinguished by the number of diodes used to model the electrical properties of a PV cell. The addition of series and shunt resistances are used in order to account for the parasitic power losses. The single-diode model is a more commonly used model in the industry as it offers a more reasonable trade-off between accuracy and complexity [32-34]. It also has the advantage that it can be easily parameterized based on typical datasheet information [35, 36]. On the other hand, the double-diode model offers higher accuracy [37-39] but suffers from longer computation times because of its additional complexity [40].

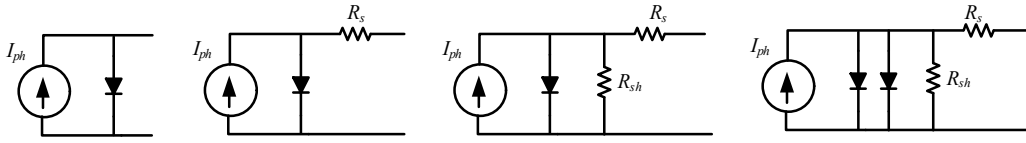


Figure 2.1 Different PV equivalent circuits

The PV modeling is based on a suitable electrical equivalent circuit, employing a set of parameters that represent properties of PV modules and operating conditions. The accurate determination of the PV model parameters is a challenge for researchers to obtain a model that simulates as close as possible the characteristics of the PV panels under a wide range of irradiance and temperature conditions. Determination of these parameters is not a trivial task, since a PV module is characterized by nonlinear  $I-V$  curves that depend mainly on irradiance and temperature the cell. Many techniques have been proposed in literature to determine the parameters of the PV model. The accuracy of the PV modeling under given conditions depends on the accuracy of the extracted parameters. The existing methods for the parameter extraction of the PV cells and modules classic models such as the single-diode and the double-diode models can be categorized into two large groups [41]: The first type, *numerical methods*, uses only the coordinates of the limited number of points on the  $I-V$  curves, such as the short-circuit, the open-circuit, and the maximum power point, which are usually provided by PV manufacturers. This approach is attractive in practical applications because of its speed and need to a few data from  $I-V$  curves. The second type is the *curve fitting methods* which yields more accurate parameter values since it utilizes all of the data of the  $I-V$  curves, but it requires all the experimental points of the  $I-V$  curves and, therefore is more complicated.

With *numerical methods*, a system of equations is formed for specific operating points, which is then solved via a numerical or iterative algorithm. A representative method of this category is introduced in [42], employing a system of five equations to determine the five parameters of the single-diode model. In particular, the fundamental equation of the model is evaluated at the short-circuit point, open-circuit point, and maximum power point, while the slope of the  $P-V$  curve at the maximum power point is set to zero. The fifth equation is formed by exploiting the linear dependence of the open-

circuit voltage on the operating temperature, utilizing the relevant temperature coefficient provided in the module datasheet. Based on the manufacturer datasheet, a generalized model of the PV array is also built in [43] and the proposed model is established using power system computer aided design (PSCAD) software. In [44], an analytical method is introduced to determine the parameters of the PV model. However, many derivations of the mathematical equations are executed, resulting in a complex model. In addition, an iterative method is proposed in [45] to estimate the parameters of the PV model. Similarly, the methods in [46-49] rely only on datasheet information, whereas other methods require also the  $I$ - $V$  curve slope at the short-circuit and/or open-circuit points [50-52].

An alternative approach to determine the model parameters is to employ a *curve fitting or optimization algorithm*, assuming that the entire  $I$ - $V$  experimental curve is available. The least-square fitting technique is applied to measured data in [53-56], while various metaheuristic algorithms have been proposed in the literature, implementing genetic algorithms [57], neural networks [58], pattern search [59], particle swarm optimization [60], differential evolution [61], and bird mating optimization [62]. A comprehensive review and comparative assessment of these methods may be found in [63]. Although the methods based on experimental data generate accurate models, they have some disadvantages such as complexity, computational cost, and convergence failure [64].

In this context, the fundamental approach of the existing works in the parameter determination of the PV model is that, first, all the parameters are extracted under standard test condition (STC). Further, some of the parameters are assumed to be invariant under environmental conditions, whereas the values of some of the equivalent circuit parameters are considered to change with respect to irradiation and temperature changes. Therefore, invariant or independent parameters are estimated using STC values and used with no modifications in arbitrary conditions, whereas dependent or variable parameters are first obtained using the STC data and then modified using some translational formula in the climatic conditions other than the STC. There is a major shortcoming for this type of characterization methods. According to the experimental observations, the values of all the parameters of the equivalent circuit model of PV panels change at different

temperature and irradiation levels. Thus, the assumption that some of the parameters are constant during arbitrary climatic conditions is physically unrealistic [65-67].

A few studies have addressed the variation of the PV model parameters. Reference [68] presents a technique to obtain the  $I-V$  characteristics of monocrystalline and polycrystalline silicon PV modules for different atmospheric conditions using numerical tools. However, the technique is based on the simplified equivalent circuit model in which the shunt resistance is ignored and a fixed series resistance is taken into account. Furthermore, the model shows deficiency in low irradiance densities.

To derive the PV curves of silicon solar modules for arbitrary temperatures and irradiance levels, a parameter extraction technique based on the single-diode equivalent circuit was investigated in [69]. However, the shunt resistance is adjusted to change solely with irradiance, and the series resistance is considered constant as calculated at STC. In [70], unknown parameters of the PV model are extracted using manufacturer datasheets for several irradiance levels at 25 °C. The parameters are then arranged in a look-up table in order to update the parameters based on interpolation for different irradiance levels. However, the modeling technique is not applicable for outdoor operating situations where temperature and irradiance vary simultaneously. Moreover, to create the look-up table, a restricted number of manufacturer-provided  $I-V$  curves are utilized which limits the model accuracy. The parameters of a single-diode model are derived in [71] by fitting the equivalent circuit equation to different sets of  $I-V$  characteristics associated with different temperature and irradiance levels. However, it demands a long computation time as well as a wide range of measured  $I-V$  curves which are hardly available.

Moreover, the existing PV modeling techniques consider a fixed solar spectral distribution where the air mass (AM) is set to 1.5 spectrum. However, in real field conditions, the AM and, consequently, the solar spectral distribution change over time. Different PV technologies respond differently to this variation. As a result, different PV technologies would experience variation in their efficiency in real field conditions. However, this fact is not reported by manufacturers and previous PV modeling studies.

## 2.5 Review of Research into Effects of Snow on PV Systems

The significance of sunlight as a major energy source of snow accumulation energy balance was recognized very early in 1889 [72]. Albedo which is the ratio of reflected radiation to incoming radiation is an important factor in snow energy balance. Thereafter, albedo and the reflective characteristics of snow accumulation have been investigated [73]. Models of radiative transfer in snow and optical properties of snow have also been studied [74], [75]. These studies have found applications in different research areas including inspection of climate feedbacks, snow chemistry and ecology, as well as hydrology and remote-sensing interpretation.

The accumulation of snow weakens the intensity of incoming solar radiation, and hence, reduces output of PV modules. A few studies have addressed the issue of energy losses of PV systems caused by snow and ice. Power loss of a 100-kW PV system in the U.S. as a function of snow depth, weather conditions, and tilt angle has been described in [76]. An average daily power loss of 11% to 45% for a tilt angle of 30° and 5% to 26% for a tilt angle of 40° has been reported. Application of PV systems in the northern Canadian climate condition was discussed in [77]. Many issues such as the impacts of snow/ice accumulation on PV modules, pertinent properties of snow/ice, thermal performance of PV module, and snow removal from PV modules have been investigated in [78]. It also proposed a technology for the snow/ice removal and used computer programs to model the snow melting rate on PV modules at four sites across Canada. Reference [79] studied the effects of snow on a rooftop PV system in the New Munich Trade Fair Centre, where the amount of proportional annual yield reduction by snow was estimated to lie between 0.3 and 2.7% from 1999 to 2004.

A monthly snow loss model has been developed [80] by incorporating parameters such as temperature, humidity, ground interference, tilt angle, and irradiation. The model has been employed to calculate the snow loss for two sites in the U.S. during two winters. Using meteorological information and regressive analysis, an empirical model based on [81] has been developed [82] to determine the short-circuit current of PV modules which takes into account parameters such as albedo. However, it did not consider the snow cover on PV modules. The impacts of snow on PV modules have been verified in [3], and a methodology was proposed to estimate the snowfall losses using climatic parameters and

time-series performance data for several PV technologies with different tilt angles. Detailed effects of albedo on PV modules have been investigated in [83, 84], which analyze the role of factors including cloud optical thickness, PV and ground surface materials, and the type of PV system. Reference [25] presented a model to predict the PV system snow losses based on snow depth, meteorological data, and performance data. An electrical installation on PV modules was proposed in [85] for defrosting of the modules when snow covers them. Reference [86] calculated the energy losses for seven modules with different tilt angles due to snow. Methods for removing snow from PV solar cell roofs, especially various material surface solutions, have been discussed in [87], and a strategy was addressed for the measurement of friction between snow/ice and different panel surfaces.

In all of the previous work, an average daily, monthly and annual energy loss due to snow was estimated by either comparing the expected energy against the collected data from the PV system or using an approximate offline model based on field and meteorological factors. These offline methodologies cannot be incorporated in power electronics and control topologies for analysis under snowy climates. Moreover, the penetration of insolation into the snow coverage on the PV modules was ignored in the aforementioned models. In addition, the  $P$ - $V$  and  $I$ - $V$  characteristics that are required for accurate evaluation of electrical performance of the PV modules for advanced design and control have not been modeled.

## **2.6 Review of MPPT Techniques under Partial Shading Condition**

PV systems normally need a power electronic interface along with an MPPT controller to be connected to the utility grid or a load. A major challenge in using a PV source is to tackle its nonlinear output characteristics, which vary with temperature and insolation. The characteristics get more complicated if the entire array does not receive uniform insolation, as in partially shaded conditions due to passing clouds, neighboring buildings, towers, trees, or telephone poles. Moreover, snow and ice are complex phenomena which pose a different distribution of solar irradiation due to the sunlight penetration and refraction. These conditions lead to changing the electrical characteristic of the PV array and producing multiple local MPPs on  $P$ - $V$  characteristic [88].

Over recent years, several MPPT techniques in combination with power electronic devices have been proposed to deliver maximum power from a PV array. These techniques vary in some general parameters such as complexity, accuracy, cost, and speed. The category of hill-climbing techniques such as P&O and incremental conductance (InCond) has achieved popularity mainly because of their simplicity, accuracy, and few tuning parameters [89-92]. The P&O algorithm works by injecting a change in the operating point of the converter (perturbation) and checking for a condition to determine the better operating point [93]. The output power is the determining factor in increasing or decreasing control parameters (voltage or duty cycle) to reach the MPP. The InCond is another commonly used MPPT technique [94, 95]. The MPP is reached when the slope of the PV power curve is zero [96, 97]. However, the major drawback of these algorithms is that they are unable to find the GMPP under partial shading condition leading to a significant reduction in PV system efficiency.

The issue of partial shading condition in PV systems and shade-tolerant MPPT (STMPPT) or global MPPT (GMPPT) solutions have been addressed by researchers in the PV field. Soft computing techniques have been proposed to find the global MPP (GMPP) of PV array in partial shading condition. The particle swarm optimization (PSO) algorithm and its modifications were used in several studies. A PSO method was used in [98] to find the GMPP of modular PV systems with a centralized MPPT control. In [99], the PSO method and the conventional P&O technique were used to enhance the convergence time of PSO. In [100], a combination of PSO and differential evolution algorithm was investigated where the two algorithms are applied consecutively in odd and even iterations. A centralized GMPPT control approach based on PSO was presented in [101] for distributed PV generation. Other soft computing techniques have been also studied such as artificial bee colony [102], grey wolf optimization [103], simulated annealing [104], fireworks algorithm [105], and natural cubic spline guided Jaya algorithm [106]. However, the accuracy of these approaches are greatly dependent on the proper initialization of their parameters in the governing equations [107]. Although the algorithms could find the GMPP for a set of conditions, they suffer from problems such as considerable fluctuations and a weak dynamic performance. The algorithms are also complex and require undesirable computational burden.

In [108], a global phase and a local phase using P&O technique are called consecutively up until the GMPP is found. The nearest local MPP is searched first. Then, other local MPPs are searched at predefined points based on the open-circuit voltage of the PV modules. A comparison is made between MPP of consecutive peaks to locate the GMPP. The same concept is utilized in [107] based on InCond technique instead of P&O technique. The GMPPT algorithm in [109] based on P&O method could achieve a good performance. The algorithm uses measurements of all PV module voltages to detect a partial shading condition and find the GMPP. Thus, it requires a large number of sensors. In [110], initially, the shading pattern is determined by producing several duty-cycles and comparing their currents. Next, the local MPPs are found using a hill-climbing technique and are compared to reach the GMPP. Therefore, the algorithm speed is restricted especially for large PV systems as the number of duty-cycles at the first stage should be at least equal to the number of bypass diodes of series-connected PV panels.

Methods in [111] and [112] could achieve a successful GMPPT by smoothly sweeping all the possible operating points of the  $P$ - $V$  curve. In [113], the multi-peak PV characteristic is split into several single-peak curves based on a PV equivalent model. Then, an improved beta GMPPT algorithm is proposed. However, the value of beta and its bounding range depend on the environmental conditions such as irradiance and temperature. The method also needs information about the configuration of the PV array and PV panel datasheet. In [114], a trapezoidal area which contains all the possible peaks is initially introduced based on the PV string characteristics. The proposed GMPPT then progressively reduces the voltage range that contains the PV array GMPP to avoid scanning unnecessary voltage range. However, the study considers limited operating conditions of PV modules (irradiance: 100-1000 W/m<sup>2</sup> and temperature: 25-75 °C). Moreover, it needs detailed information about the PV module and PV array arrangement.

Many of the proposed GMPPT techniques have been developed based on critical assumptions which are not necessarily true under actual outdoor operation. The authors of [108], for example, stated that the local peaks of a partially shaded PV array would be located around multiples of  $0.8V_{oc}$ , where  $V_{oc}$  is the open-circuit voltage of a PV module. This assumption was used in several GMPPT methods [107] [115]. However, this observation is not generally true for different PV array configurations and different

ambient conditions [116] [117]. In addition, the algorithms are complex with too many conditions and parameters that need to be tuned for a specific PV system. In most cases, the GMPPT methods require detailed information of PV array configuration and placement of the bypass diodes. However, the power electronic conversion stage which incorporates the MPPT algorithm is manufactured without the detailed knowledge of a specific PV array configuration. The MPPT algorithm is programmed to search for the true MPP within a predefined voltage window. The PV system designer then selects the PV module and decides on a proper array configuration. Therefore, it is essential to develop an independent GMPPT algorithm. The algorithm also needs to possess features such as simplicity, no extra hardware, and fast and reliable tracking in order to be a proper candidate for control of PV converter products.



## CHAPTER 3

---

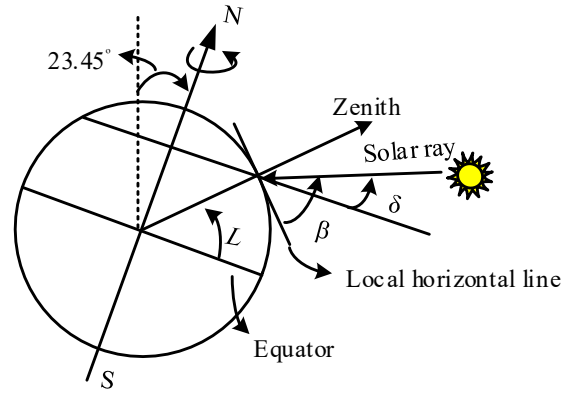
# AN IMPROVED PROCEDURE IN DETERMINATION OF PV CHARACTERISTICS IN REAL FIELD CONDITIONS

### 3.1 Introduction

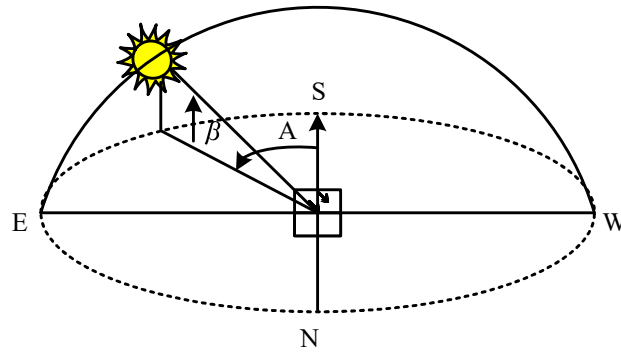
This chapter aims to develop an accurate model for predicting the electrical characteristics of PV modules under real operating conditions [R1, R5]. Variation of parameters of a PV module model is taken into account since the output characteristics depend on the surrounding conditions. The analytical expressions of the single-diode model along with experimental data are utilized to support the modeling approach. The proposed PV modeling technique updates the parameters to precisely predict the characteristics of the PV modules. Necessary corrections to the photocurrent are made through including air mass ( $AM$ ) and angle of incidence ( $AOI$ ) in the model. This can characterize the spectral and optical effects. The experimental results of outdoor measurements in conjunction with several comparative studies are used to verify the model. Furthermore, the capability of the proposed model in determining the annual energy yield of a 12-MW PV farm is assessed.

### 3.2 Solar Angles

In order to realize a portion of sunlight converted to electricity, the influence of the position of the sun with respect to the PV module surface need to be assessed. This assessment would verify angular relationship of solar rays, the earth, and the PV module at any time of a day and at any location. The solar angles formed between the sun and the earth are shown in Figure 3.1. As can be seen from Figure 3.1(a), the angle between a



(a)



(b)

Figure 3.1 Solar angles: (a) the altitude  $\beta$  and declination angle  $\delta$  of the sun, (b) position of the sun in terms of azimuth  $A$  and altitude angle  $\beta$ .

ray of the sun and the plane of the equator is defined as the "sun declination angle",  $\delta$ , which can be estimated by a sinusoidal relationship [118]

$$\delta = 23.45 \sin \left[ \frac{360}{365} (n - 81) \right], \quad (3.1)$$

where  $n$  is the day number of a year starting from 1<sup>st</sup> of January ( $n = 1$ ). This angle changes between the extremes of  $-23.45^\circ$  (winter solstice, 21<sup>st</sup> of December) and  $+23.45^\circ$  (summer solstice, 21<sup>st</sup> of June). At the vernal and autumnal equinoxes, 21<sup>st</sup> of March and 21<sup>st</sup> of September, the center of the sun lies in the plane of the equator, i.e.,  $\delta = 0$ . During fall and winter when the earth moves from autumnal equinox to winter solstice to vernal

equinox, the sun declination angle is less than zero ( $\delta < 0$ ), and during spring and summer when the earth rotates from vernal equinox to summer solstice to autumnal equinox, the sun declination angle is greater than zero ( $\delta > 0$ ).

Figure 3.1(b) illustrates the position of sun at any time of day in terms of two angles, the "sun altitude angle"  $\beta$  and the "sun azimuth angle"  $A$ . The sun altitude angle is defined as the angle between the incident sun ray and the local horizon. The sun azimuth angle is normally measured in degrees off of due south and north for the Northern Hemisphere and the Southern Hemisphere, respectively. In the Northern Hemisphere, for example, the azimuth angle is the angle between the direction of due south and the vertical projection of the sun ray down onto the horizon line (Figure 3.1(b)). It should be mentioned that, by convention, the sun azimuth angle takes positive values in the morning, when the sun is in the east, and negative values in the afternoon, when the sun is in the west. The sun altitude and azimuth angle can be calculated as [119]

$$\beta = \sin^{-1}(\cos L \cos \delta \cos \omega + \sin L \sin \delta) \quad (3.2)$$

$$A' = \sin^{-1}\left(\frac{\cos \delta \sin \omega}{\cos \beta}\right)$$

$$\text{if } \cos \omega \geq \frac{\tan \delta}{\tan L} \text{ then } A = A' \quad (3.3)$$

$$\text{otherwise, } \cos \omega < \frac{\tan \delta}{\tan L} \text{ and } A = 180 - A',$$

where  $L$  is the latitude of a location on the earth, and  $\omega$ , the "hour angle" which corresponds to the time of a day, is the angular distance between the sun ray meridian and the local meridian. By taking into account that the earth rotates  $15^\circ$  per hour, and a 24-hour time scale for a day [118],

$$\omega = 15 * (12 - ST), \quad (3.4)$$

where  $ST$  is the solar time. In order to use (3.4), the local time should be converted to the solar time [120]. As can be observed from the aforementioned equations, the sun altitude and azimuth angles, i.e., the instantaneous position of the sun, depends on the latitude of a specified location, date and time of a day. Another useful angle to be defined is the "angle of incidence",  $AOI$ , that is the angle between a line perpendicular to the PV module

surface and the direct sun ray, which can be calculated as

$$AOI = \cos^{-1}(\cos \beta \cos(A - \varphi) \sin \theta_T + \sin \beta \cos \theta_T), \quad (3.5)$$

where  $\theta_T$  is the tilt angle of the PV module, and  $\varphi$  is the deviation of the PV module face from due south for the Northern Hemisphere and due north for the Southern Hemisphere, which takes positive values toward the east and negative values toward the west.  $AM$  is described as the mass of air through which the sun rays travel to reach a surface, which influences the intensity and spectral distribution of sunlight, and is calculated as [120]

$$AM = \sqrt{(708 \sin \beta)^2 + 1417} - 708 \sin \beta. \quad (3.6)$$

Therefore,  $AM$  changes depending on different days of a year as well as at different times of a day which affects the spectral distribution of sunlight. Different PV technologies react differently to these variations.

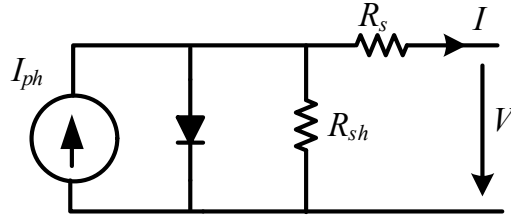


Figure 3.2 Single-diode PV circuit model.

### 3.3 Proposed Methodology

The basic unit of a PV system is the PV cell that is composed of layers of semiconductors to convert the solar energy to electricity by directly absorbing the solar photons. Various PV cell technologies have various material arrangements and configuration designs, thus, featuring different photo carrier transports. Nonetheless, PV cells can be electrically characterized by performing regular current-voltage tests. The proposed methodology is based on the single-diode equivalent circuit model of the solar module, which is shown in Figure 3.2. An implicit equation characterizes the relationship between voltage and current of the single-diode PV model as

$$I = I_{ph} - I_s \left[ \exp\left(\frac{V + R_s I}{a V_t}\right) - 1 \right] - \frac{V + R_s I}{R_{sh}}. \quad (3.7)$$

In this equation,  $R_s$  is the series resistance,  $R_{sh}$  is the shunt resistance,  $a$  is the ideality factor of the model diode,  $I_{ph}$  is the photo-generated current of the PV module,  $I_s$  is the diode saturation current, and  $V_t = N_s k T_c / q$  is the thermal voltage of the solar module, as  $T_c$  is the  $p$ - $n$  junction temperature in Kelvin,  $q = 1.60217646 \times 10^{-23}$  C is the charge of an electron,  $k = 1.3806503 \times 10^{-23}$  J/K is the Boltzmann constant, and  $N_s$  is the number of solar cells connected in series. To describe a solar module, the model requires a set of five parameters, i.e.,  $R_s$ ,  $R_{sh}$ ,  $I_{ph}$ ,  $I_s$ , and  $a$ . A systematic approach is proposed here to derive the parameters so that the model can be updated for arbitrary atmospheric conditions.

### 3.3.1 Updating $I_{ph}$ and $I_s$

As insolation generates the photocurrent of PV cells, its measurement is the primary source of error when evaluating the solar modules characteristics. Soiling of the module surface, for example, can result in a steady decrease in the current of the PV module. The photocurrent is basically impacted by the solar irradiance density hitting the surface of the PV module and marginally influenced by temperature. The photocurrent of the PV module  $I_{ph}$  can be precisely calculated as [21]

$$I_{ph} = f(AM)f(AOI) \frac{G}{G_{STC}} K_{sf} [I_{ph,STC} + K_I(T_c - T_{STC})] \quad (3.8)$$

where  $G$  is the solar irradiance,  $f(AM)$  and  $f(AOI)$  characterize the impact of changes of the solar spectral distribution and optical losses, respectively.  $K_{sf}$  quantifies derating of PV cells because of factors such as aging and dirt.  $K_I$  is the temperature coefficient of short-circuit current provided by manufacturers, and  $I_{ph,STC}$  is the photocurrent of PV module at STC in which the irradiance level is  $G_{STC} = 1000$  W/m<sup>2</sup>, the temperature of PV cells junction is  $T_{STC} = 25$  °C, and the solar spectral distribution is set to an  $AM = 1.5$  spectrum.  $I_{ph,STC}$  will be calculated by writing (3.7) for short-circuit condition.  $f(AM)$  and  $f(AOI)$  can be obtained as [81]

$$f(AM) = a_0 + a_1(AM) + a_2(AM)^2 + a_3(AM)^3 + a_4(AM)^4 \quad (3.9)$$

$$f(AOI) = b_0 + b_1(AOI) + b_2(AOI)^2 + b_3(AOI)^3 + b_4(AOI)^4 + b_5(AOI)^5. \quad (3.10)$$

The coefficients of (3.9) and (3.10),  $a_0$ - $a_4$  and  $b_0$ - $b_5$ , for different solar modules can be obtained from a module database provided in [121], or by regression methods using real operating measurements. Therefore, to obtain the photo-generated current, (3.8) leads to the effective irradiance, i.e., the irradiance that is converted to electricity which is different from the plane-of-array irradiance. The following relationships are obtained by applying the short-circuit and the open-circuit conditions to (3.7) at STC:

$$I_{ph,STC} = I_{sc,STC} + I_{s,STC} \left[ \exp\left(\frac{R_s I_{sc,STC}}{aV_t}\right) - 1 \right] + \frac{R_s I_{sc,STC}}{R_{sh}} \quad (3.11)$$

$$I_{ph,STC} - I_{s,STC} \left[ \exp\left(\frac{V_{oc,STC}}{aV_t}\right) - 1 \right] - \frac{V_{oc,STC}}{R_{sh}} = 0, \quad (3.12)$$

where  $I_{sc,STC}$ ,  $I_{s,STC}$ , and  $V_{oc,STC}$  are the short-circuit current, the reverse saturation current of the diode, and the open-circuit voltage under STC, respectively. The short-circuit current  $I_{sc,STC}$  and open-circuit voltage  $V_{oc,STC}$  are provided by manufacturer datasheets. By substituting (3.11) into (3.12), the reverse saturation current of the diode  $I_{s,STC}$  can be calculated as

$$I_{s,STC} = \frac{\left\{ \frac{(V_{oc,STC} - R_s I_{sc,STC})}{R_{sh}} - I_{sc,STC} \right\}}{\left\{ \exp\left(\frac{R_s I_{sc,STC}}{aV_t}\right) - \exp\left(\frac{V_{oc,STC}}{aV_t}\right) \right\}} \quad (3.13)$$

Consequently, the photo-generated current of the PV module  $I_{ph}$  can be updated by (3.8).

The PV module output voltage is mainly influenced by temperature and slightly by the level of irradiance. However, the effect of irradiance becomes more significant at low irradiance levels. As a result, the open-circuit voltage is calculated as a function of both cell temperature and insolation as

$$V_{oc} = V_{oc,STC} + aV_t \ln(G_{eff}) + K_V(T_c - T_{STC}), \quad (3.14)$$

where  $K_V$  is the temperature coefficient of the open-circuit voltage available from manufacturer datasheet, and  $G_{eff}$  is the effective irradiance ratio introduced as

$$G_{eff} = f(AM)f(AOI) G K_{sf}/G_{STC} \quad (3.15)$$

Therefore, the diode reverse saturation current  $I_s$  is dependent on both temperature and irradiance, and is updated as

$$I_s = (I_{ph} - (V_{oc,STC} + aV_t \ln(G_{eff}) + K_V(T_c - T_{STC}))/R_{sh}) / (\exp(V_{oc}/aV_t) - 1) \quad (3.16)$$

### 3.3.2 Updating $R_s$ and $R_{sh}$

The MPP of the  $I$ - $V$  curve varies nonlinearly as temperature and irradiance level change. The voltage and current of the MPP of a PV module in different atmospheric conditions can be estimated as [81]

$$I_m = (C_0 G_{eff} + C_1 G_{eff}^2) * (I_{m,STC} + K_{Im}(T_c - T_{STC})) \quad (3.17)$$

$$V_m = V_{m,STC} + C_2 aV_t \ln(G_{eff}) + \frac{C_3 (aV_t \ln(G_{eff}))^2}{N_s} + K_{Vm}(T_c - T_{STC}), \quad (3.18)$$

where  $V_{m,STC}$  and  $I_{m,STC}$  are the voltage and current of the MPP at STC, respectively, provided by manufacturer datasheet.  $K_{Vm}$  and  $K_{Im}$  are the MPP voltage and current temperature coefficients, respectively.  $K_{Vm}$  and  $K_{Im}$  together with other coefficients of (3.17) and (3.18), i.e.,  $C_0$ - $C_3$ , can be achieved for different solar modules from the module database, or by regression methods from real operating measurements. Using (3.17) and (3.18), the MPP of the PV characteristic can be updated as  $P_{m,cal} = V_m \times I_m$  for arbitrary ambient conditions. The series and parallel resistances of the model,  $R_s$  and  $R_{sh}$ , are obtained based on the fact that only one pair of these resistances fulfils the condition in which the estimated MPP  $P_{m,cal}$  is equal to the MPP of the modeled PV characteristic. The following equation for  $R_{sh}$  is derived from (3.7) by applying the MPP condition

$$R_{sh} = \frac{V_m(V_m + R_s I_m)}{V_m I_{ph} - V_m I_s \exp\left(\frac{V_m + R_s I_m}{aV_t}\right) + V_m I_s - P_{m,cal}} \quad (3.19)$$

By initializing the two parameters as

$$R_s' = 0; \quad R_{sh}' = [V_m/(I_{sc} - I_m)] - [(V_{oc} - V_m)/I_m], \quad (3.20)$$

the standard Newton-Raphson iterative method is used to calculate the resistors. In each iteration of the iterative procedure,  $R_s$  is increased slightly with a predefined step-size and  $R_{sh}$  is calculated simultaneously by (3.19) up until the criterion at the MPP is satisfied. Therefore, the two resistances of the model  $R_s$  and  $R_{sh}$  are updated for arbitrary atmospheric conditions.

### 3.3.3 Determining Diode Ideality Factor

The diode ideality factor  $a$  indicates the extent of ideality of the circuit model diode and its value resides in a known range (e.g.,  $1 < a < 2$  for monocrystalline and polycrystalline silicon). By adopting an arbitrary value of  $a$  and calculating the other four parameters, the  $I-V$  and  $P-V$  curves would cross through the three major points provided by the manufacturer datasheet. Nonetheless, a proper value of  $a$  is required to appropriately model the remaining of the PV characteristics. In this research, diode ideality factor is obtained based on the fitting approach proposed in [70]. Scanning different values of  $a$  within its allowable range while determining four other parameters produces different sets of five-parameter. The best set among these sets is the one with minimum difference between the measured  $I-V$  curve (possibly at STC) and the modeled one. The diode ideality factor associated with the best set is then derived and considered constant in the modeling technique because of its dependence on the PV material and technology.

To realize the development of PV characteristics, a simplified algorithm in Figure 3.3 illustrates the proposed technique in conjunction with the criterion of iterative approach. The input data contain temperature, irradiance level, module database, manufacturer datasheet, and field information. In the iterative process, the condition to reach the estimated MPP is checked and if it is satisfied, the parameters of the model are derived. Otherwise, the procedure proceeds by an increment in  $R_s$ , and new parameters will be obtained.

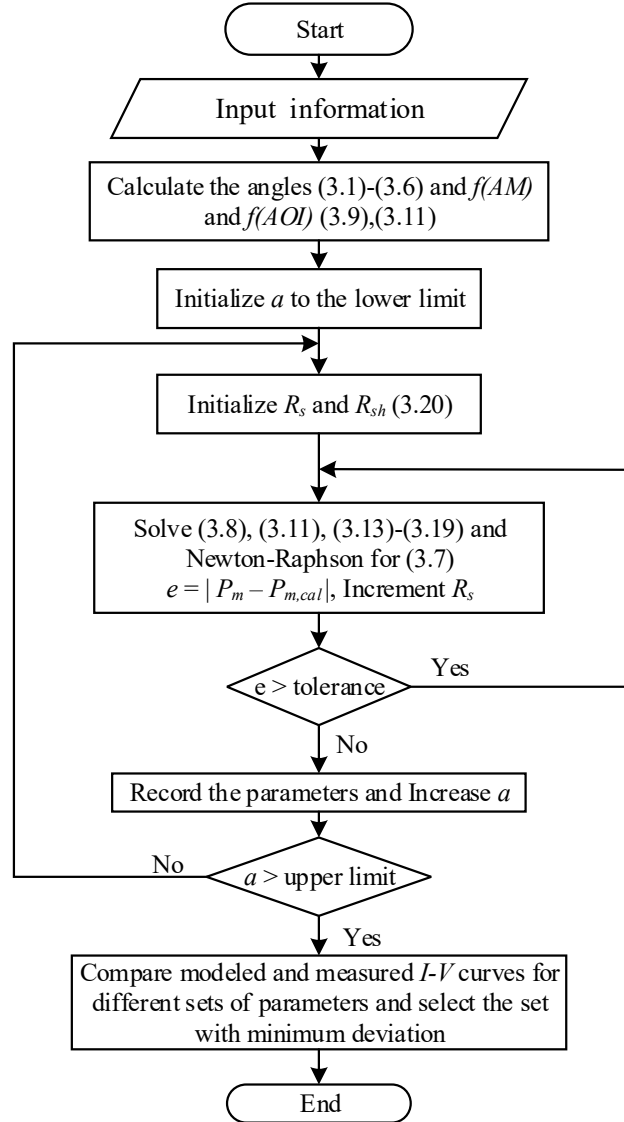


Figure 3.3 Algorithm of the proposed technique.

### 3.4 Results and Model Validation

This section studies the effectiveness of the proposed modeling technique in characterizing the real performance of PV modules under varying ambient conditions. Different PV technologies from different manufacturers have been under evaluation.

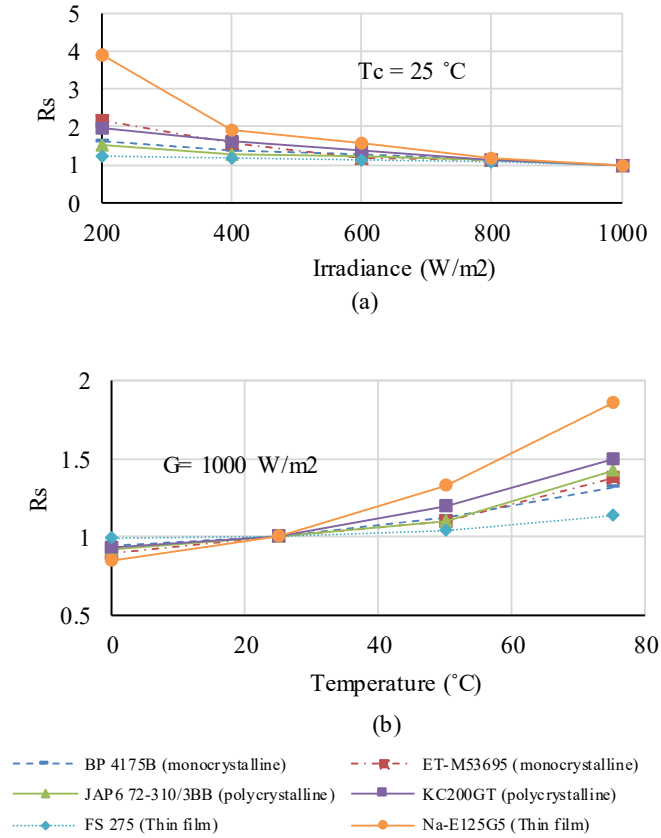


Figure 3.4 Variation of series resistance with (a) irradiance, and (b) temperature.

### 3.4.1 Parameters Variation

The impact of temperature and insolation levels on the parameters of the PV module model is investigated in this section. The short-circuit current is primarily dependent on irradiance and increases (decreases) as irradiance level increases (decreases). On the other hand, temperature primarily influences the output voltage of the PV module. As the temperature decreases, the open-circuit voltage increases while the output current decreases slightly and vice versa. The open-circuit voltage is slightly affected by variation of irradiance at high irradiance levels. However, this effect could be considerable at low irradiance levels.

Dependency of series and shunt resistances on irradiance and temperature is illustrated in Figure 3.4 and Figure 3.5. Different PV technologies from different manufacturers were studied. The values are normalized with respect to STC. An increase

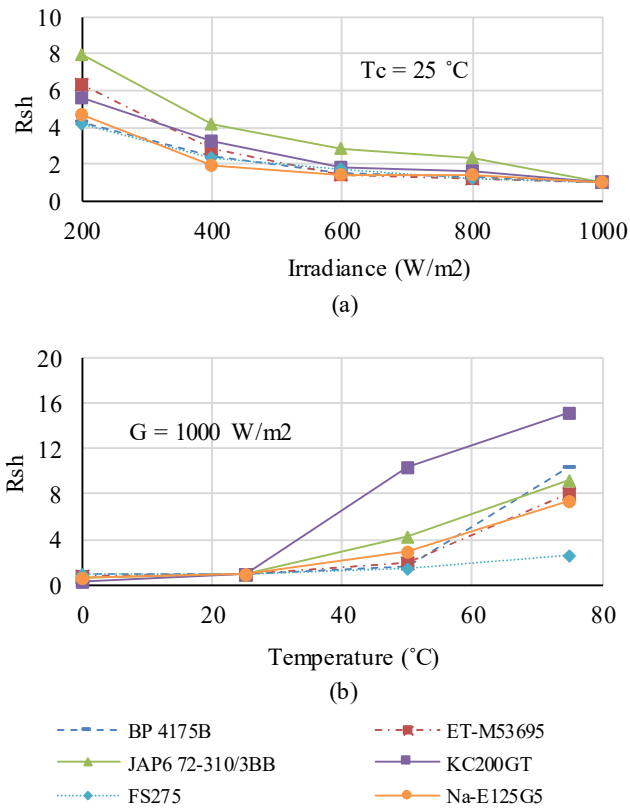


Figure 3.5 Variation of shunt resistance with (a) irradiance, and (b) temperature.

in irradiance level leads to a decrease in series resistance due to the formation of additional charges which results in an increase in conductivity of the PV cells (Figure 3.4(a)). However, the series resistance increases as temperature increases, as shown in Figure 3.4(b), because of a decrease in charge carrier mobility. Figure 3.5 shows that the parallel resistance behaves rather the same way while experiencing larger magnitude variation. As observed, the resistances depend on both cell temperature and insolation level, and their relationship is nonlinear. Furthermore, the variation differs not only among various PV technologies but also among various manufacturers of the same technology because of different cell configurations.

The series and shunt resistances affect the performance and efficiency of PV modules during operation. Therefore, considering constant values of resistances for wide range of ambient conditions would cause error in PV modeling in conventional methods, specifically in studies of PV modules under low irradiance or mismatch conditions.

### 3.4.2 Experimental Validation

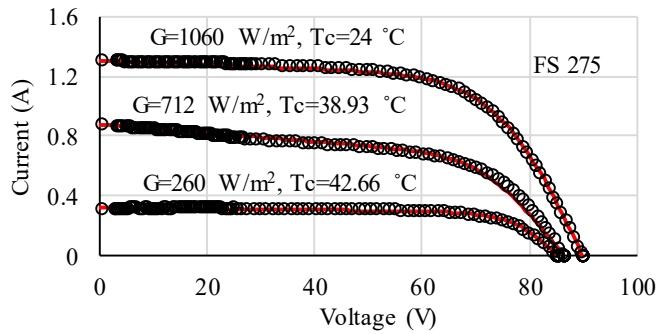
#### 3.4.2.1 Experimental Setup

To investigate experimentally the feasibility of the developed model for real operating conditions, tests were carried out on three PV modules with different technologies: an ET-M53695 monocrystalline PV module from ET Solar manufacturer, a CS6P-260P polycrystalline PV module from Canadian Solar manufacturer, and a FS-275 thin film PV module from First Solar manufacturer. The value of  $K_{sf}$  can be obtained from a comparison between the short-circuit current of the PV panel under test and the short-circuit current data provided by manufacturer datasheet. The CS6P-260P and FS-275 PV panels are new so that this factor was calculated as almost unity, whereas it was obtained as 0.97 for the ET-M53695.

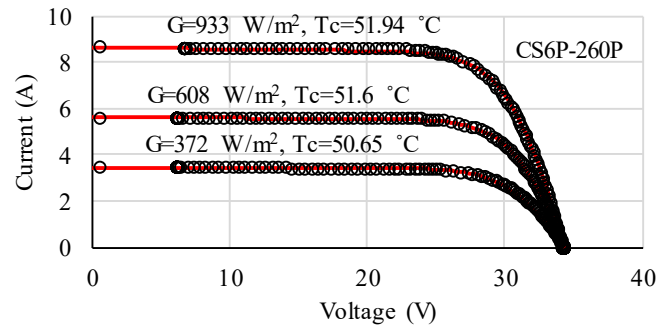


Figure 3.6 Outdoor experiments of PV modules.

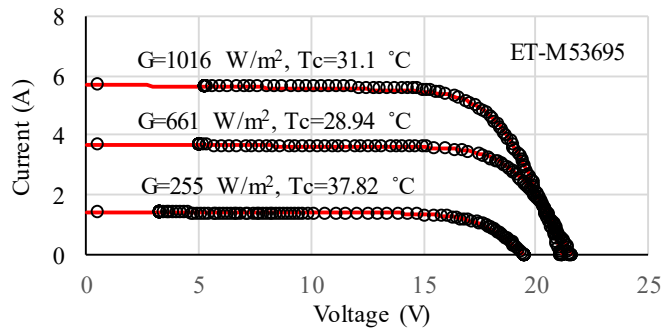
The experiments were conducted in a south-faced balcony of Lucien Brault building of UQO as depicted in Figure 3.6. The ET-M53695 and CS6P-260P PV modules consist of 36 PV cells (with two bypass diodes) and 60 PV cells (with three bypass diodes), respectively. The FS-275 PV module comprises 116 PV cells without bypass diodes. The PV characteristics of the PV panels were measured using HT Instruments I-V 400 PV Panel Analyzer and irradiance meter test kit. The PV modules were faced due south during tests with a tilt angle of  $30^\circ$ . The temperature of the back surface of the modules



(a)



(b)



(c)

○ Experimental measurements — Modeled curves

Figure 3.7 Modeled and experimentally measured  $I-V$  curves in different operating conditions for (a) FS-275 (thin film), (b) CS6P-260P (polycrystalline), and (c) ET-M53695 (monocrystalline).

were measured by a Fluke 62 Mini infrared thermometer which offers quick and reliable surface temperature readings.

### 3.4.2.2 Experimental Results

The date and time of the experiments were recorded and entered into the model along with the installation angle to realize the spectral response and reflection losses. By

feeding the proposed model with the field information and the manufacturer data, the performance of the PV modules for real outdoor conditions can be predicted. Estimated  $I-V$  curves by the proposed modeling technique along with experimental measurements are shown in Figure 3.7 for different PV technologies. The circular markers demonstrate the experimental results, while the solid lines in red represent the modeled curves. It is shown that the electrical characteristics and energy production of the PV modules are highly dependent on ambient conditions. There is a good agreement between the experimental measurements and the simulated model in different ambient conditions, with errors of less than 1%. The main source of this error is the instantaneous variation of irradiance level during the measurements.

### 3.4.2.3 Comparative Study

The precision of the proposed approach was also verified by comparing the modeled  $I-V$  characteristics of the PV modules with the  $I-V$  characteristics provided by manufacturer datasheets at different irradiance levels. Verifications were conducted for crystalline and thin film PV technologies and with reference to the existing models proposed in [16, 18]. Figure 3.8(a) and Figure 3.8(b) demonstrate the  $I-V$  curves of the thin film Na-E125G5 [18] and the polycrystalline KC200GT [16] PV modules, respectively, at STC and four different irradiance densities. The manufacturer-provided  $I-V$  curves of the PV modules are shown with circular markers, while the red solid lines represent the  $I-V$  curves of the proposed approach. The dashed black lines illustrate the  $I-V$  curves of the previous models where the parameters were obtained at STC and considered fixed at different conditions.

As can be observed from Figure 3.8, there is an obvious mismatch between the manufacturer-provided  $I-V$  curves and the curves predicted by conventional models when moving away from STC. This mismatch is less considerable in the polycrystalline PV module for which the variation of parameters is smaller, whereas, a significant mismatch occurs in the case of thin film PV module, especially at lower irradiance levels. Nevertheless, larger deviation would be expected at irradiance levels lower than  $200 \text{ W/m}^2$  which are common in outdoor conditions. The  $I-V$  characteristics of the proposed

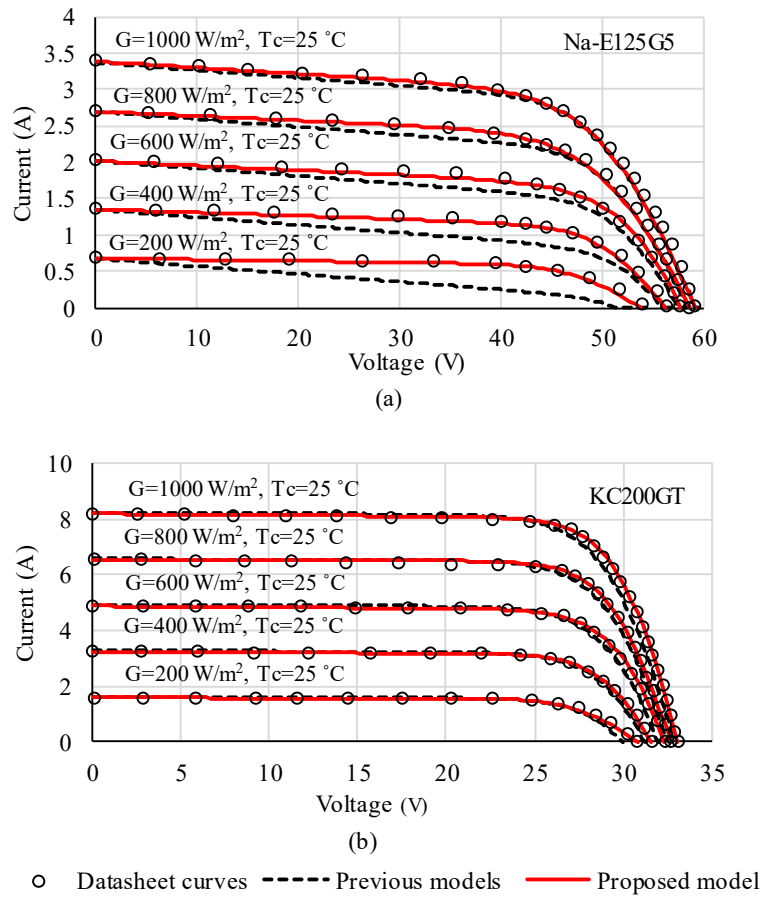


Figure 3.8 Comparison with respect to manufacturer provided  $I-V$  curves between the proposed model and previous models with constant parameters presented (a) in [18] for thin film Na-E125G5 PV module, and (b) in [16] for polycrystalline KC200GT PV module.

approach and the manufacturer-provided curves are closely matched at different irradiance levels of 200-1000  $\text{W/m}^2$  that indicates the validity of the proposed modeling.

#### 3.4.2.4 Discussion

It is essential to properly assess the PV modules efficiency and performance because of large investment on PV installations. This could help appropriately evaluate the payback time and would be beneficial for both operation and preconstruction design of PV systems.

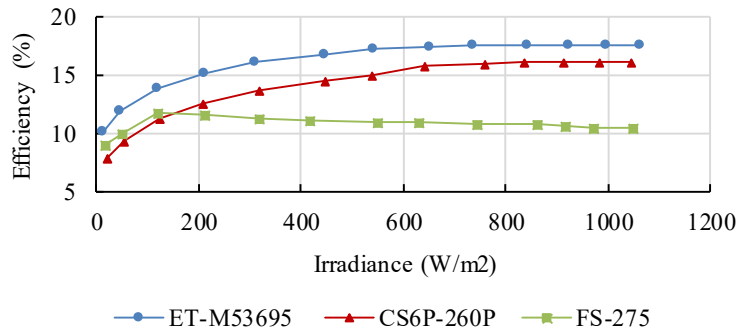


Figure 3.9 Efficiency of PV modules as a function of irradiance.

Field evaluation of PV modules performance is complicated due to the fact that their efficiency is affected by both temperature and irradiance levels. The effect of temperature on the PV modules efficiency is known and normally reported by manufacturers. The relationship between the MPP and temperature with a constant irradiance could be approximated by a straight line whose slope is interpreted as the temperature coefficient of the output power of the PV module. In practice, this is true for high irradiance levels, however, low irradiance samples are neglected to obtain the temperature coefficient. In fact, the effect of irradiance level on efficiency of the PV modules is not reported by manufacturer datasheets.

Figure 3.9 shows the measured efficiency of the PV modules versus irradiance level. The results are translated to STC temperature of 25 °C. PV cells efficiency is affected by irradiance and deviates from those predicted by manufacturers as irradiance level decreases. Monocrystalline PV cells generally experience higher efficiency as they utilize a broader range of wavelengths of sunlight. The FS-275 thin film module demonstrates lower variation of efficiency. On the other hand, wider decrease in the efficiency of the CS6P-260P polycrystalline PV module is observed. The extent of PV module efficiency reduction in low irradiance levels depends on the selected PV technology.

The above analysis implies that PV modeling without considering the variation of parameters and efficiency would lead to considerable error in PV energy generation. To realize this error, the energy yield of a 12-MW grid-connected PV farm located in southwest of the city of Ottawa, Canada, was investigated. The thin film PV panels in the

Table 3.1 Annual energy yield of a 12-MW grid-connected PV farm.

| Year                                              | 2013      | 2014      |
|---------------------------------------------------|-----------|-----------|
| PV farm SCADA database                            | 14.86 GWh | 14.32 GWh |
| Conventional PV model with uncorrected parameters | 15.35 GWh | 14.85 GWh |
| Relative error                                    | 3.36 %    | 3.7 %     |
| Proposed PV model                                 | 14.98 GWh | 14.44 GWh |
| Relative error                                    | 0.81 %    | 0.83 %    |

farm are installed due to south with a fixed tilt-angle. The PV arrays are simulated using the proposed PV model in this study and a conventional modeling method in [16]. The measured current and voltage from the DC-side of the inverters are utilized to obtain the annual energy yield of the PV farm. The results of the simulated models along with the data collected by the SCADA system of the PV farm are shown in Table 3.1. The proposed PV model provides a more precise energy prediction of the PV farm in comparison with the conventional PV model in [16].

### 3.5 Conclusion

This chapter demonstrated the necessity for an accurate PV model which can predict the behavior of a PV module in real field conditions. In order to make precise estimations of performance of outdoor operated PV modules, a more extended investigation of PV characteristics rather than STC parameters is needed. A new method based on the single-diode PV model along with a parameter extraction procedure was proposed, which is able to update its parameters. A simple and fast iterative approach was employed to obtain the series and parallel resistances. A correction of the insolation measurements was introduced to represent the spectral and optical effects. A good agreement was achieved between the PV characteristics predicted by the proposed model and those obtained from the manufacturers and experimental measurements. The methodology proposed in this thesis offers a simple electrical model instead of laborious field measurements to obtain accurate characteristics of PV modules. Moreover, the performance of different PV technologies and configurations for a specific site could be successfully assessed through

this model. This enables the proper selection of the PV technology and configuration that leads to an optimum design of the PV installation.



## **CHAPTER 4**

---

# **A NOVEL MODELING TECHNIQUE FOR PV MODULES COVERED WITH SNOW/ICE**

### **4.1 Introduction**

As the application of PV systems is increasing in cold areas, it is vitally important to address this issue through an appropriate method capable of estimating PV performance under snow conditions. This research project proposes a novel PV modeling approach that can represent instantaneous electrical characteristics of PV modules in the presence of uniform snow coverage [R2]. The proposed model utilizes the Bouguer-Lambert Law to estimate the level of insolation reaching surface of snow-covered PV cells. This is achieved by introducing an extinction coefficient which depends on the snow properties. To study the efficiency of PV cells at low insolation levels, a two-diode equivalent circuit model is employed. The true impact of uniform and nonuniform snow accretion on PV system performance is investigated [R4]. The simulation results of the proposed model are validated with experimental measurements from field tests for different commercial PV modules as well as real data collected by the SCADA system of a 12-MW grid-connected PV farm. Good agreement was observed between power generation results estimated from the proposed model and those obtained experimentally on snow-covered PV systems. This model will be helpful for researchers and PV systems developers in cold regions.

### **4.2 Proposed Methodology for Modeling of Snow-Covered PV Modules**

The electrical characteristics of the PV cells vary depending on environmental conditions. At higher insolation levels, the series resistance mainly determines the

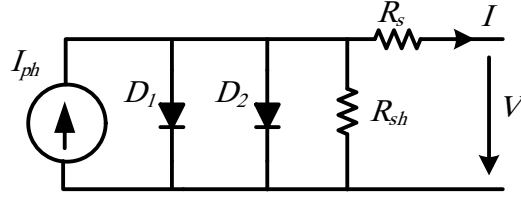


Figure 4.1 Two-diode PV module model.

efficiency of the PV cells which is the efficiency at STC reported by manufacturers. Snow coverage significantly decreases the insolation intensity reaching the surface of PV modules. The efficiency of the PV cells varies considerably at low insolation levels where the shunt resistance and the second diode affect the PV cell efficiency [122]. Therefore, the proposed methodology utilizes the two-diode equivalent circuit model of the PV module which is depicted in Figure 4.1. The PV module can be electrically characterized by an implicit equation as

$$I = I_{ph} - I_{s1} \left[ \exp\left(\frac{V + R_s I}{a_1 V_{t1}}\right) - 1 \right] - I_{s2} \left[ \exp\left(\frac{V + R_s I}{a_2 V_{t2}}\right) - 1 \right] - \frac{V + R_s I}{R_{sh}} \quad (4.1)$$

where  $R_s$  is the series resistance,  $R_{sh}$  is the shunt resistance,  $I_{ph}$  is the photo-generated current by the incidence of light,  $I_{s1}$  and  $I_{s2}$  represent the diodes reverse saturation current,  $a_1$  and  $a_2$  are the ideality factor of the diodes, and  $V_{t1,2} = N_s k T_c / q$  is the PV module thermal voltage with  $N_s$  cells connected in series, as  $T_c$  is the  $p$ - $n$  junction temperature in Kelvin,  $k = 1.3806503 \times 10^{-23}$  J/K is the Boltzmann constant, and  $q = 1.60217646 \times 10^{-23}$  C is the charge of an electron.

In order to model the instantaneous electrical characteristics of PV modules in the presence of snow, a systematic methodology is proposed in following subsections.

#### 4.2.1 Solar Radiation Penetration in Snow

In order to obtain the photo-generated current, it is essential to specify the amount of insolation received by the PV module. A layer of snow/ice on the PV module lessens the insolation reaching the surface of the PV cells. Radiation striking the snow coverage penetrates deeper layers of snow depending on the light wavelength and snow properties

[123]. Hence, to model the electrical performance of a PV module that is covered with snow, the penetration of the insolation into the snow should be taken into account. The attenuation of insolation travelling through the snow/ice cover can be modeled using the Bouger-Lambert Law [124]:

$$G_{\downarrow}(h) = G_{\downarrow}(0) \exp(-k_{ext}h) \quad (4.2)$$

where  $G_{\downarrow}(0)$  is the intensity of insolation on the surface of snow cover,  $h$  is the depth of snow cover,  $G_{\downarrow}(h)$  is the intensity of insolation remaining in depth  $h$  below the snow surface, and  $k_{ext}$  is the extinction coefficient. All radiation that is absorbed or scattered out of the incident direction is extinct [125]. This is characterized by the extinction coefficient which generally depends on the characteristics of snow and illumination conditions [126]. A formulation of the extinction coefficient as a function of snow properties is presented in [127] and [128] as

$$k_{ext} = \frac{3\rho}{2\rho_i r_{ef}} \quad (4.3)$$

where  $\rho$  is the snow density,  $\rho_i$  is the ice density ( $= 917 \text{ kg m}^{-3}$ ), and  $r_{ef}$  is the effective grain radius. The values of the insolation extinction coefficient of different types of snow may range from around  $10 \text{ m}^{-1}$  for soft new snow to  $55 \text{ m}^{-1}$  for hard powder snow [78]. The accumulation of ice also affects the incoming radiation with extinction coefficients ranging from  $2 \text{ m}^{-1}$  for clear ice to  $20 \text{ m}^{-1}$  for cloudy ice. The transmitted radiation through snow coverage generally reveals spectral dependence. However, the Bouger-Lambert Law can be used for the whole solar spectrum by calculating an average value for the extinction coefficient based on the snow/ice properties [124].

#### 4.2.2 Determining the Photocurrent of the PV Module

The photocurrent is basically impacted by the insolation intensity hitting the surface of the PV module and marginally influenced by temperature. Conventional electrical models for PV modules fail to describe the various physical processes that influence the conversion of photon energy into electricity, and thus, cannot be used to characterize the

PV modules under snow condition. The photocurrent of a snow-covered PV module  $I_{ph}$  can be obtained as

$$I_{ph} = \frac{G_{\downarrow}(h)}{G_{STC}} K_{sf} [I_{ph,STC} + K_I(T_c - T_{STC})] \quad (4.4)$$

In this equation,  $K_{sf}$  quantifies the derating of PV module because of factors such as aging and dirt,  $K_I$  is the temperature coefficient of short-circuit current provided by manufacturers.  $I_{ph,STC}$  is the photocurrent of PV module at STC which will be analytically calculated in the next step. Therefore, to determine the photocurrent, the effective insolation, i.e. the insolation that is converted to electricity, is recognized by (4.4).

#### 4.2.3 Obtaining the Saturation Current and the Ideality Factor of the Model Diodes

The PV module output voltage is mainly influenced by temperature and more slightly so by the intensity of insolation. However, the effect of intensity of insolation becomes more significant at low irradiance levels in the presence of snow. As a result, the open-circuit voltage is calculated as a function of both cell temperature and the insolation penetrated through the snow cover as follows

$$V_{oc} = V_{oc,STC} + V_t \ln(G_{\downarrow}(h) K_{sf}/G_{STC}) + K_V(T_c - T_{STC}) \quad (4.5)$$

Therefore, the saturation currents of the diodes are dependent on both temperature and insolation, and are obtained with a simplified equation as [129], [18]

$$I_{s1} = I_{s2} = I_s = (I_{ph} - V_{oc}/R_{sh}) / (\exp(V_{oc}/\{(a_1 + a_2)/p\}V_t) - 1) \quad (4.6)$$

where  $(a_1 + a_2)/p = 1$ . This simplification enables the analytical calculation of the diodes saturation currents. Equation (4.1) could be rewritten in terms of  $p$  as

$$I = I_{ph} - I_s \left[ \exp\left(\frac{V + R_s I}{V_t}\right) + \exp\left(\frac{V + R_s I}{(p-1)V_t}\right) - 2 \right] - \frac{V + R_s I}{R_{sh}} \quad (4.7)$$

The diode ideality factors  $a_1$  and  $a_2$  indicate the diffusion and recombination current components, respectively. According to the Shockley's diffusion theory,  $a_1$  is considered as unity [130]. The value of  $a_2$  is adaptable depending on the PV technology and configuration, however, its value resides in a known range. In the modeling algorithm, the lower limit and upper limit for  $a_2$  were considered 1 and 2.5, respectively. However, based on vast simulation studies in conjunction with the experimental tests, it was found that if  $a_2$  is between 1.1 and 2, the best agreement between the proposed PV model and experimental results is achieved. Scanning different values of  $a_2$  within its allowable range while determining other parameters produces different sets of parameters. The best set among these sets is the one with minimum difference between the measured  $I$ - $V$  curve (possibly at STC) and the modeled one by (4.7). The diode ideality factor  $a_2$  associated with the best set is then derived.

The following equations are obtained by applying the short-circuit and the open-circuit conditions to (4.7) at STC:

$$I_{ph,STC} = I_{sc,STC} + I_{s,STC} \left[ \exp\left(\frac{R_s I_{sc,STC}}{V_t}\right) + \exp\left(\frac{R_s I_{sc,STC}}{(p-1)V_t}\right) - 2 \right] + \frac{R_s I_{sc,STC}}{R_{sh}} \quad (4.8)$$

$$I_{ph,STC} - I_{s,STC} \left[ \exp\left(\frac{V_{oc,STC}}{V_t}\right) + \exp\left(\frac{V_{oc,STC}}{(p-1)V_t}\right) - 2 \right] - \frac{V_{oc,STC}}{R_{sh}} = 0, \quad (4.9)$$

where  $I_{sc,STC}$  and  $I_{s,STC}$  are the short-circuit current and the reverse saturation current of the diode under STC, respectively. The short-circuit current  $I_{sc,STC}$  is provided by manufacturer datasheet. By substituting (4.8) into (4.9), the reverse saturation current of the diode  $I_{s,STC}$  under STC can be calculated as

$$I_{s,STC} = \left\{ \frac{(V_{oc,STC} - R_s I_{sc,STC})}{R_{sh}} - I_{sc,STC} \right\} / \left\{ \exp\left(\frac{R_s I_{sc,STC}}{V_t}\right) + \exp\left(\frac{R_s I_{sc,STC}}{(p-1)V_t}\right) - \exp\left(\frac{V_{oc,STC}}{V_t}\right) - \exp\left(\frac{V_{oc,STC}}{(p-1)V_t}\right) \right\} \quad (4.10)$$

#### 4.2.4 Obtaining the Model Resistances

The series and parallel resistances of the model,  $R_s$  and  $R_{sh}$ , are obtained based on the fact that only one pair of these resistances fulfils the condition in which the experimental MPP  $P_{max,e}$ , is equal to the MPP of the modeled PV characteristics. The following equation for  $R_{sh}$  is derived based on (4.7) by applying the MPP condition as  $P_{max,e} = V_{mp}I_{mp}$ :

$$R_{sh} = V_{mp}(V_{mp} + R_s I_{mp}) / \left\{ V_{mp} I_{ph} - V_{mp} I_s \left[ \exp\left(\frac{V_{mp} + R_s I_{mp}}{V_t}\right) + \exp\left(\frac{V_{mp} + R_s I_{mp}}{(p-1)V_t}\right) - 2 \right] - P_{max,e} \right\} \quad (4.11)$$

where  $V_{mp}$  and  $I_{mp}$  are the voltage and current of MPP. By initializing the two parameters as

$$R_s' = 0; \quad R_{sh}' = [V_{mp}/(I_{sc,STC} - I_{mp})] - [(V_{oc,STC} - V_{mp})/I_{mp}], \quad (4.12)$$

the standard Newton-Raphson iterative method is used to calculate the resistors. In each iteration of the iterative procedure,  $R_s$  is increased slightly with a predefined step-size and  $R_{sh}$  is calculated simultaneously by (4.11) up until the criterion at the MPP is satisfied. Therefore, the two resistances of the model  $R_s$  and  $R_{sh}$  are obtained so that the peak of the modeled  $P$ - $V$  curve coincides with the experimental maximum power point.

To realize the development of PV characteristics in the presence of snow, a simplified algorithm in Figure 4.2 illustrates the proposed technique in conjunction with the iterative approach criteria. The input data include temperature, insolation, manufacturer datasheet, and snow depth and properties. In this process, first the effective insolation producing the photocurrent is determined. Then, the parameters of the two-diode model are extracted. In the iterative process, the condition to reach the MPP is checked and if it is satisfied, the parameters of the model are derived. Otherwise,  $R_s$  is incremented and new parameters are obtained.

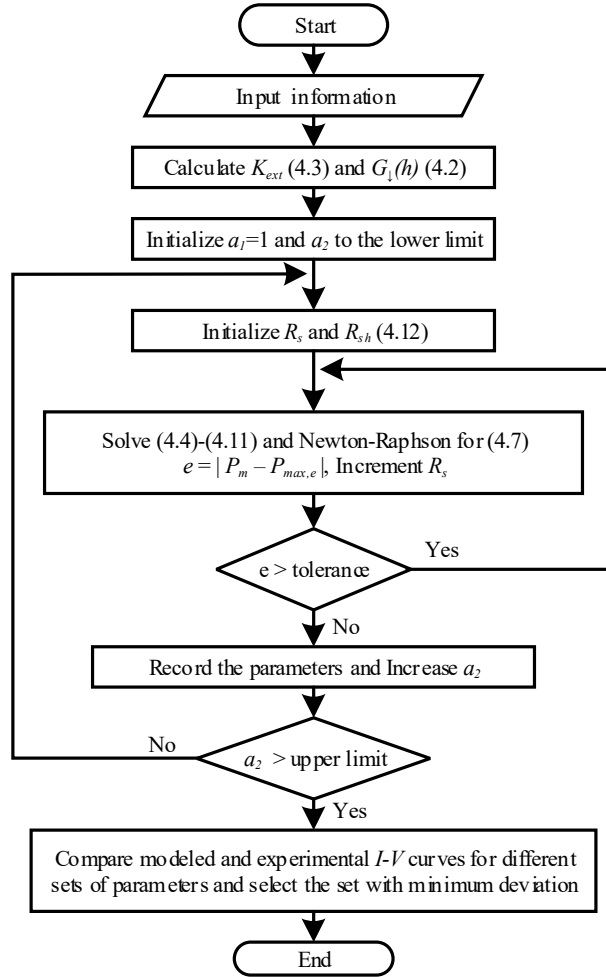


Figure 4.2 Algorithm of the proposed modeling methodology for snow-covered PV modules.

### 4.3 Model Evaluation and Results

In this section, the effectiveness of the proposed approach will be assessed by characterizing the real performance of snow-covered PV modules under varying ambient conditions. For this purpose, the simulation model was implemented with MATLAB/SIMULINK, and different PV technologies from different manufacturers were evaluated. The same experimental setup explained in section 3.4.2.1 is used during cold months as shown in Figure 4.3. The experiments were carried out at different days of December 2016 and January-March 2017.



Figure 4.3 Experimental measurements of PV modules in cold months.

The extinction coefficient represents the geophysical feature of snow that determines the amount of insolation penetration for a given snow depth. This coefficient basically depends on the properties of snow, namely the grain size and density, and can be obtained by (4.3). Moreover, the snow properties are affected by climatological parameters like snow temperature and accumulation. The experiments were supplemented by physical characteristics of the snow coverage, including snow depth, density, and an estimation of grain size. The snow depths were measured using an electronic digital caliper. A digital scale was also used to determine the snow densities. The snow grain size was obtained using a millimeter-scale grid and a magnifying glass. The extinction coefficient was obtained for different snow accumulation over the course of experiments. The range of the extinction coefficient in the experiments was recognized between  $18 \text{ m}^{-1}$  and  $54 \text{ m}^{-1}$ .

#### **4.3.1 PV Performance under Uniform Snow Accumulation**

In this section, performance of PV systems under uniform snow coverage is investigated.

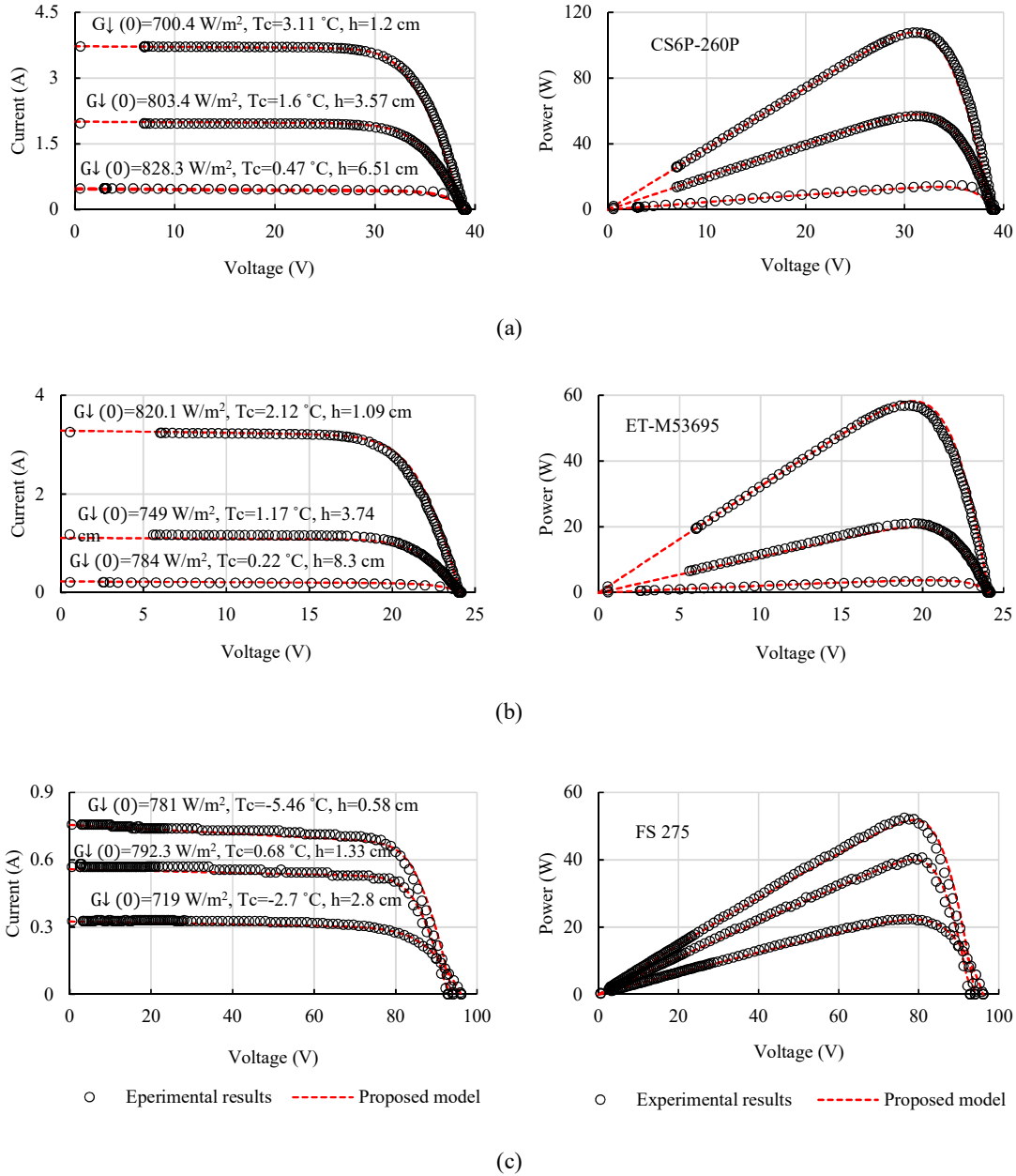


Figure 4.4  $I$ - $V$  and  $P$ - $V$  curves of proposed model and experimental results in different operating conditions and snow depths for (a) CS6P-260P (polycrystalline), (b) ET-M53695 (monocrystalline), and (c) FS-275 (thin film).

#### 4.3.1.1 PV Electrical Characteristics

The effectiveness of the proposed methodology is verified by comparing the  $I$ - $V$  and  $P$ - $V$  characteristics of the simulated model with the ones measured experimentally

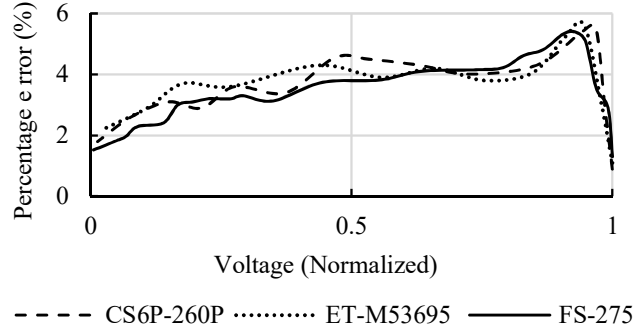


Figure 4.5 Percentage error between the proposed PV model and the experimental measurements.

outdoors for different PV modules. By feeding the proposed model with the field information as well as the manufacturer data, it is possible to predict the performance of the PV modules for a variety of climatic conditions and snow depths. Figure 4.4 shows simulated  $I-V$  and  $P-V$  curves along with experimental measurements for different uniform snow depths. The circular markers in black demonstrate the experimental results, while the dashed lines in red represent the modeled curves. It is observed that photocurrent decreases considerably as snow depth increases. In fact, insolation transmittance through the snow coverage is greatly dependent on snow depth as well as snow properties. As can be observed from Figure 4.4, the proposed model successfully estimates the electrical characteristics of snow-covered PV modules, demonstrating the effectiveness of the proposed methodology. Minor deviations between the modeled and experimental curves could be due to slight nonuniformity of snow coverage on the PV module. An increase in open-circuit voltage of  $I-V$  and  $P-V$  curves with respect to STC is seen in the results due to the lower temperatures in cold weather conditions. This implies that the peak power tracking window of the MPPT controller integrated to the power electronic interface should increase for cold temperatures. This tracking window is actually the voltage range in which the MPPT controller searches for the maximum power of the PV array.

Figure 4.5 presents the percentage error of the proposed model with reference to the experimental measurements. This analysis has been carried out for the three PV technologies under study based on different measurements with different snow depths.

Generally, an average percentage error of 3.6% was observed between the proposed PV model and the experimental results.

#### 4.3.1.2 Power Loss due to Snow

The performance of the PV modules was analyzed after they were covered with snow in different days. Figure 4.6 illustrates the changes of the MPPs of PV modules under test for different snow depths as compared to the expected MPPs. The amount of power generated did not have a fixed pattern because of the variation of parameters like insolation and temperature. The electricity production of the PV modules is dependent on

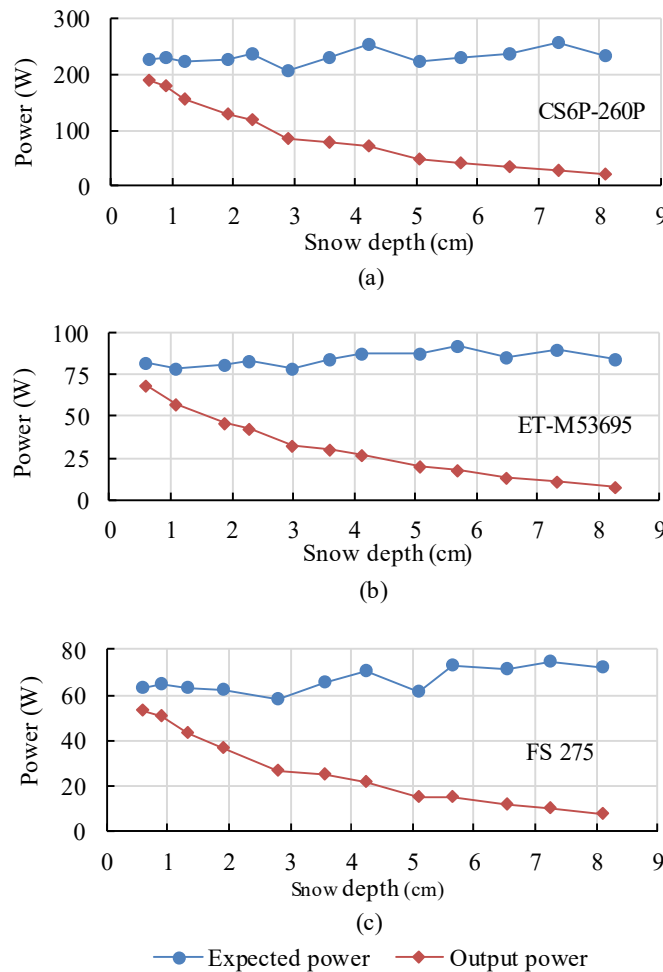


Figure 4.6 Effect of different snow depths on power production of (a) CS6P-260P, (b) ET-M53695, and (c) FS 275.

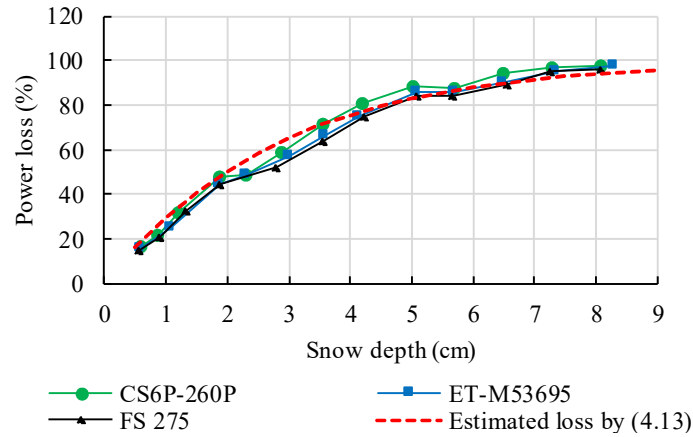


Figure 4.7 Power loss due to snow coverage for different PV technologies.

the snow depth, and the MPPs decline nonlinearly as the snow depth increases as a result of a decrease of insolation penetration.

The percentage of power loss of PV modules due to snow, which was determined by comparing the MPPs of the snow-covered PV modules against their expected MPPs without snow cover in the same condition, is shown in Figure 4.7. It should be noted that by covering the PV modules with a mere 2.5 cm of snow, a power loss of more than 50% was experienced. The PV modules could generate almost no electricity, power loss of nearly 100%, for uniform snow accumulation of deeper than 8 cm. Small differences in percentage of snow loss of different PV technologies under test were observed for the same snow depths. These differences could be results of uncertainties in PV characteristics measurements in snowy conditions. Moreover, different PV technologies show different spectral responses. Light transmittance through snow demonstrates spectral dependence as well as dependency on snow depth and snow properties. The maximum values of transmitted light intensities are at wavelengths between 450 nm and 550 nm, while the near-infrared portion of light penetrates less effectively. Therefore, different PV technologies would respond differently to this spectral dependence.

The percentage of power loss of a snow-covered PV module as a function of snow thickness can be represented by the following equation based on an average value of extinction coefficient

$$P_{loss}(\%) = [1 - \exp(-k_{ext}h)] \times 100 \quad (4.13)$$

In the tests, an average value of 34.9 was obtained for the extinction coefficient for which the estimated power loss based on (4.13) is illustrated in Figure 4.7 with dashed line in red. As can be observed, this equation offers a good tool for estimating the power loss of PV systems due to a uniform snow coverage. It is worth mentioning that (4.13) recognizes the power loss solely due to snow as it is obtained in comparison with the expected power under same conditions.

In order to obtain the output power of a snow-covered PV array which is controlled by a power electronic converter with an MPPT algorithm, the following expression based on (4.2), (4.4), and (4.5) is proposed as

$$P_{out} = N \cdot \frac{G_{\downarrow}(h)}{G_{STC}} K_{sf} [I_{mp,STC} + K_I(T_c - T_{STC})] [V_{mp,STC} + V_t \ln(G_{\downarrow}(h) K_{sf}/G_{STC}) + K_V(T_c - T_{STC})] \quad (4.14)$$

where  $I_{mp,STC}$  and  $V_{mp,STC}$  are the MPP current and voltage of a PV module under STC, and  $N$  is the number of PV modules in the PV array. Equation (4.14) entails the effect of temperature and module quality degradation as well as the snow coverage. This equation is useful for estimating the PV power production in cold regions.

#### 4.3.1.3 Case Study

Conventional PV modeling methods cannot be used to simulate the snow-covered PV arrays. In order to further verify the suitability of the proposed approach, the PV model is utilized to simulate a 12-MW grid-connected PV farm located in Ontario, Canada. The thin film PV panels in the farm are installed due south with a fixed tilt-angle. The SCADA system of the PV farm yields hourly-average data such as tilted irradiance, back-surface temperature of PV panels, as well as DC current, DC voltage, and AC power of the inverters. The grid-connected inverters in the PV farm incorporate an MPPT control to extract the maximum power from the PV arrays. The data of the SCADA system of the PV farm were derived for two typical days when snow existed on the PV panels after a snowfall.

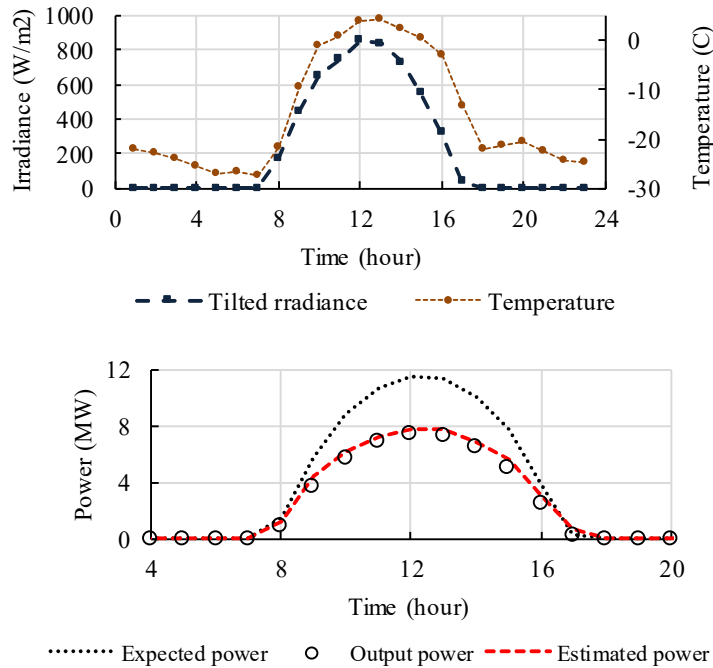


Figure 4.8 Tilted irradiance, back-surface temperature, and output DC power of a 12-MW grid-connected PV farm from SCADA database, along with estimated output power using the proposed model for day 1 with a snow depth of  $h=1.6$  cm.

The irradiance and temperature data along with the field measurements of snow depth and snow properties are fed to the proposed model. The PV farm had been in operation for six years by the end of year 2015. The quality degradation was assessed by testing several separated PV modules and comparing the results against manufacturer datasheet. An average value of 95.9% was obtained for  $K_{sf}$ .

The results of the simulated models along with the data collected by the SCADA system of the PV farm for two typical days of December 2015 and January 2016 with different snow depths are shown in Figure 4.8 and Figure 4.9. A snow-covered PV farm can still produce a considerable amount of energy depending on the depth of snow accumulation. The proposed PV modeling technique provides a good power prediction of the PV farm. However, small differences are seen between the data collected by the SCADA system and the estimated power. Table 4.1 shows the energy yield of the PV farm for these two days. The proposed model overestimates the energy production of the

PV farm mainly as a result of electrical mismatching losses that exist in the PV farm due to the nonuniformity of snow coverage on different strings.

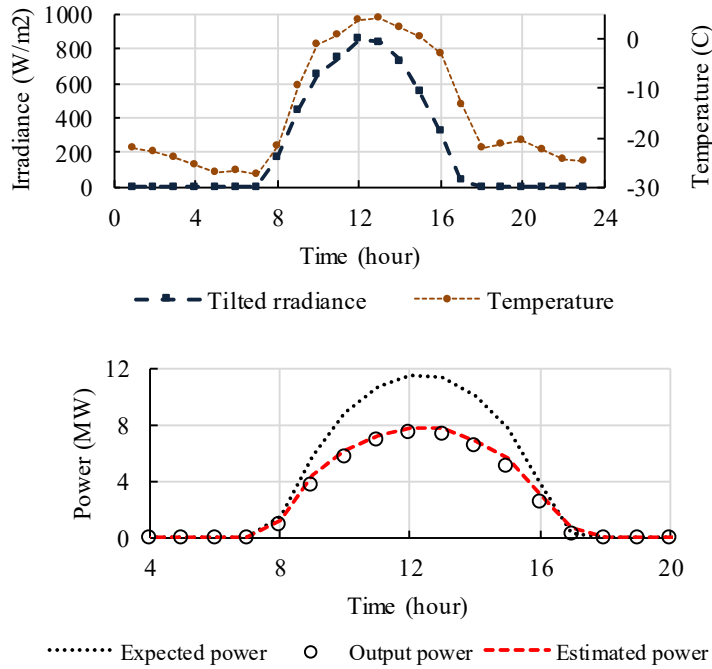


Figure 4.9 Tilted irradiance, back-surface temperature, and output DC power of a 12-MW grid-connected PV farm from SCADA database, along with estimated output power using the proposed model for day 2 with a snow depth of  $h=2.55$  cm.

Table 4.1 Energy production of a 12-MW PV farm for two typical days with uniform snow coverage.

|                        | Day 1 ( $h=1.6$ cm) | Day 2 ( $h=2.55$ cm) |
|------------------------|---------------------|----------------------|
| PV farm SCADA database | 46.234 MWh          | 29.418 MWh           |
| Proposed PV model      | 49.15MWh            | 31.43MWh             |
| Relative error         | 6.3 %               | 6.8 %                |

#### 4.3.1.4 Variation of Photocurrent and Diode Saturation Current

The photocurrent is a very important parameter which represents the portion of sunlight converted to electricity. The photocurrent will change for different operating

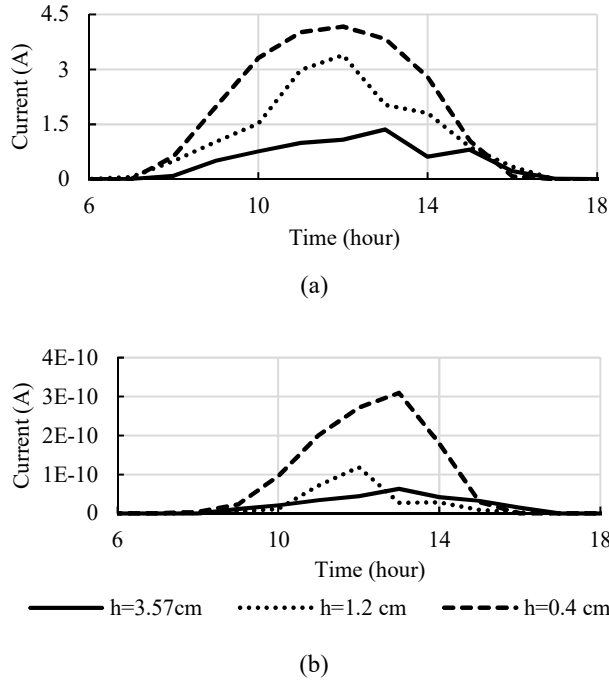


Figure 4.10 Variation of (a) the photocurrent and (b) the diode saturation current of the CS6P-260P PV module for three different days with different snow depths.

conditions with different temperature and irradiance. Moreover, the presence of snow on PV modules affects the incoming irradiance. The diode saturation current is another important parameter of a PV model and depends on the PV technology.  $I_s$  decreases as the quality of the PV material improves. Moreover, the operating condition, mainly the operating temperature, influences this parameter. Figure 4.10(a) and Figure 4.10(b) show the variation of the photocurrent and the diode saturation current of the CS6P-260P PV module, respectively, for three different days with different snow depths.

### 4.3.2 PV Performance under Nonuniform Snow Accretion

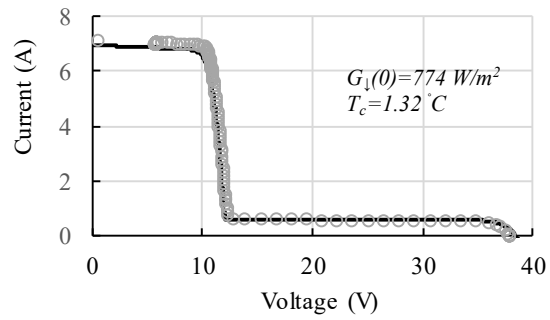
The performance of a PV module is affected by temperature, solar irradiance, shading, and module configuration. The power produced by a PV module is directly proportional to the amount of light that the PV module absorbs. However, when a number of series-connected PV cells in a PV module receive less irradiance, they behave as a load instead of a generator which may cause hot-spot problem. To avoid this, many PV

manufacturers utilize bypass diodes. This section verifies the performance of PV systems under nonuniform snow accretion. A PV array is composed of arrays of PV panels. Each PV panel is formed by a string of PV cells, possibly in conjunction with bypass diodes. Hence, the PV model in section 4.2 can be scaled down/up to a PV cell/array by knowing their arrangement.

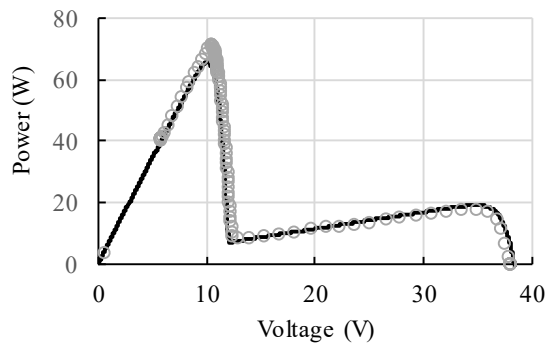
#### 4.3.2.1 PV Electrical Characteristics

When the PV modules are uniformly covered by snow, the resulting  $P-V$  characteristic exhibits a single MPP, as shown in Figure 4.4. Nonuniform snow accretion on PV panels often occurs due to ambient conditions such as wind, temperature variation, partial snow shedding, and ground interference. This leads to a power loss which is dependent on the configuration of the PV system.

Extensive outdoor experiments have been conducted in cold months during which many natural nonuniform snow patterns were observed. Moreover, artificial nonuniform patterns were created by partly removing the snow coverage. Figure 4.11 and Figure 4.12 show the simulated and experimental  $I-V$  and  $P-V$  graphs for two nonuniform snow patterns as well as their associated photos. The PV characteristic becomes more complex, characterized by multiple peaks, due to the bypass diodes under nonuniform snow coverage. In the case of Figure 4.11, almost two third of the PV module is covered with a snow depth of 6.82 cm. Consequently, two peaks are created at 17.6 W and 71.4 W. In the case of Figure 4.12, two different snow depths of 7.53 cm and 1.7 cm partially cover the PV module. As a result, three peaks are produced at 8W, 59.4 W, and 55.4 W. Pattern of the snow coverage and the snow depths influence the resulting PV characteristics exhibiting local MPP/MPPs along with a global MPP. It is obvious from these figures that the difference between the local MPP/MPPs and the global MPP is noticeable which indicates the importance of an appropriate MPPT controller to operate at the true global MPP in these situations. The results show that the proposed model is capable of predicting the electrical behavior of the PV module for different ambient conditions and snow depths.



(a)



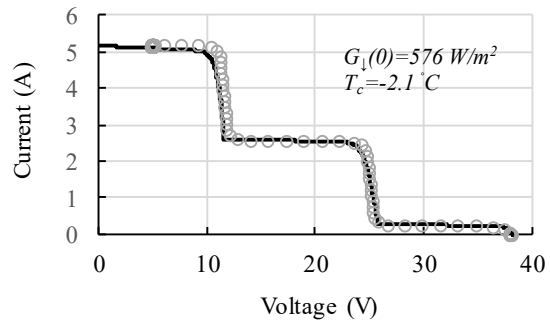
○ Experimental — Proposed Model

(b)

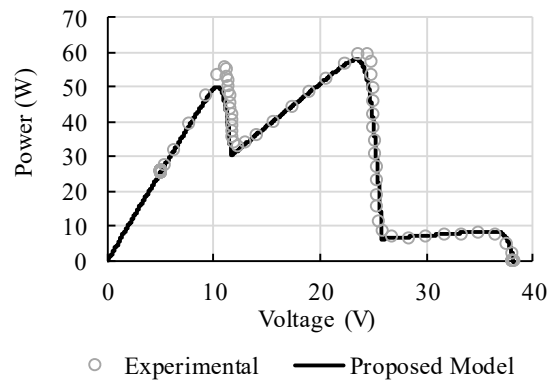


(c)

Figure 4.11 Simulated and experimental (a)  $I$ - $V$  graph and (b)  $P$ - $V$  graph, along with (c) field photo, under nonuniform snow accretion on the CS6P-260P PV panel (two peaks).



(a)



(b)



(c)

Figure 4.12 Simulated and experimental (a)  $I$ - $V$  graph and (b)  $P$ - $V$  graph, along with (c) field photo, under nonuniform snow accretion on the CS6P-260P PV panel (three peaks).

### 4.3.2.2 Effect of Bypass Diodes

This section verifies the effect of bypass diodes on snow loss of a PV string. The PV string consists of four series-connected CS6P-260P PV panels, as shown in Figure 4.13. Two simulation models of the PV string are developed with and without the bypass diodes. Snow accumulation with three different depths of 1 cm, 4 cm, and 7.5 cm is considered. The simulation studies are carried out when each snow depth covers different areas of the PV string. Actually, it is assumed that the snow-covered area expands from the bottom cells of the leftmost PV panel and continues to cover more cells in each simulation run.

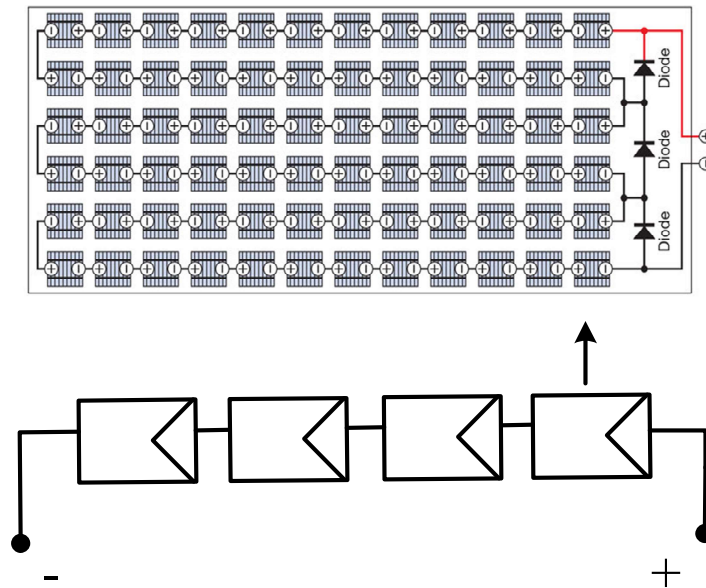
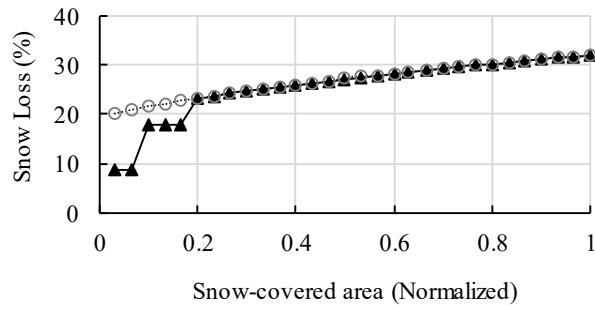
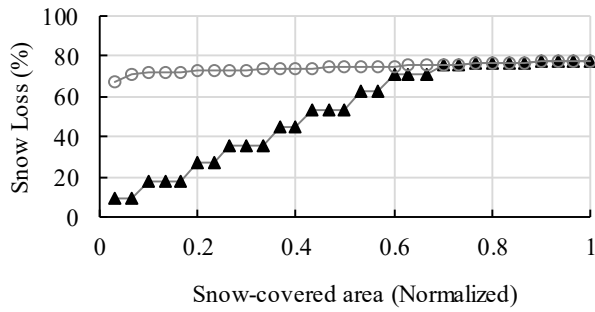


Figure 4.13 A PV string of four series-connected panels.

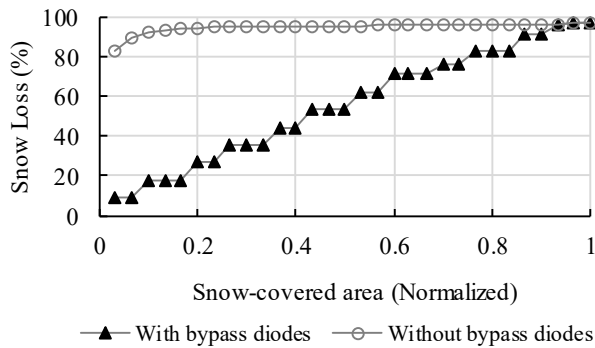
Figure 4.14 shows the power loss due to nonuniform snow accretion versus snow-covered area with and without bypass diodes. The snow-covered area is normalized with respect to the total area of the PV string. The percentage of power loss was determined by comparing the global MPP of the snow-covered PV string against its expected MPP without snow cover in the same irradiance and temperature condition. The amount of power loss of a PV string without bypass diodes significantly increases as the snow depth



(a)



(b)

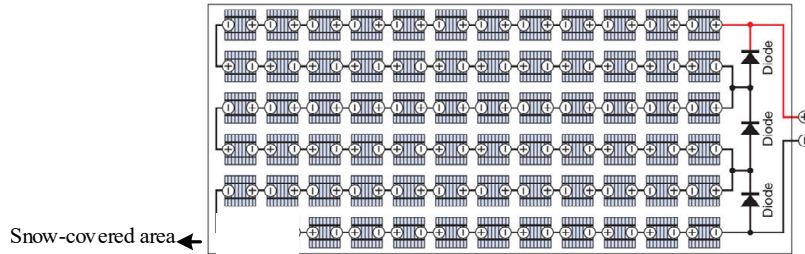


(c)

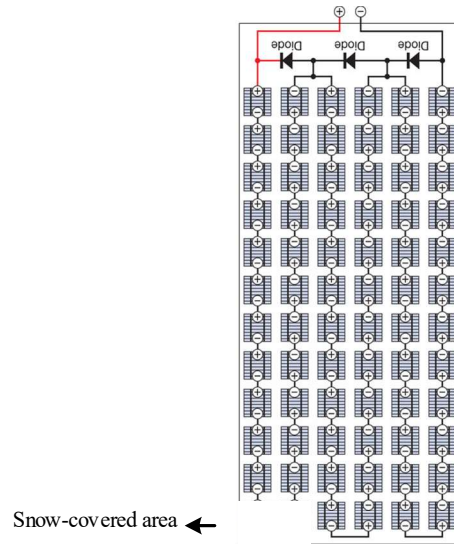
Figure 4.14 Power loss of a PV string due to different snow depths of (a) 1 cm, (b) 4 cm, and (c) 7.5 cm

increases. It can be seen that even a small area of snow accretion on the PV string without bypass diodes noticeably restricts its power generation. The PV string with bypass diodes generally experiences less power loss. The difference is more obvious for bigger snow depths and smaller snow-covered areas. In fact, the negative effects of nonuniform snow

accretion could be greatly mitigated by utilizing the bypass diodes if the MPPT controller is capable of tracking the global MPP.



(a)



(b)

Figure 4.15 Snow-covered area change on PV panel in (a) landscape position, and (b) portrait position.

### 4.3.2.3 Effect of PV Panels Layout

PV panels layout could affect the power loss due to snow. This is investigated by comparing the power loss of the PV panel when installed in landscape and portrait position, as shown in Figure 4.15. The white rectangle on the PV panel demonstrates the snow-covered area variation. Figure 4.16 shows the simulation result of snow loss when a snow depth of 2 cm covers different areas of the PV panel starting from the bottom

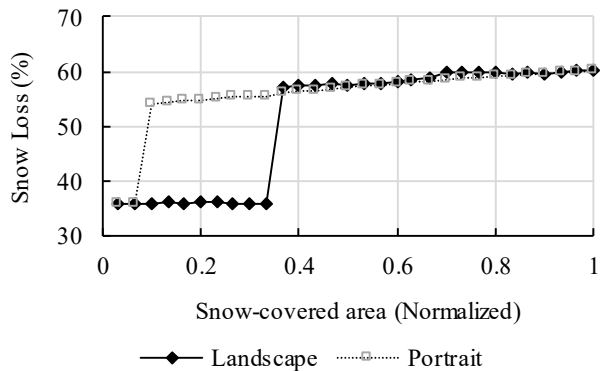
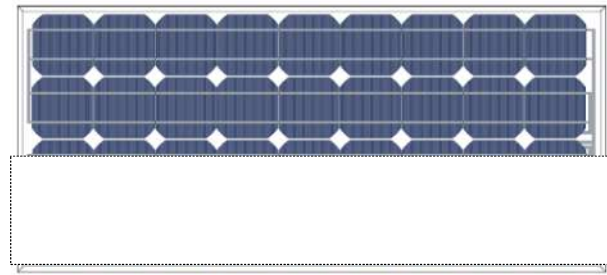


Figure 4.16 Power loss due to different snow-covered areas of a depth of 2 cm for landscape and portrait positioning.

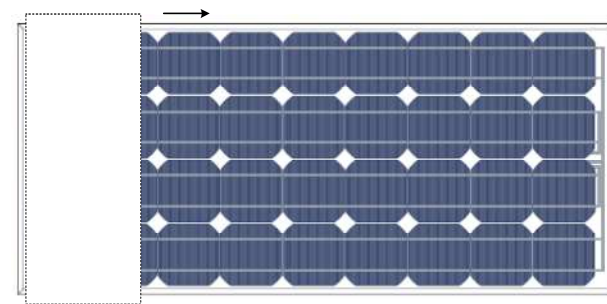
cells. Generally, the PV panel with landscape position experiences less power loss, especially for smaller snow-covered areas. This difference would be greater for higher snow depths.

The power loss due to snow is also verified experimentally when the snow-covered area on PV panels change horizontally and vertically, as shown in Figure 4.18. The white rectangle on the PV panel demonstrates the snow-covered area variation. These tests were performed outdoor for the ET-M53695 monocrystalline PV module (with 36 series-connected PV cells and three bypass diodes) and FS-275 thin film PV module (with 116 series-connected PV cells and no bypass diode). Figure 4.17 shows the experimental results of snow loss for different horizontal/vertical snow coverage variations. As snow coverage reduces vertically, the reduction in snow loss is small. On the other hand, for horizontal snow coverage variation, the reduction in snow loss when snow-covered area reduces is significant. This analysis along with knowledge of snow-melting patterns would be helpful for proper installation of PV panels in cold climates to minimize power loss due to snow.

The PV panels in an array can be electrically connected together in either a series, a parallel, or a mixture of the two, to yield the desired voltage and current level. The output power of a PV array not only depends on ambient condition, but also depends on

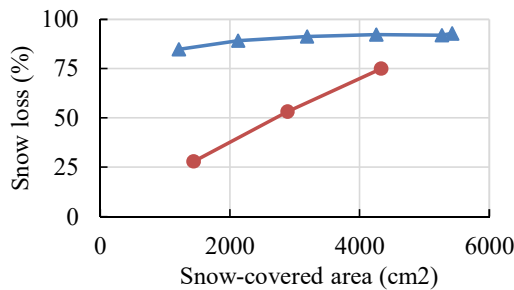


(a)

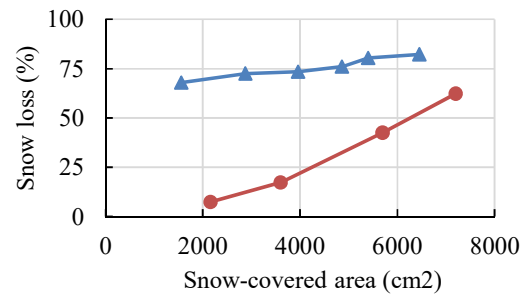


(b)

Figure 4.18 Snow-covered area change on PV panel, (a) horizontal change, (b) vertical change.



(a)



(b)

Figure 4.17 Experimental snow loss due to different snow-covered areas for (a) ET-M53695 PV module and (b) FS-275 PV module.

other factors such as the interconnection of the individual PV panels. In cold climate regions, there are many sunny days where snow still exists on PV modules after a snowfall. A snow layer may melt or partially shed which causes accumulation of snow at the bottom or top of PV modules. Hence, the physical layout of PV modules mounting

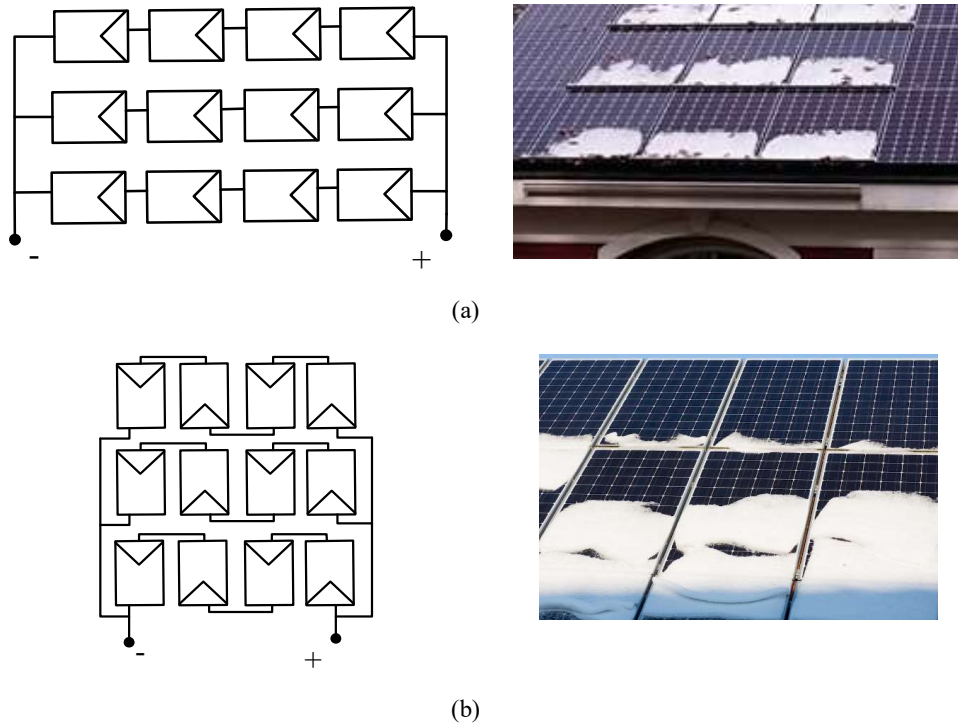


Figure 4.19 A PV array configuration with (a) horizontal layout, and (b) vertical layout.

Table 4.2 Power loss for two PV array layouts

| Layout                 | Horizontal | Vertical |
|------------------------|------------|----------|
| Average power loss (%) | 34%        | 48%      |

could also affect the PV power production. To study this effect, two PV arrays with horizontal and vertical layout, as shown in Figure 4.19, were simulated. Both PV arrays have the same series-parallel structure and include 12 identical PV modules. Simulations were conducted for a variety of snow depths starting from 1cm to 10 cm and different snow patterns on the PV panels. In fact, for each snow depth, different possible nonuniform patterns with different areas were examined. Table 4.2 shows the average snow loss for the two layouts based on 500 different nonuniform snow patterns. The vertical PV array layout faces greater power loss due to nonuniform snow accretion. Hence, the horizontal PV array layout would be more effective in snowy climates.

## 4.4 Conclusion

The primary objective of this chapter was to address the necessity of an accurate model of PV modules applicable for snowy climates. This research may be regarded as a basis for the development of PV models and a practical tool for the design and selection of PV modules subjected to snowfall. Outdoor measurements of PV panels during cold months were used to evaluate the PV model. The proposed model is capable of interfacing with power electronics converters and MPPT control techniques, allowing the simulation of whole PV systems and their interaction with other systems. The model successfully predicts the electrical characteristics of the PV modules covered with uniform/nonuniform snow for a large range of conditions. It also enables development of predictive models for power generation of PV systems in snowy climates using meteorological information. Different simulations for verifying the effect of bypass diodes and different layouts have been carried out. The snow-covered PV panels can still produce a significant amount of energy depending on the pattern and depth of the snow accumulation. The portion of this energy that could be collected is decided by configuration of the PV array as well as the MPPT technique. Hence, a proper design of a PV system considering the effect of snow accretion is essential to benefit from the solar energy potential in cold regions. As PV systems are expected to make a significant contribution to supply worldwide electricity in a more secure and economic way, it is essential to carry on verifying the effect of snowfall on their performance. This research could be a helpful reference for future studies in the applications of PV systems in cold weather regions.



## CHAPTER 5

---

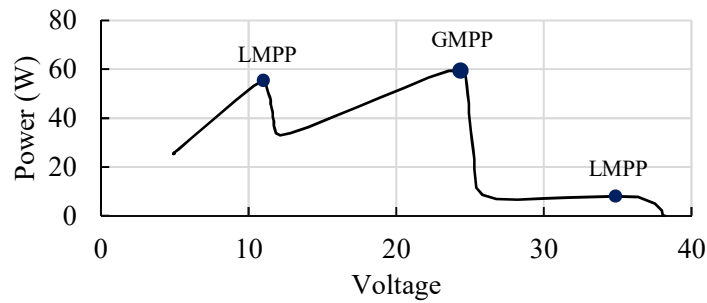
# A HIGH PERFORMANCE SHADE-TOLERANT MPPT BASED ON CURRENT-MODE CONTROL

### 5.1 Introduction

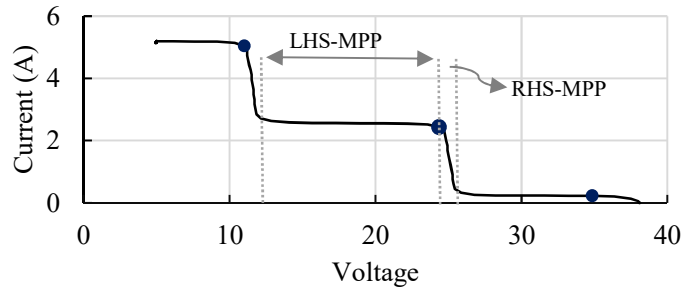
This chapter proposes a high performance shade-tolerant MPPT (STMPPT) technique for DC-DC converter stage of PV applications [R3]. The average current-mode control (ACMC) is utilized to regulate the PV array current using two feedback control loops. The current-mode control is a superior scheme in control of DC-DC power electronic converters. The proposed STMPPT technique operates in two modes. The ACMC with the P&O MPPT algorithm functions in a local MPPT (LMPPT) mode under normal irradiance condition. When the PV array is likely to be partially shaded, a global MPPT (GMPPT) subroutine effectively scans the PV profile to optimize the PV system operation. This is achieved by implementing simple innovations to the ACMC-based P&O algorithm. The innovations benefit from useful observations of  $I-V$  characteristics. The idea behind using the  $I-V$  characteristics is to significantly reduce the search space, make the algorithm independent of shading conditions and PV array configuration, and inherently recognize the occurrence of partial shading conditions. The proposed STMPPT technique enables very fast and reliable tracking of global maximum power point (GMPP). In addition, it can stably work under dynamic environmental change without losing correct sense of tracking direction. Its simplicity and independency would offer a viable solution for PV converter products. Simulation and experimental performance assessments are presented under different operating conditions that could happen in outdoor PV installations.

## 5.2 Worthwhile $I$ - $V$ Characteristics of Shaded PV Arrays

The PV characteristic exhibits a singular power peak when a PV array is homogeneously irradiated. A traditional dynamic MPPT could track the singular power peak and attain a suitable PV harvest performance. Partial shading often occurs due to shadows created by passing clouds, presence of snow, trees, and nearby objects. The shaded cells could become reverse biased, behaving as a load, and dissipating power from the irradiated cells [131]. The PV manufacturers and installers normally use bypass diodes to prevent hot-spot problem and to stop unproductive cells from disrupting the production of active cells. The resultant PV characteristics of the shaded PV array introduce new challenges for the control of power electronic interface to optimize energy harvesting.



(a)



(b)

Figure 5.1 Experimental PV characteristics under partial shading condition. (a)  $P$ - $V$  graph. (b)  $I$ - $V$  graph.

Figure 5.1(a) and Figure 5.1(b) show the  $P-V$  graph and  $I-V$  graph of the CS6P-260P PV module under partial shading, when nonuniformly covered with snow. The  $P-V$  graph exhibits three power peaks as a result of two different snow depths on the PV module. In practice, the PV modules are assembled in parallel-series configuration to form a PV array in order to provide the expected power. This configuration is not fixed for a certain level of power, and the PV developers design the PV array for specific objectives. The number of power peaks appearing in the  $P-V$  graph depends on the configuration of the partially shaded PV array and the shading pattern. Moreover, location and magnitude of the power peaks are greatly variable due to the infinite variety of possible partial shading conditions.

On the other hand, the  $I-V$  graph of a partially shaded PV array represents a simpler characteristic. Some simple observations, which are true for any PV array configuration under different partial shading conditions, are presented as follow:

1. The  $I-V$  graph features several steps. Starting from the right-most step towards left, the current level at each step is greater than the previous step current level. Hence, the current magnitude at local MPP (LMPP) would actually present an increasing trend when moving from the right-most step towards the left-most step no matter the partial shading pattern or PV array configuration, as can be seen in Figure 5.1(b).
2. In each step, the operation of PV array could be categorized into two stages: (1) left-hand side of MPP (LHS-MPP) and (2) right-hand side of MPP (RHS-MPP). In the LHS-MPP, the PV characteristic experiences very small variation of current level. Hence, if the PV system works on the MPP of a step, a small perturbation in current level would force the operating point to the RHS-MPP of next step.
3. In the RHS-MPP, the voltage range is small. Thus, if the operating point happens to be in this range, the MPP of this step could be reached quickly with a small decrease in PV array voltage.

These observations could be easily realized from any  $I-V$  graph of partially shaded PV arrays. They are not dependent on the PV module arrangement within the PV array, datasheet information of PV module manufacturer, shading pattern, or ambient condition.

### 5.3 Proposed ACMC-Based STMPPT

A high performance STMPPT control is presented in this section targeting very fast and reliable tracking of true maximum power of PV systems under partial shading condition. Figure 5.2 illustrates the control structure operating on a DC-DC boost converter. The main reason for using this control structure is that the current-mode control is the industry standard technique for controlling the switching power supplies [132]. The ACMC contains two feedback loops, a voltage-control loop and a current-control loop. The signals that are sensed and fed back to the controller unit include the PV array output voltage  $V_{pv}$  and the boost stage inductor current  $I_L$ . Since the average inductor current of the boost converter represents the PV array current, it is used to implement the STMPPT control. The outer voltage-control loop regulates the PV array voltage at the level determined by the MPPT algorithm. This is achieved by modulating the reference current of the inner current-control loop which enables fast tracking of the reference current.

PV converters operate within a given MPPT voltage window which is normally available from the manufacturer specification:

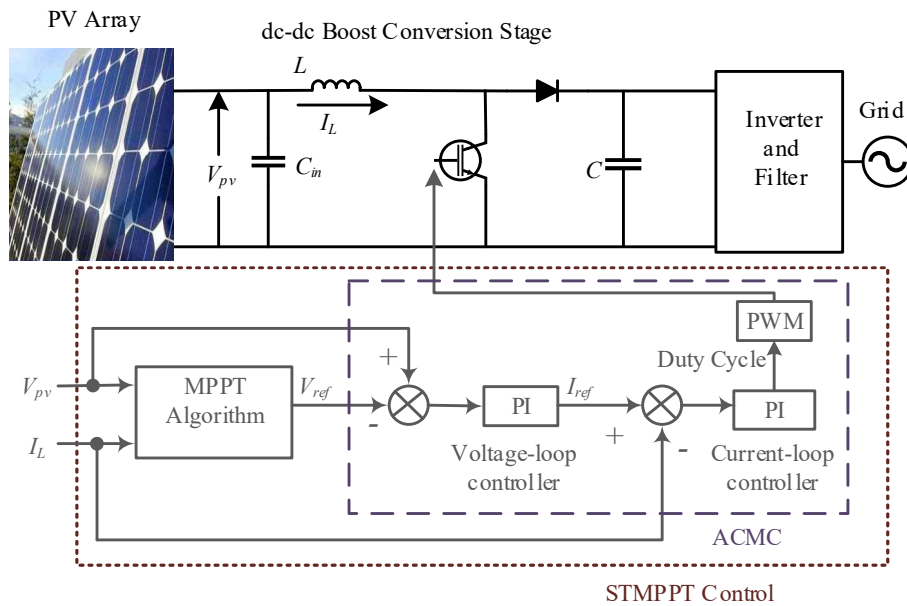


Figure 5.2 Configuration of the ACMC-based STMPPT with the front-end boost converter.

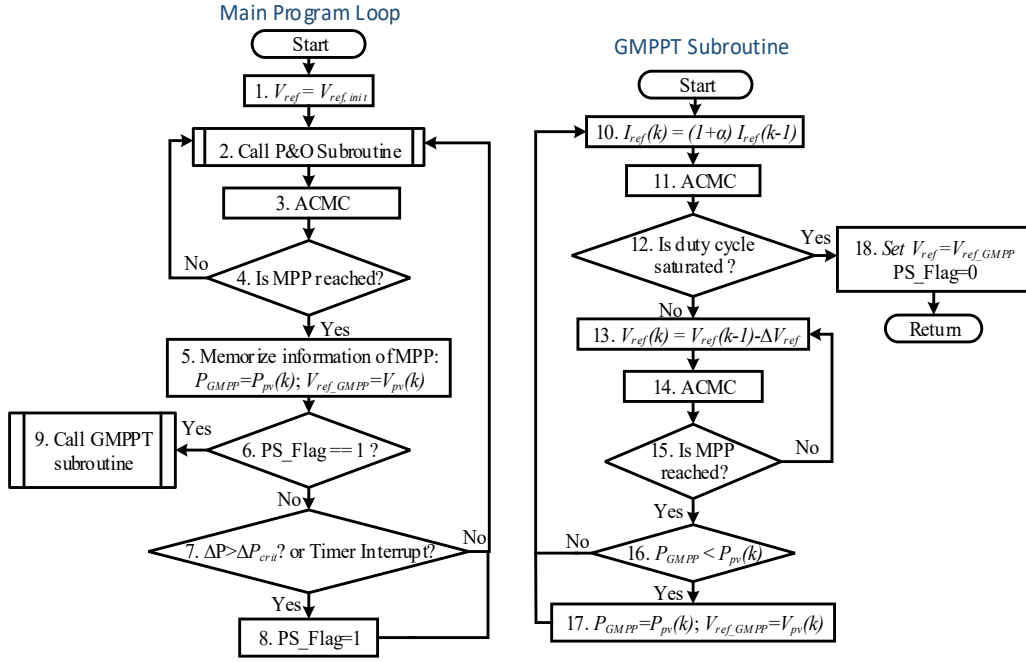


Figure 5.3 Flowchart of the proposed STMPPT technique.

$$V_{MPPT,min} \leq V_{MPPT,range} \leq V_{MPPT,max} \quad (5.1)$$

PV array designers need to ensure that the coldest temperature MPP voltage does not exceed the upper limit  $V_{MPPT,max}$ . Flowchart of the proposed STMPPT technique is shown in Figure 5.3. The main program loop starts with an initial reference voltage (Block 1). This voltage could be selected as

$$V_{ref,init} = 0.85 * V_{MPPT,max} \quad (5.2)$$

The proposed STMPPT operates in two modes: LMPPT mode and GMPPT mode.

### 5.3.1 LMPPT Mode

At uniform irradiance condition, the P&O MPPT algorithm and ACMC keep operating at the MPP (Block 2, Block 3, and Block 4). The P&O algorithm verifies change of power and voltage of PV array and determines the set-point voltage  $V_{ref}$  regularly. To maximize the output power from the PV array, its output voltage needs to be maintained at the level determined by the P&O algorithm. The DC-DC boost converter extracts a DC current from the PV array so that the PV array works at its maximum power transfer point. This is achieved through the two feedback control loops, as shown in Figure 5.2. The sensed PV array voltage  $V_{pv}$  is compared against the reference voltage set by the P&O algorithm. The consequent voltage error signal is then passed into the voltage-loop controller which regulates the PV array voltage at the reference level. The output of this controller provides the reference current signal  $I_{ref}$  for the inner current-control loop. This reference current is compared with the sensed inductor current  $I_L$ . The consequent current error signal is fed into the current-loop controller producing the duty-cycle signal to be used by the pulse width modulation (PWM) for the boost converter switch.

In fact, the PV array voltage is regulated by controlling the inductor current. The average value of the inductor current of the boost converter is the PV array current. Hence, the current-loop controller basically controls the PV array current by controlling the average value of the inductor current. In the control structure, as the PV array voltage exceeds the reference voltage provided by the P&O algorithm, the voltage-control loop increases the reference current for the inner current-control loop to regulate the PV array voltage at its reference level. On the other hand, as the PV array voltage becomes lower than the reference voltage, the control loop decreases the reference current.

### 5.3.2 GMPPT Mode

As discussed in section 5.2, the  $I-V$  characteristics under partial shading condition show interesting features through which a simpler GMPPT could be realized. Simple innovations are introduced to the P&O MPPT system based on ACMC to fulfill the proposed STMPPT.

A timer could be utilized to produce an interrupt to ensure periodic checking of partial shading condition. Otherwise, a sudden variation in PV array power could imply

a possible partial shading condition. Hence, a flag is set to 1 (Block 8) using a timer interrupt on a timely basis or when a sudden change in operating condition is detected (Block 7). Consequently, the LMPPT mode finds the right-most peak first. The relevant information of this peak is saved (Block 5).  $P_{GMPP}$  and  $V_{ref\_GMPP}$  always hold power and voltage information of the highest available power peak. Then, the GMPPT subroutine is called (Block 9) and simple steps are followed to intelligently find the GMPP.

**Step 1:** A perturbation is implemented in the current reference as (Block 10)

$$I_{ref}(k) = (1 + \alpha) I_{ref}(k - 1) \quad (5.3)$$

This perturbation would force the operating point to RHS-MPP of the next step, as per the first and second observations of  $I$ - $V$  graph in section 5.2.

**Step 2:** The reference voltage is decreased (Block 13) until the MPP of the next step is reached (Block 15):

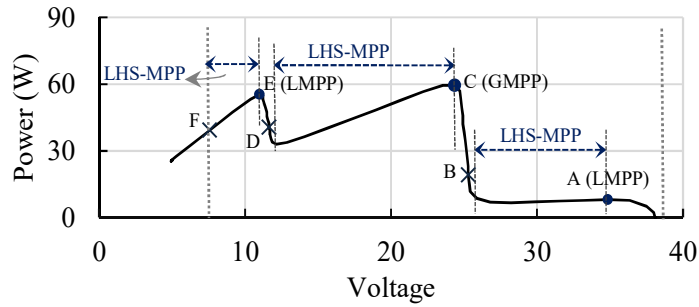
$$V_{ref}(k) = V_{ref}(k - 1) - \Delta V_{ref} \quad (5.4)$$

This stage would be quick since the voltage range of RHS-MPP is small, as per the third observation in section 5.2.

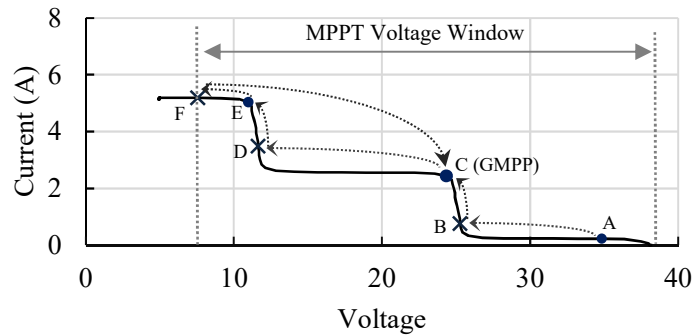
**Step 3:** When the operating point gets to the MPP of the present step, a comparison is made (Block 16). If the power of the new peak is greater than the previous highest peak power,  $P_{GMPP}$  and  $V_{ref\_GMPP}$  are updated (Block 17). Otherwise, they keep the information of the previous highest peak.

**Step 4:** The algorithm goes to Block 10, and the steps 1-3 are repeated until the perturbation of reference current causes saturation of the duty-cycle of the current-control loop (Block 12). This actually happens when the algorithm reaches the MPP of the left-most step. At this time, the operating point is transferred to the GMPP which is the peak with the highest power, and the partial shading flag is cleared (Block 18). The algorithm then returns to the main routine, and the P&O subroutine operates at the GMPP.

The procedure of GMPPT mode is demonstrated with an example in Figure 5.4. When the partial shading flag is set to 1 ( $PS\_Flag=1$ ), the LMPPT mode tracks the right-



(a)



(b)

Figure 5.4 Tracking principle of the proposed STMPPT for a shaded PV characteristic

most peak at point A. Upon calling the GMPPT subroutine, a perturbation is applied to the present reference current. The operating point moves to RHS-MPP of the next step, point B. A descending reference voltage will find the MPP of this step, at point C. Since the power of this MPP is greater than the previous peak power, the information of GMPP is replaced with the new MPP. Another perturbation in the reference current is implemented and the controller forces the operating point to RHS-MPP of the third step, at point D. The MPP of this step is found, at point E, by reducing the reference voltage. Since the power of this peak is less than the power of point C, the information of GMPP remains unchanged. A perturbation to the reference current of point C leads to a quick saturation of the duty-cycle. When this is recognized by the algorithm, the operating point is transferred to point C which is the peak with the highest power, and the flag is cleared ( $PS\_Flag=0$ ). Hereafter, the LMPPT mode will operate at the GMPP.

The current at MPP of a PV array  $I_{MPP}$  is linearly proportional to its short-circuit current  $I_{sc}$  under uniform irradiance condition [133]

$$I_{MPP} \approx \beta_{sc} I_{sc} \quad (5.5)$$

where the value of  $\beta_{sc}$  resides between 0.78 and 0.92. Hence, by choosing  $\alpha = 0.3$  in (5.3), the ACMC would force the operating point to RHS-MPP of the next step in case of partial shading condition. In Step 2, the consecutive reduction in reference voltage is implemented with a faster frequency, as the frequency of voltage-control loop, to speed up the GMPPT mode.

Thanks to the ACMC, both reference current and reference voltage are available within the program. The basic idea of the GMPPT mode is to implement a reference current perturbation when the MPP of each step is found. This prevents blind search of the whole set of PV characteristics. As can be seen from Figure 5.4, the LHS-MPP of different steps form the large majority of the PV profile voltage range. At a given step, when the MPP is reached from RHS-MPP, the remaining operating points in LHS-MPP would experience lower power than the MPP. The proposed STMPPT would not intelligently search the LHS-MPP of the PV characteristics using the perturbation in reference current. Moreover, the MPP search from RHS-MPP is executed quickly because of short voltage range. Hence, the proposed STMPPT could reliably track the GMPP at a great speed.

### 5.3.3 Dynamic Changing Environment

The PV systems are normally operated outdoors where the ambient condition changes overtime. Irradiance intensity increases/decreases, for instance when it is partly clouded resulting in oscillations of PV power. Duration of these oscillations is highly unpredictable. On the other hand, the GMPPT techniques are mostly dependent on power information at different stages, and their convergence speed differs depending on the specific method and PV system condition. If variation of irradiance intensity happens during the search process, the GMPPT algorithms could become confused and converge to a wrong position instead of GMPP [134]. This could also lead to frequent restarting of

the algorithms, considerable oscillations, and loss of energy as atmospheric conditions may change significantly in real outdoor environment.

A simple solution is presented in this paper to overcome the issue. The algorithm in Figure 5.3 shows that when a sudden variation in PV power occurs (Block 7), the GMPPT subroutine is not called immediately. The LMPPT mode first finds the right-most MPP. The condition in Block 4 plays an important role in detecting the power variation due to a changing environment. The following tests are verified first in Block 4:

$$\Delta P_{pv}(k) < 0 \text{ and } \Delta P_{pv}(k-1) < 0$$

$$\text{Sign}(\Delta V_{ref}(k)) \neq \text{Sign}(\Delta V_{pv}(k)) \text{ OR } \text{Sign}(\Delta V_{ref}(k)) = \text{Sign}(\Delta I_L(k)) \quad (5.6)$$

The first condition implies that the PV power reduction for two consecutive samples is a result of a changing environment. This could be realized from the  $P$ - $V$  graph as the MPPT algorithm would not decrease the PV array power for two consecutive samples [116]. The second condition in (6) indicates that if there is no changing environment, the sign of reference voltage perturbation must be the same as the sign of the PV array voltage variation and negative to the sign of the PV array current variation. Otherwise, the variation of the PV array condition is dictated by a changing environment. A flag is set to 1 ( $En\_Flag=1$ ) when any condition in (5.6) is satisfied, demonstrating a changing environment. Otherwise, this flag is set to 0 when a stable environment is realized. The following conditions are tested in Block 4 to ensure reaching the MPP:

$$\text{Sign}(\Delta P_{pv}(k)) \neq \text{Sign}(\Delta P_{pv}(k-1)) \text{ and } En\_Flag(k) = 0 \text{ and } En\_Flag(k-1) = 0 \quad (5.7)$$

The sign of the power variation and the changing environment flag in two subsequent samples are used to identify whether the peak is reached. Hence, when a sudden change in the PV array power is detected, the proposed STMPPT operates in the LMPPT mode until a steady environment is realized. Then, the GMPPT subroutine is called. This is an essential feature that could restrict frequent restarting of the GMPPT program without environmental sensors. Moreover, it enhances the proper sense of tracking during LMPPT mode in the presence of a dynamic changing environment.

### 5.3.4 Inherent Partial Shading Recognition

The GMPPT methods are mostly launched by a sudden variation in PV power. Then, the method searches the  $P$ - $V$  profile to track the GMPP. This could cause considerable oscillations and loss of energy when the PV power variation is a result of uniform irradiance change. The situation becomes more serious when the uniform irradiance changes dynamically for a longer period.

The method in [109] uses measurements of all PV module voltages to detect a partial shading condition. Thus, it requires large number of sensors. In [111], an index along with two other conditions were introduced to detect the occurrence of partial shading condition. However, the proposed method needs the parameters of the PV module and information of the configuration of the PV array. Moreover, extra temperature and voltage sensors are required to measure the temperature and voltage of one PV module. In [105], the load line and the trend of variation of the PV string MPP voltage and current are used to realize the partial shading condition with verifying too many conditions. A critical slope is introduced which is dependent on the PV string specifications. Moreover, the method sets a minimum irradiance of  $100 \text{ W/m}^2$ , even if shading of lower irradiance is common in real field conditions. In fact, the proposed methods could not detect the partial shading condition independently with a simple strategy. Furthermore, these methods would suffer from frequent restarting when the partial shading condition is accompanied by a dynamic irradiance variation. This, for instance, could happen when a PV array is nonuniformly covered with snow and the irradiance level changes overtime.

The proposed STMPPT is able to inherently recognize the incident of partial shading condition. This is another useful feature achieved independently without extra measurements or setting parameters and conditions. A perturbation in reference current is implemented when the GMPPT subroutine is called. If the PV array is partially shaded, this perturbation moves the operating point to the next step. Hence, the duty-cycle is not saturated and the program recognizes inherently that there is a partial shading condition. In this case, the program continues to find the GMPP.

Otherwise, if there is a change in uniform irradiance condition, the duty-cycle is saturated immediately after the first perturbation in the reference current, and the

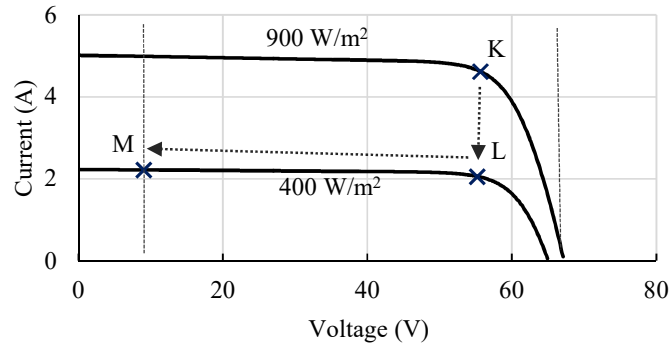


Figure 5.5 Tracking behavior of the proposed STMPPT for a uniform irradiance change

algorithm returns to LMPPT mode. This is depicted in Figure 5.5 for the  $I$ - $V$  graph of a typical PV array when irradiance level changes from  $900 \text{ W/m}^2$  to  $400 \text{ W/m}^2$ . This change in irradiance level could take a while during which the main program loop stays in the LMPPT mode until a steady condition is realized. The operating point is transferred by the LMPPT mode from point K to the MPP of the new characteristic at point L. The power and voltage of point L are memorized as GMPP. When the GMPPT subroutine implements the perturbation, the operating point moves to point M very quickly. The duty-cycle is saturated and the program sets the reference voltage to the voltage of point L. The algorithm then returns to the LMPPT mode. In fact, the proposed STMPPT inherently realizes the uniform irradiance condition with the first perturbation in the reference current.

#### 5.4 Simulation Verification

In order to verify the effectiveness of the proposed GMPPT, simulation analyses were conducted with Matlab/Simulink. Different partial shading conditions and dynamic variation of irradiance as per the EN50530 standard were examined. Moreover, different PV systems and state-of-the-art GMPPT methods were investigated.

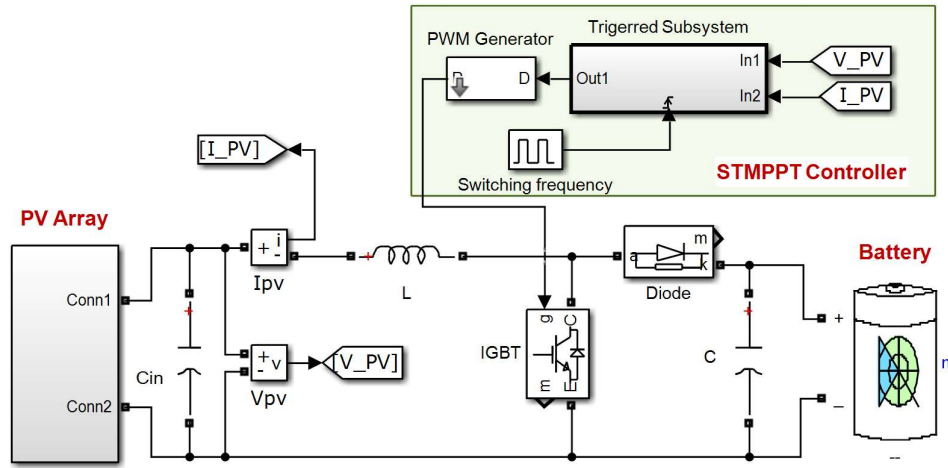


Figure 5.6 Simulation schematic of the PV system.

Table 5.1 Parameters of the PV system

| $C_{in}$   | $C$         | $L$  | Switching frequency | $V_{MPPT,min}$ | $V_{MPPT,max}$ |
|------------|-------------|------|---------------------|----------------|----------------|
| 10 $\mu$ F | 210 $\mu$ F | 2 mH | 20 kHz              | 7 V            | 70 V           |

Simulation study of a PV system similar to the experimental setup, which will be verified in section 5.5, was conducted under different partial shading scenarios. Figure 5.6 illustrates the circuit schematic of the PV system which consists of a DC-DC boost converter, a PV array, a battery pack, and the STMPPT controller. The ratings of the parameters of the PV system are presented in Table 5.1. A typical MPPT voltage window was established by  $V_{MPPT,min}$  and  $V_{MPPT,max}$ . Nevertheless, this voltage range depends on the topology and functionality of the PV converter and is decided by the manufacturer.  $\Delta V_{ref}$  in (5.4) was selected at around 1% of the MPPT voltage window. The PV array was composed of three series-connected ET-M53695 monocrystalline PV modules. Each PV module included 36 series-connected PV cells in conjunction with two bypass diodes. The electrical parameters of the ET-M53695 PV module is listed in Table 5.2. Figure 5.7 shows the physical layout of the PV array which consists of six sub-strings (SS) created by the bypass diodes.

Table 5.2 Electrical parameters of the ET-M53695 PV module at STC

| Peak Power | Maximum Power Voltage | Maximum Power Current | Open Circuit Voltage | Short Circuit Current |
|------------|-----------------------|-----------------------|----------------------|-----------------------|
| 95 W       | 18.52 V               | 5.13 A                | 22.5 V               | 5.57 A                |

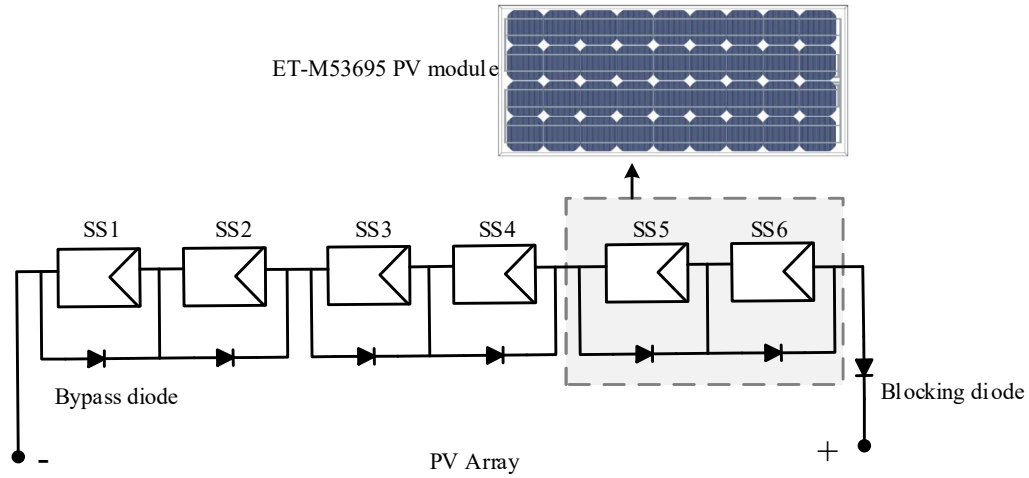


Figure 5.7 Layout of the PV array with three series-connected ET-M53695 PV module

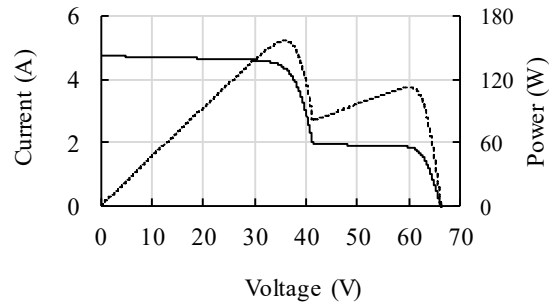
#### 5.4.1 Simulation Results under Different Partial Shading Conditions

In order to verify the performance of the proposed STMPPT, three partial shading cases were examined as presented in Table 5.3. The corresponding  $I-V$  and  $P-V$  graphs

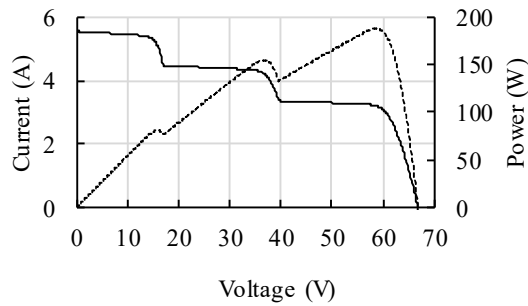
Table 5.3 Different partial shading cases.

|        | SS1 (W/m <sup>2</sup> ) | SS2 (W/m <sup>2</sup> ) | SS3 (W/m <sup>2</sup> ) | SS4 (W/m <sup>2</sup> ) | SS5 (W/m <sup>2</sup> ) | SS6 (W/m <sup>2</sup> ) |
|--------|-------------------------|-------------------------|-------------------------|-------------------------|-------------------------|-------------------------|
| Case 1 | 850                     | 850                     | 850                     | 850                     | 350                     | 350                     |
| Case 2 | 600                     | 600                     | 800                     | 800                     | 1000                    | 1000                    |
| Case 3 | 200                     | 300                     | 650                     | 650                     | 850                     | 850                     |

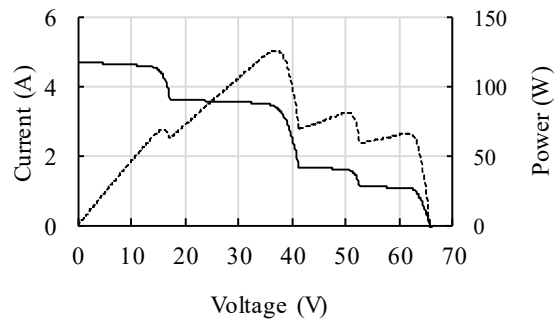
are depicted in Figure 5.8. The results were compared with a PSO GMPPT method presented in [98].



(a)



(b)



(c)

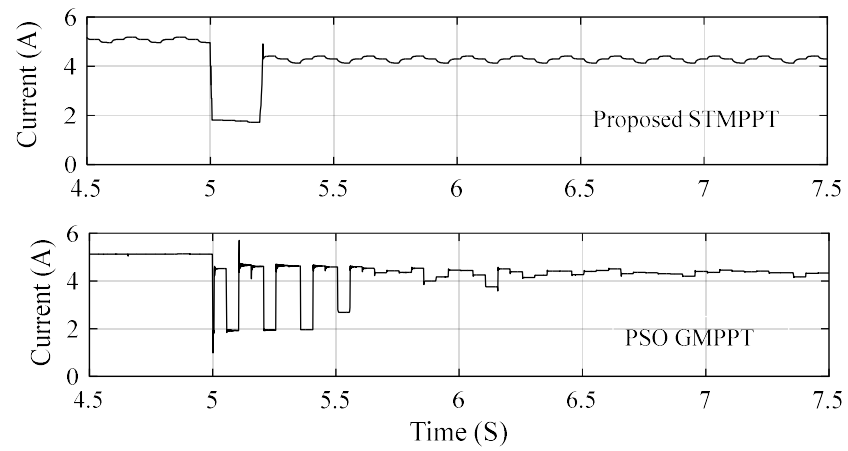
—— I-V graph      - - - - - P-V graph

Figure 5.8  $I$ - $V$  and  $P$ - $V$  graphs of different partial shading cases: (a) Case 1, (b) Case 2, and (c) Case 3.

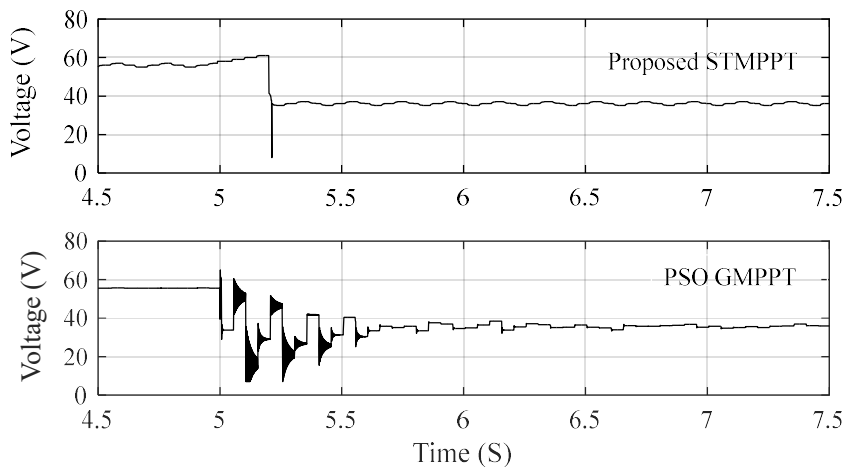
Figure 5.9 shows the simulation results for the proposed technique and the PSO GMPPT when the uniform irradiance condition changes to Case 1 at  $t=5$  s. A flag is set to 1 after recognizing the condition variation. The LMPPT mode will continue to track the right-most peak at point (1.87 A, 60 V, 112 W). Thereafter, the GMPPT subroutine is called. To realize the performance of the proposed method, the expanded results of Case 1 during the GMPPT mode are shown in Figure 5.10. A perturbation in the reference current is implemented. The operating point will jump to the RHS-MPP of the next step. The MPP of this step is then found at point (4.36 A, 35.7 V, 155.9 W). This is done quickly as the voltage range of the RHS-MPP of PV characteristic is short. As the power of this peak is greater than the power of the previous peak, the information of this peak is saved as GMPP. Another perturbation in reference current will follow which results in saturation of the duty-cycle. At this time, the flag is cleared to zero. The algorithm returns the operating point to the GMPP (second peak in this case), and the LMPPT mode will make fine adjustments. As can be seen, the search time for the GMPPT mode is 14 ms in this case.

The simulation results for Case 2 and Case 3 are shown in Figure 5.11 to Figure 5.14. The proposed STMPPT experiences considerably less power oscillations. The proposed algorithm follows the same simple procedure when the power variation is recognized. Using the perturbation in reference current and reference voltage decrease, the GMPPT mode can locate the true peak within 15 ms and 24 ms for Case 2 and Case 3, respectively. These results demonstrate very fast and efficient GMPPT under different partial shading conditions.

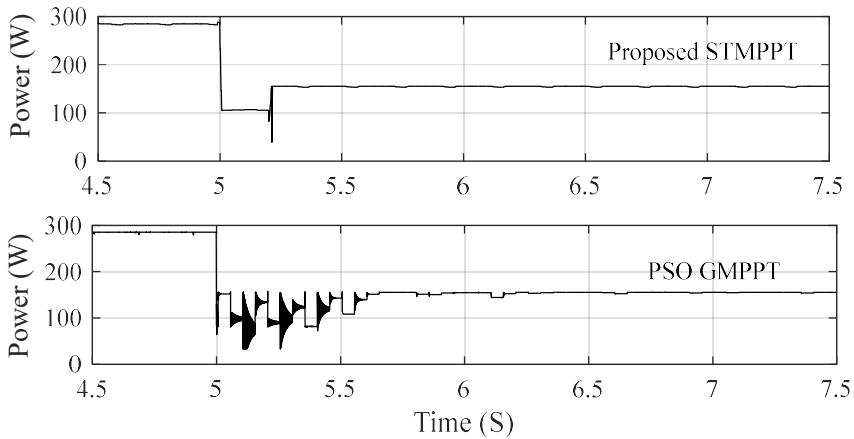
To highlight the capability of the proposed STMPPT technique, further verification was made by comparing it with respect to a more recent study in [113] where a two-stage GMPPT technique was presented. The multi-peak PV characteristic was split into several single-peak curves based on a PV equivalent model. Then, an improved beta algorithm was utilized to locate the GMPP.



(a)



(b)



(c)

Figure 5.9 Simulation results of the proposed STMPPT and the PSO GMPPT for Case 1: (a) current waveforms, (b) voltage waveforms, and (c) power waveforms.

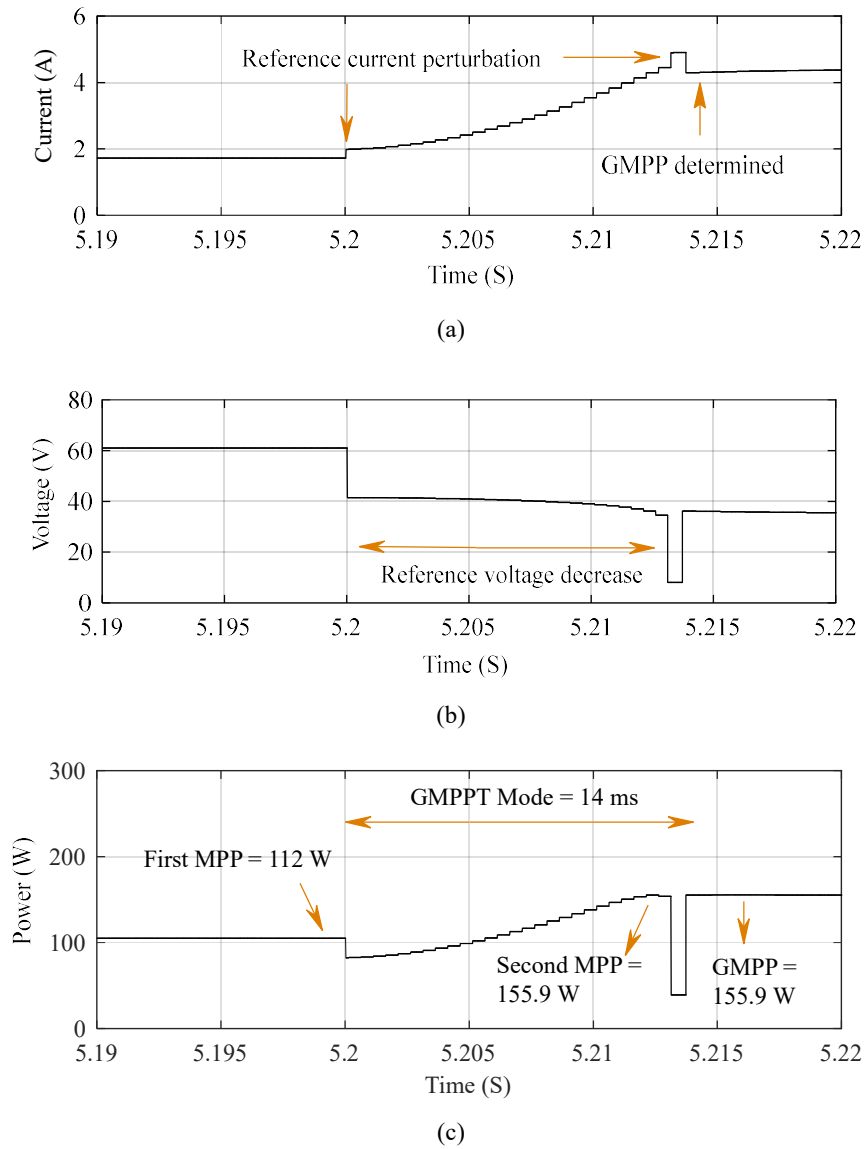
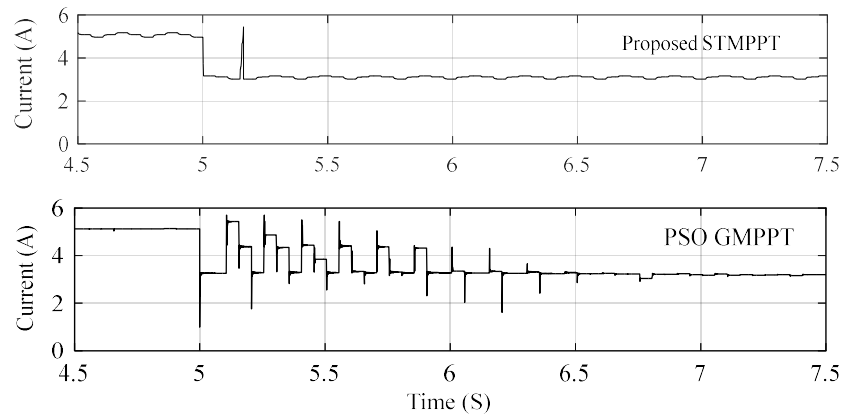
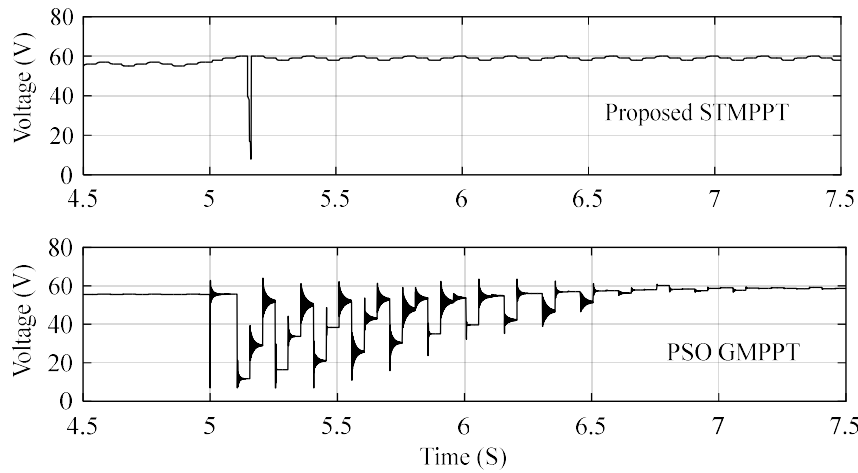


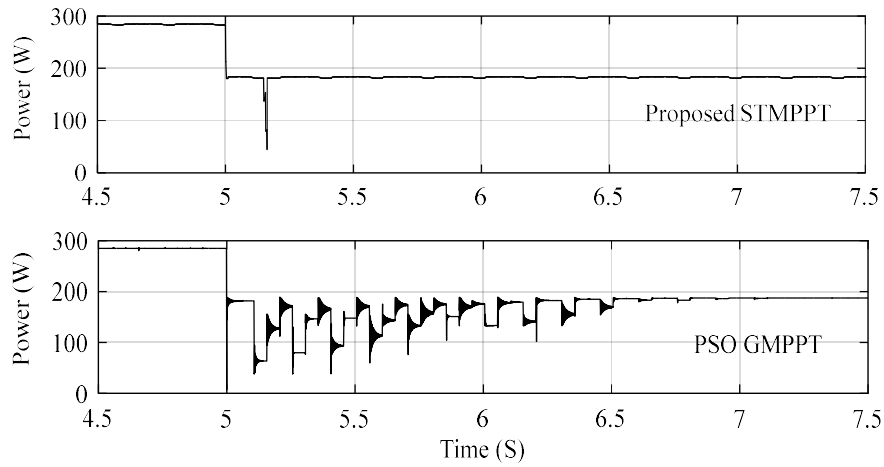
Figure 5.10 Expanded simulation results of the proposed STMPPT showing GMPP mode performance for Case 1: (a) current waveform, (b) voltage waveform, and (c) power waveform.



(a)



(b)



(c)

Figure 5.11 Simulation results of the proposed STMPPT and the PSO GMPPT for Case 2: (a) current waveforms, (b) voltage waveforms, and (c) power waveforms.

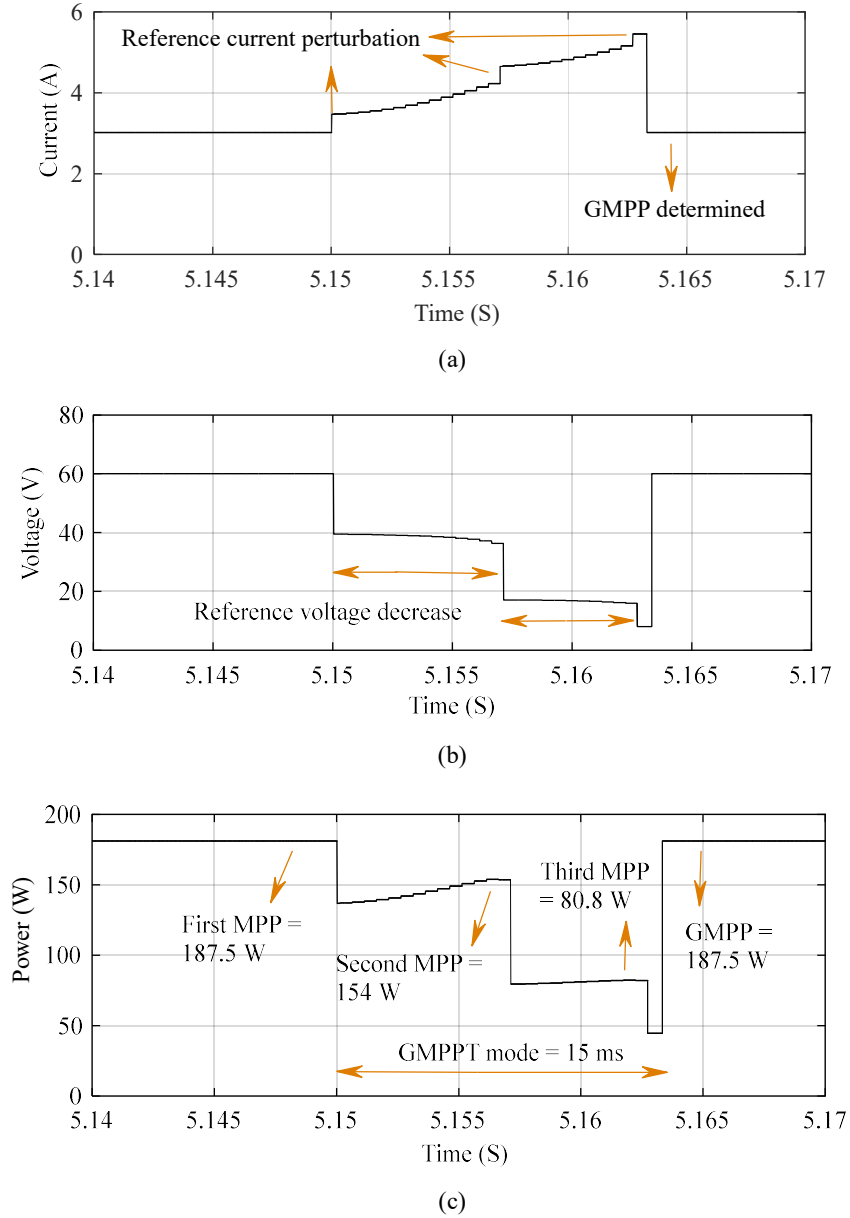
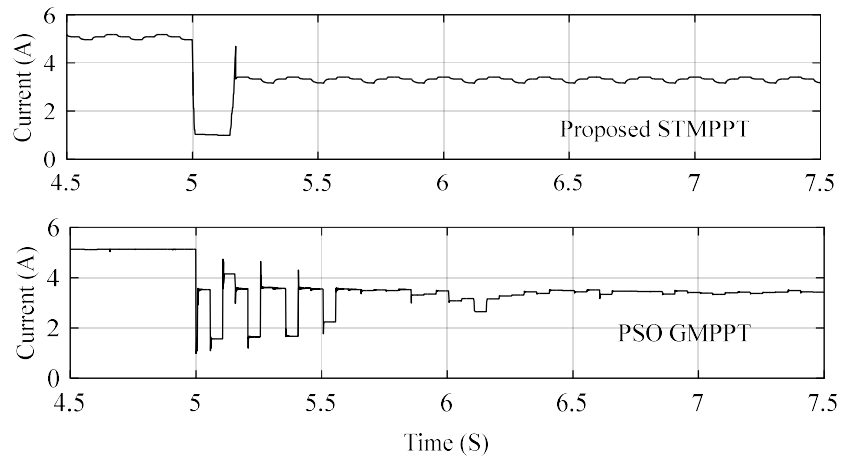
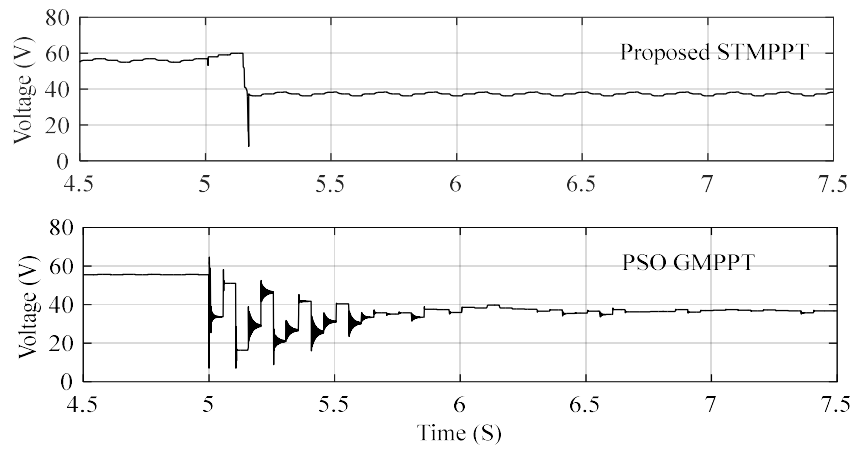


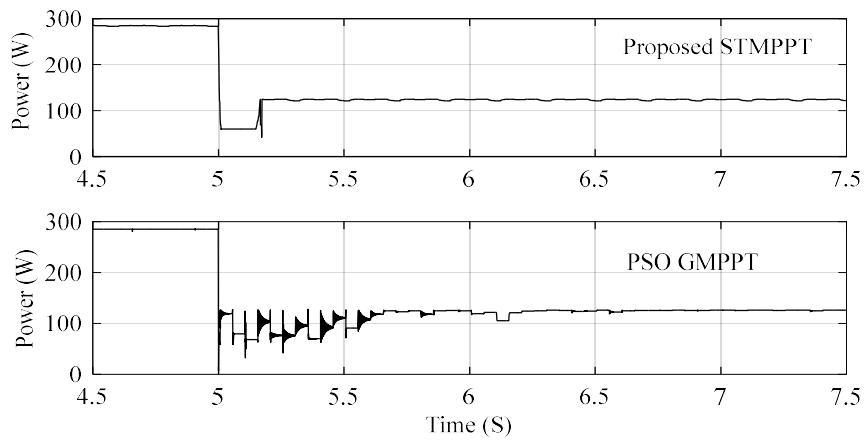
Figure 5.12 Expanded simulation results of the proposed STMPPT showing GMPPT mode performance for Case 2: (a) current waveform, (b) voltage waveform, and (c) power waveform.



(a)



(b)



(c)

Figure 5.13 Simulation results of the proposed STMPPT and the PSO GMPPT for Case 3: (a) current waveforms, (b) voltage waveforms, and (c) power waveforms.

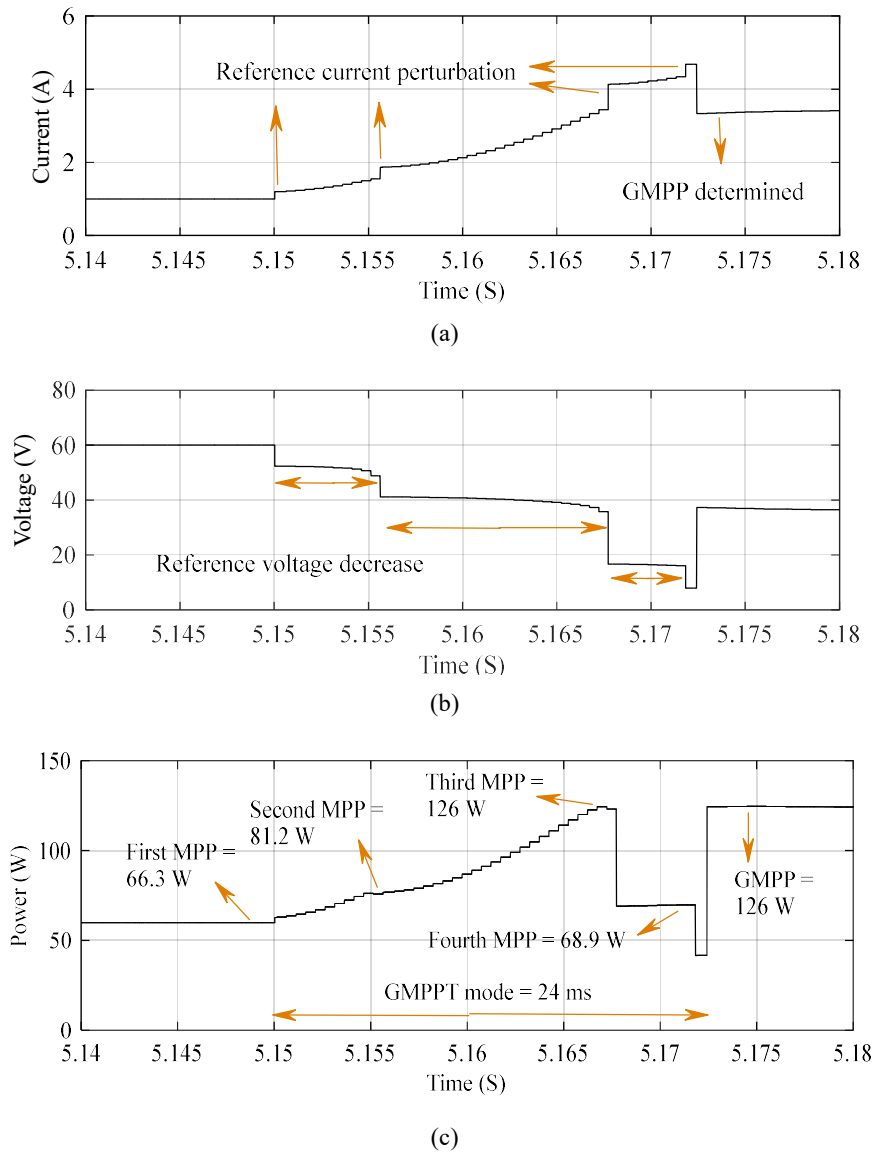


Figure 5.14 Expanded simulation results of the proposed STMPPT showing GMPP mode performance for Case 3: (a) current waveform, (b) voltage waveform, and (c) power waveform.

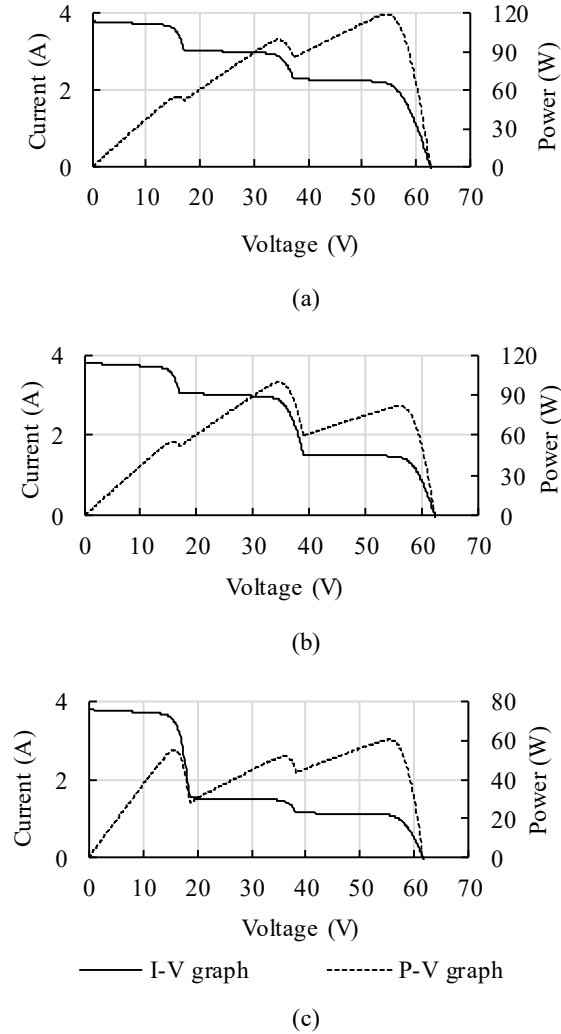


Figure 5.15 PV graphs of different partial shading patterns verified in [113]: (a) Pattern 1, (b) Pattern 2, and (c) Pattern 3.

The method in [113] was simulated based on a PV system consisting of a PV array, a buck-boost converter, and a load. The PV array comprised three series-connected Solarex MSX-60W PV modules. A bypass diode was connected in parallel with each PV module. Three different shading patterns were examined as shown in Figure 5.15. The same PV system with the same parameters was used to verify the proposed method in this chapter. The three partial shading patterns in Figure 5.15 were examined with the proposed STMPPT.

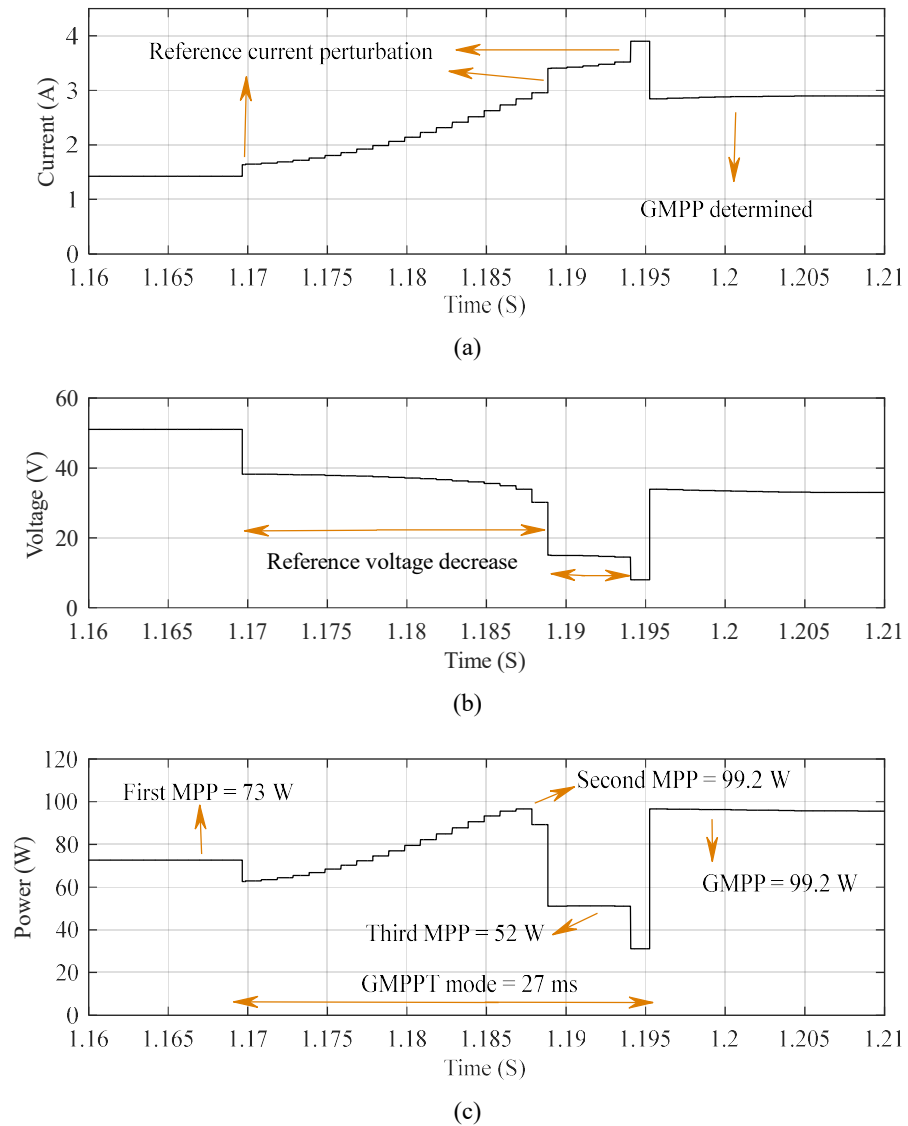


Figure 5.16 Simulation results of proposed STMPPT for Pattern 2: (a) current waveform, (b) voltage waveform, and (c) power waveform.

As an example, the simulation results for Pattern 2 are presented in Figure 5.16. These results are comparable with Figure 12 of [113]. The GMPP mode of the proposed technique in this paper tracks the true peak with a faster dynamic in 27 ms. Table 5.4 presents a comparison between the proposed STMPPT technique and the modified beta algorithm. The average tracking time of the three patterns is listed to show the speed of the algorithms. The proposed technique achieved a significantly faster speed. The

Table 5.4 Comparison of the simulation results for three patterns in Figure 5.15

|                             | Method in [113] | Proposed technique |
|-----------------------------|-----------------|--------------------|
| Average GMPPT time          | 250 ms          | 29 ms              |
| Average tracking efficiency | 88.52%          | 99.06%             |
| Steady-state efficiency     | 99.40%          | 99.68%             |
| Computational burden        | High            | Low                |
| Dependency on PV array      | Yes             | No                 |

tracking efficiency is calculated within the same time span to have a reasonable comparison. The energy loss is reduced as a result of the faster and more reliable GMPPT of the proposed technique. Moreover, the value of beta and its bounding range in [113] depend on the environmental conditions such as irradiance and temperature. The method also needs information about the configuration of the PV array and PV panel datasheet. However, the proposed technique offers a simple solution to partial shading condition without being dependent on environmental condition and PV array arrangement.

#### 5.4.2 Dynamic Tracking Performance and Inherent Recognition of Partial Shading

The intensity of irradiance is constantly changing, and the PV array experiences dynamic shadows. Hence, the dynamic MPPT performance would affect the long-term solar production investment benefits when the PV system is installed in real field condition. In this regard, the EN50530 test standard sets up a procedure to investigate the static and dynamic MPPT performance under dynamic change of irradiance intensity [135], [136]. However, partial shading is not considered in the EN50530 standard.

Based on this standard, a test sequence was examined using the simulation setup in Figure 5.6 and Figure 5.7. Figure 5.17(a) and Figure 5.17(b) illustrate the irradiance condition on the substrings of the PV array during the dynamic test. As a result, the PV

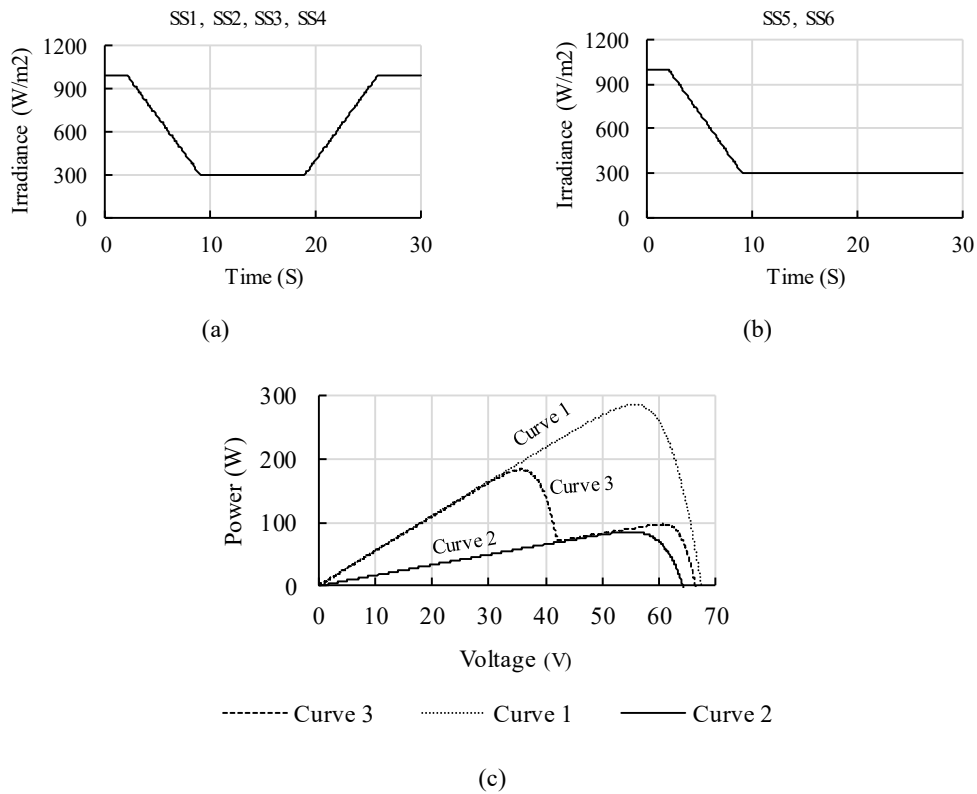


Figure 5.17 Test conditions for a dynamic test. (a) Changing irradiance condition on SS1, SS2, SS3, and SS4. (b) Changing irradiance condition on SS5 and SS6. (c) Resulting  $P$ - $V$  curves.

array experienced three curves at steady-state conditions as shown in Figure 5.17(c). The test sequence includes dynamic transitions among the curves. The whole PV array received a uniform irradiance of  $1000 \text{ W/m}^2$  (Curve 1) before  $t=2 \text{ s}$ . From  $t=2 \text{ s}$  to  $t=9 \text{ s}$ , the uniform irradiance condition changed from Curve 1 to Curve 2, and remained unchanged until  $t=19 \text{ s}$ . Thereafter, the condition of the PV array changed to partial shading condition of Curve 3 dynamically from  $t=19 \text{ s}$  to  $t=26 \text{ s}$  and stayed in this condition. It is noted that the EN50530 standard only presents dynamic variation of uniform irradiance, and the dynamic change to partial shading condition is taken into account here to verify more severe situations.

Figure 5.18 shows the power waveform of the proposed STMPPT technique during the dynamic test. The program does not call the GMPPT subroutine during the dynamic variation of irradiance, and the LMPPT mode operates on the PV array. This provides a

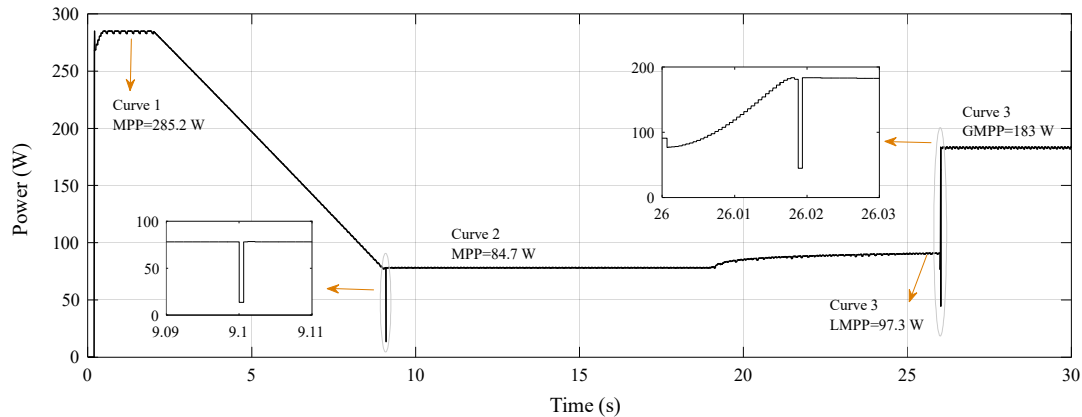


Figure 5.18 Power waveform of dynamic test results

better tracking performance and a stable operation. The enlarged waveforms in Figure 5.18 show the GMPPT after the dynamic variations around  $t=9$  s and  $t=26$  s. The program calls the GMPPT subroutine when a stable condition is realized after an unstable situation. After the first dynamic variation at  $t=9$  s, from Curve 1 to Curve 2, the GMPPT subroutine implements a current perturbation immediately causing a saturation of the duty-cycle as the new condition is uniform. Hence, the GMPP search is ended and the algorithm quickly returns to the LMPPT mode. In fact, the proposed algorithm inherently recognizes the uniform irradiance condition with one perturbation in reference current. When the second dynamic transition ends at  $t=26$  s, from Curve 2 to Curve 3, the LMPPT mode first converges to the LMPP of 97.3 W. Then, the algorithm calls the GMPPT subroutine. The perturbation in reference current does not lead to a saturation of the duty-cycle. Consequently, the algorithm inherently realizes that this is a partial shading condition. The GMPPT subroutine finds the GMPP of Curve 3 quickly in 18 ms. The LMPPT mode then operates at this GMPP.

## 5.5 Experimental Verification

### 5.5.1 Experimental Setup and Digital Design Overview

Figure 5.19 shows the experimental setup of the PV system under study. The experimental tests were conducted using a PV array consisting of three series-connected

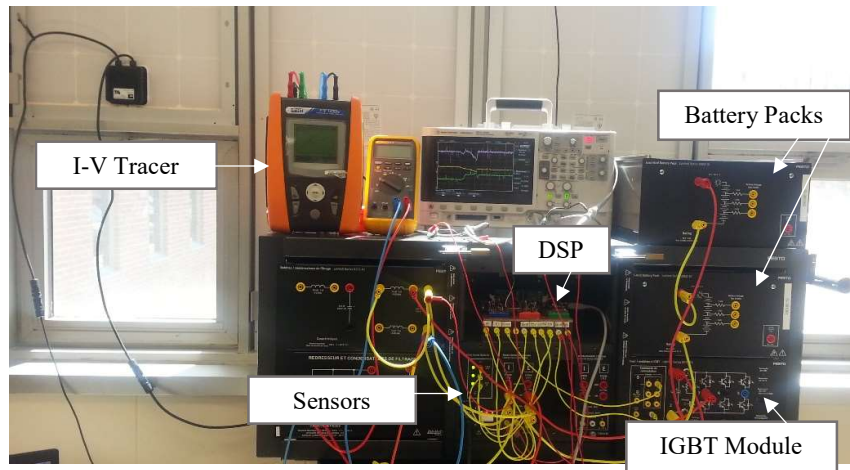


Figure 5.19 Experimental setup, PV array, and PV simulator

ET-M53695 PV modules and a programmable PV simulator power supply. The terminal voltage of the PV array needs to be controlled by the duty-cycle of the switching device of the boost converter to optimize the PV system operation. One leg of a three-phase Lab-Volt IGBT Chopper/Inverter was used to realize the IGBT switch and diode of the boost converter. The PV array was connected to a Lab-Volta Lead-Acid Battery Pack via the

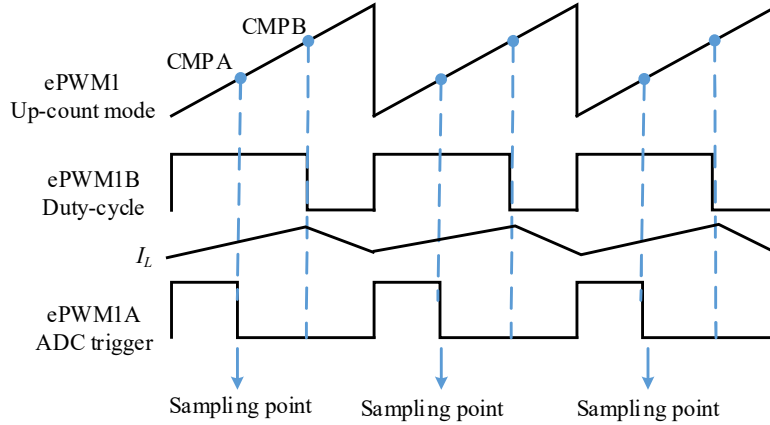


Figure 5.20 PWM generation and ADC sampling in DSP

boost converter. The parameters of the experimental setup are listed in Table 5.1. A voltage sensor and a current sensor were used to measure the PV array voltage and the inductor current. The algorithms were implemented using the Texas Instrument TMS320F28335 DSP. The platform for software development was the Code Composer Studio (CCS 7.0.0). The control programs were developed in C environment.

The enhanced PWM (ePWM) module of DSP is used as a time base to produce the duty-cycle and set the sampling rates, as shown in Figure 5.20. Hence, the ePWM1 is configured to work in up-count mode. A compare register of ePWM1 (CMPB) is adjusted regularly by the control algorithm to implement the boost converter duty-cycle command through ePWM1B. The sensed signals,  $V_{pv}$  and  $I_L$ , are fed back to the DSP via two analog to digital converter (ADC) channels. The ePWM1A is configured to produce a start of conversion (SOC) trigger for ADC measurements. The inductor current of the boost converter is sampled at the middle point of the ePWM1B ON state so that the measurement indicates the average current. The voltage sampling is also done at the same point. Hence, another compare register of ePWM1 (CMPA) is modified to trigger the SOC at this point on up-count through ePWM1A.

### 5.5.2 Experimental Results Using a Real PV Array

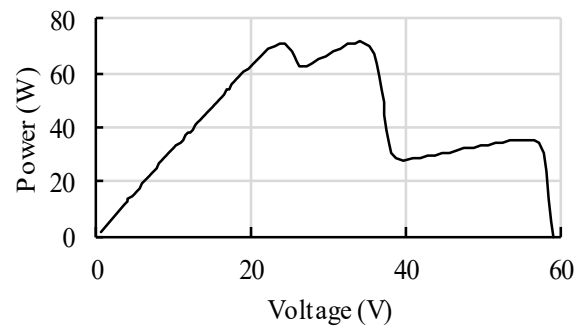
The goal of this section is to experimentally demonstrate how fast the proposed technique can help maximize a real PV system harvest. The PV array consisting of three

series-connected PV modules was installed on a south-faced window of a laboratory. The DC-DC boost converter is controlled by two feedback loops in conjunction with the STMPPT controller. The performance of the whole control system depends on the rate at which the control loops run. The update frequency of the P&O MPPT algorithm is 40 Hz. The PV array voltage is regulated by the voltage-control loop with a dynamic of 1 kHz while the inner current-control loop that shapes the inductor current has a much faster dynamic of 10 kHz. The MPPT algorithm modifies the reference voltage, and the feedback loops steer the PV array operating voltage to that reference point. Hence, the feedback loops need to feature a faster dynamic than the MPPT algorithm, so that the PV array voltage has sufficient time to stabilize. A number of current and voltage samples are averaged before feeding to the MPPT algorithm to mitigate the effect of noise. These samples are always the last ones before the MPPT algorithm update. This is a decisive factor as the first samples after the update could contain transient values when the internal loops try to steer the PV array voltage to the reference voltage.

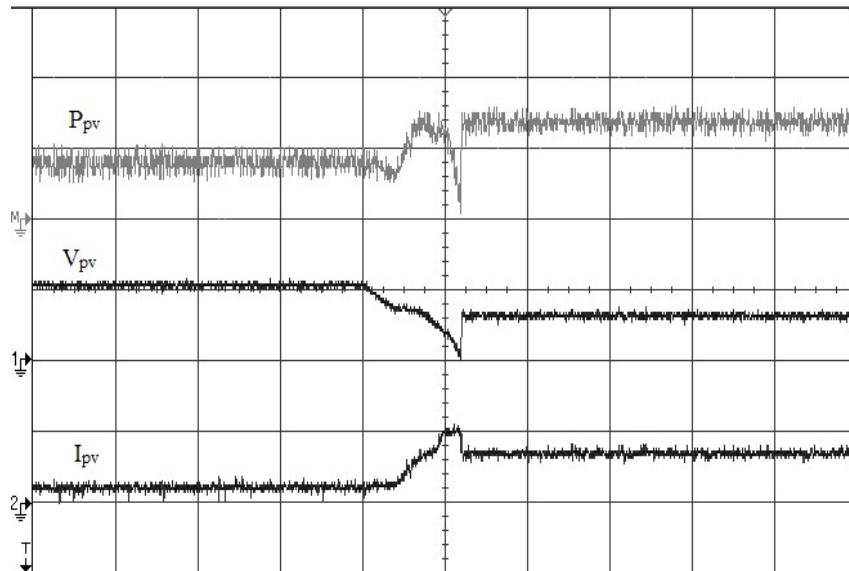
Natural partial shading conditions often occurred as a result of shadow of a nearby building. Artificial partial shading conditions were also created using plastic sheets with different transparencies. The PV characteristics were monitored using HT Instruments I-V 400 PV Panel Analyzer and irradiance meter test kit. The PV array experienced a variety of multi-peak curves during the course of the experiments. The performance of the proposed technique was tested with many partial shading conditions. A number of experimental results and their associated  $P$ - $V$  curves are presented to show the performance of the proposed technique.

Figure 5.21 illustrates the experimental results when the  $P$ - $V$  curve features three peaks at (0.63 A, 56.4 V, 35.5 W), (2.1 A, 34 V, 71.7 W), and (2.99 A, 23.6 V, 70.7 W). The LMPPT mode first tracks the right-most peak at 35.5 W. Then, the GMPPT mode of the proposed technique finds the GMPP at 71.7 W in 25 ms. In Figure 5.22, the partial shading condition features three peaks at (0.67 A, 56 V, 37.9 W), (1.86 A, 34.2 V, 63.7 W), and (2.94 A, 23.9 V, 70.4 W) where the left-most peak is the GMPP. The GMPPT mode starts after finding the right-most peak at 37.9 W. The second and third peaks are then reached at 63.7 W and 70.4 W. Hence, the program transfers the operating point to the GMPP at 70.4 W. The tracking time of GMPPT mode is 27 ms in this case. During

the course of the experiments, more complicated partial shading conditions were frequently observed. Figure 5.23 shows the experimental results when the  $P$ - $V$  curve exhibits 4 peaks and the right-most peak is the GMPP. This situation happened in an evening when the front frame of the window partially shadowed the PV panels. The GMPPT mode could successfully locate the GMPP of the partial shading condition in less than 30 ms.

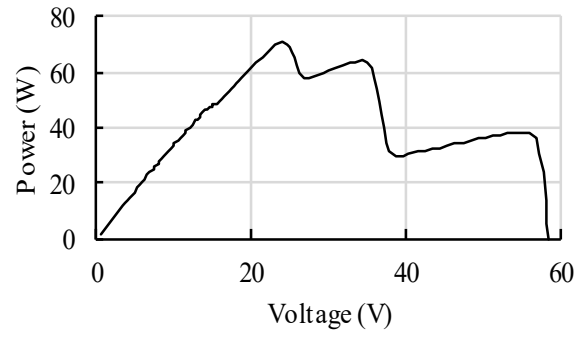


(a)

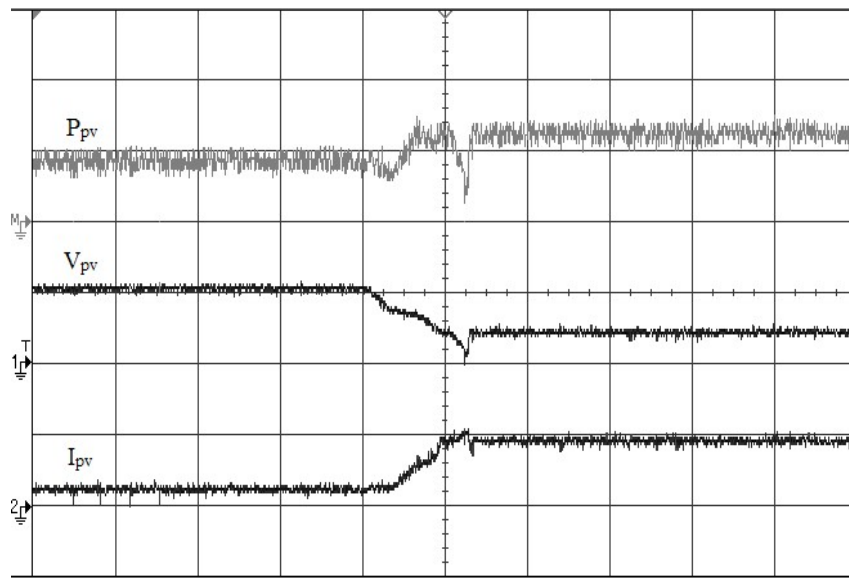


(b)

Figure 5.21 Experimental results under partial shading condition: (a)  $P$ - $V$  curve and (b) experimental waveforms during GMPPT mode of the proposed technique (Scale time: 20 ms/div,  $V_{pv}$ : 55 V/div,  $I_{pv}$ : 3 A/div,  $P_{pv}$ : 40 W/div).

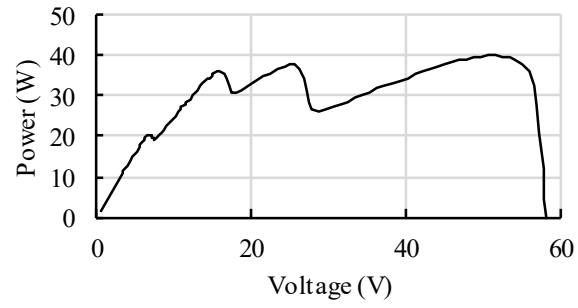


(a)

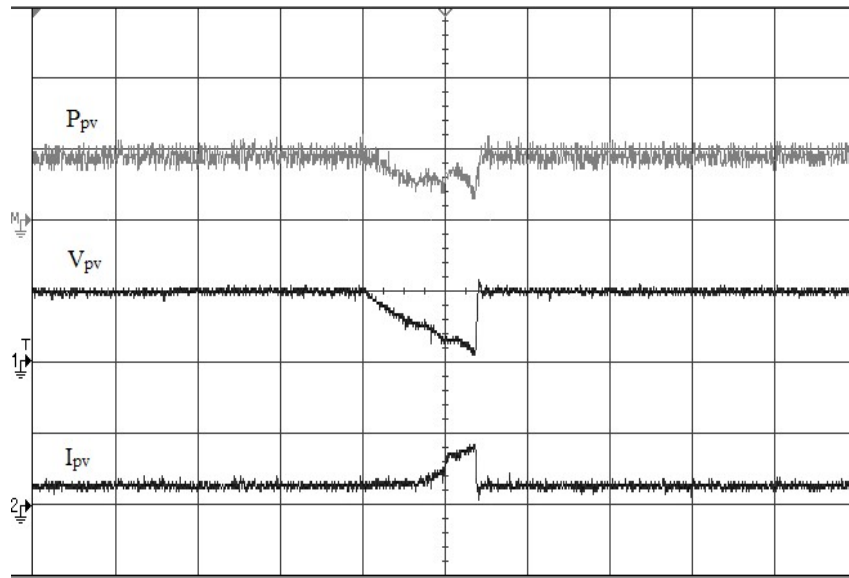


(b)

Figure 5.22 Experimental results under partial shading condition: (a)  $P$ - $V$  curve and (b) experimental waveforms during GMPPT mode of the proposed technique (Scale time: 20 ms/div,  $V_{pv}$ : 55 V/div,  $I_{pv}$ : 3 A/div,  $P_{pv}$ : 40 W/div).



(a)



(b)

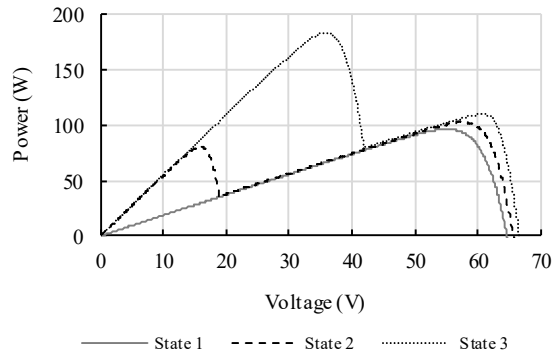
Figure 5.23 Experimental results under partial shading condition: (a)  $P$ - $V$  curve and (b) experimental waveforms during GMPPT mode of the proposed technique (Scale time: 20 ms/div,  $V_{pv}$ : 55 V/div,  $I_{pv}$ : 3 A/div,  $P_{pv}$ : 40 W/div).

### 5.5.3 Experimental Results using a PV simulator

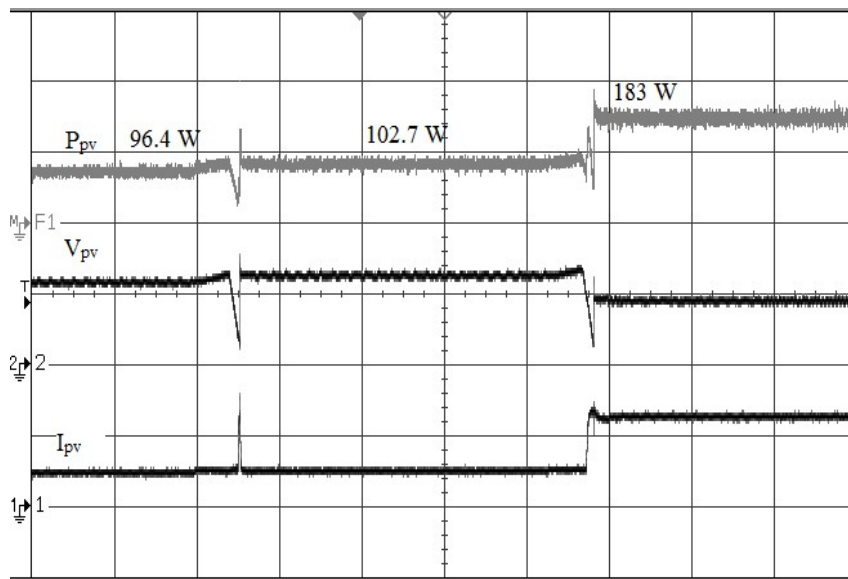
The objective of this section is to evaluate the dynamic performance of the proposed STMPPT technique using the ITECH PV simulator power supply (IT6517C). The dynamic response of the PV simulator is considerably slower than that of a real PV array. Hence, the update frequency of the P&O algorithm, the voltage-control loop frequency, and the current-control loop frequency were chosen as 2 Hz, 100 Hz, and 1 kHz, respectively. The PV simulator features built-in EN50530 testing procedure to verify static and dynamic MPPT performance. It is also capable of simulating partial shading condition and dynamic shadow movement.

Performance of the proposed STMPPT technique was tested in the presence of a moving shadow. It is assumed that the PV array is initially under a uniform shadow resulting in a single-peak  $P-V$  graph as shown by State 1 in Figure 5.24(a). The shadow is then removed from one PV panel leading to a partially shaded  $P-V$  graph shown by State 2 in Figure 5.24(a). Finally, the  $P-V$  graph of State 3 will appear by removing the shadow from another PV panel. Such moving shadow scenario often happens in real field conditions. In cold climate regions, for example, this is the case when a uniform snow coverage on a PV array from a snowfall in the night partially sheds during the next sunny day. Experimental waveforms in Figure 5.24(b) demonstrate the successful operation of the proposed technique in the presence of the moving shadow. The algorithm tracks the GMPP at 102.7 W (the right-most peak) when the condition changes to State 2. Thereafter, when two PV panels become unshaded as indicated by State 3, the algorithm finds the GMPP at 183 W (the left-most peak).

Moreover, the performance of the proposed STMPPT technique was verified with dynamic irradiance changes as per the EN50530 standard. This standard recommends testing of several irradiance ramp sequences with different slopes and irradiance levels. In more detail, irradiance variation ramps from 10% to 50%, 30% to 100%, and 1% to 10% of STC irradiance level should be tested with a variety of slopes ranging from 0.5 W/m<sup>2</sup>/s up to 100 W/m<sup>2</sup>/s. Figure 5.25 shows part of the test results under dynamic irradiance changes between 300 W/m<sup>2</sup> and 1000 W/m<sup>2</sup> with a slope of 100 W/m<sup>2</sup>/s. The proposed technique provides a stable operation during the dynamic irradiance changes without losing the correct sense of tracking direction. The algorithm will not call the



(a)



(b)

Figure 5.24 A moving shadow test. (a) the resulting  $P$ - $V$  graphs. (b) Experimental waveforms (Scale time: 7 s/div,  $V_{pv}$ : 45 V/div,  $I_{pv}$ : 5 A/div,  $P_{pv}$ : 110 W/div).

GMPPT mode until a stable condition is governed by the P&O MPPT. Thereafter, the proposed algorithm inherently recognizes a uniform irradiance condition and continues to track the MPP.

In order to assess this transitory behavior, the dynamic MPPT efficiency is defined as

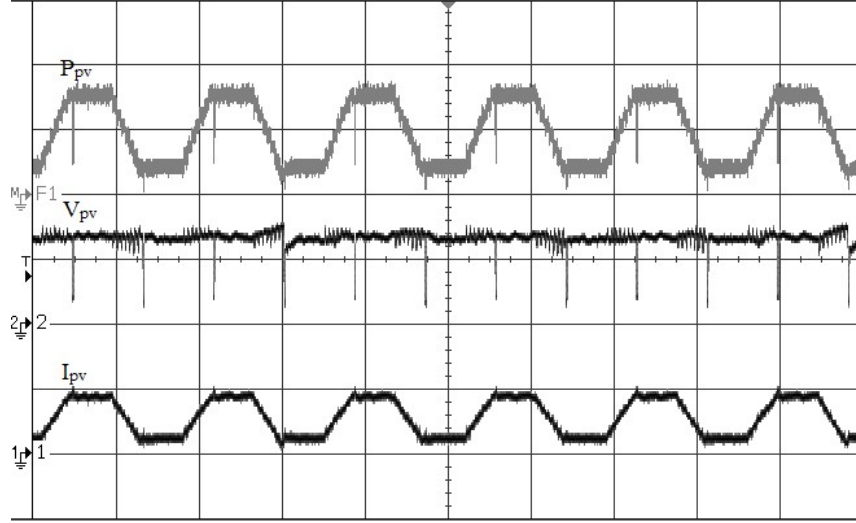


Figure 5.25 Dynamic test results as per EN50530 (Scale time: 5 s/div,  $V_{pv}$ : 45 V/div,  $I_{pv}$ : 6 A/div,  $P_{pv}$ : 180 W/div).

$$\eta_{MPPT,dyn} = \frac{\int_0^{T_M} P_{PV}(t). dt}{\int_0^{T_M} P_{MPP}(t). dt} \quad (5.8)$$

where  $P_{PV}$  is the power drawn by the MPPT control,  $P_{MPP}$  is the theoretical maximum power provided by the PV simulator, and  $T_M$  is the measuring period. The software interface of the ITECH PV simulator can generate a report of MPPT performance after the test sequences. Table V presents a dynamic efficiency comparison between the proposed STMPPT and the PSO method obtained based on the dynamic test sequences.

Table 5.5 Averaged dynamic MPPT efficiency (%)

|             | PSO   | Proposed technique |
|-------------|-------|--------------------|
| 10% to 50%  | 90.19 | 99.28              |
| 30% to 100% | 91.34 | 99.31              |
| 1% to 10%   | 85.6  | 98.65              |

The proposed STMPPT could achieve a solid performance under dynamically changing environment which essentially alleviates power oscillations and loss of energy leading to an enhanced dynamic tracking efficiency.

## **5.6 Conclusion**

This chapter proposed a high performance STMPPT technique based on ACMC to track the true peak of a PV system under partial shading condition. The simplicity and independency of the proposed technique makes it applicable to most PV system configurations. The current-mode controller of the proposed technique has a very good transient response for input and output disturbances. This technique successfully copes with dynamic environmental change without losing correct sense of tracking direction and without frequent restarting of the GMPPT mode. The hardware requirements to implement the proposed STMPPT for industrial applications are as simple as those used for the fundamental P&O MPPT controller. The occurrence of partial shading or uniform irradiance change is inherently recognized in case of power variation. Very fast and reliable GMPPT is achieved using an effective scan of PV profile. The proposed STMPPT achieves the main features needed for modern PV converter products.



## CHAPTER 6

---

# CONCLUSIONS AND FUTURE WORK

### 6.1 Concluding Remarks

PV systems have quickly increased all over the world as one of the most promising alternative energy technologies. The aim of this research project is to address the challenges in integration of PV systems in different environmental conditions, especially in snowy climates. Because of high total installed cost of PV systems, it is important to properly assess the performance and efficiency of the plants. As PV systems are expected to make a significant contribution to the supply of electricity worldwide in a more secure and economic way, it is essential to verify the effect of environmental conditions on their performance. Moreover, a proper control of the power electronics interface is needed to harvest the maximum available power from a PV array. As a result, three major problems concerning the PV systems were investigated in this research project: 1) determination of PV characteristics in real field operating conditions under a wide range of environmental variation, 2) the effects of snow accumulation on the PV systems, and 3) the problem of optimal MPPT control under partial shading conditions. Throughout this research work, detailed steps of proposed approaches have been performed and validated by simulation and experiments. Based on the results obtained, the following conclusions are drawn:

- 1) In order to make precise estimations of performance of outdoor operated PV modules, a more extended investigation of PV characteristics rather than STC parameters is needed. Field evaluation of PV modules performance is complicated as their efficiency is affected by both temperature and irradiance levels. Although the effect of temperature on PV efficiency is reported by manufacturer datasheets, the effect of irradiance variation on efficiency of the PV modules is more complex and depends on the PV technology. In fact, the parameters of the PV model change as a result of changing environmental conditions, and PV modeling without considering the variation of parameters and efficiency would lead to considerable error in the PV energy estimation and generation. The methodology proposed in this study offers a simple electrical model instead of laborious field measurements to precisely realize

the characteristics of PV modules. There was a good agreement between the experimental measurements and the simulated model under different ambient conditions, with discrepancies of less than 1%. Moreover, the performance of different PV technologies and configurations for a specific site can be successfully assessed through this model. This also allows for proper selection of PV technology and configuration which leads to an optimum design of the PV installation.

2) Snowfall during cold months reduces output of PV modules. To benefit from solar energy in snowy climates, a proper performance assessment of the snow-covered PV modules is of great importance as substantial investments are made on the PV systems. A knowledge of interaction of sun light with snow is essential to determine the influence of snow coverage on the PV modules performance. A PV modeling technique was proposed to determine the electrical characteristics of snow-covered PV cells. The PV model was then used to verify the effect of uniform/nonuniform snow accretion. An average discrepancy of 3.6% was observed between the proposed PV model and the experimental results. Generally, the power loss due to snow increases as the snow depth increases on PV modules. It should be noted that by covering the PV modules with a mere 2.5 cm of uniform snow, a power loss of more than 50% was experienced. The PV modules could generate almost no electricity, power loss of nearly 100%, for uniform snow accumulation of deeper than 8 cm. Under nonuniform snow coverage, the PV characteristic becomes more complex, characterized by multiple peaks, due to the bypass diodes. Pattern of the snow coverage and snow depth influence the location and magnitude of the maximum power points. In these situations, the difference between the local maximum power points and the global maximum power point is significant which indicates the importance of an appropriate MPPT controller to operate at the true global maximum power point. In fact, a snow-covered PV array can still produce a significant amount of energy, which depends on the pattern and depth of snow accumulation. The PV string with bypass diodes experienced an average power loss of around 19% lower than the PV string without bypass diodes. The difference is more obvious for bigger snow depths and smaller snow-covered areas. In fact, the negative effects of nonuniform snow accretion could be greatly mitigated by utilizing the bypass diodes if the MPPT controller is capable of tracking the global maximum power point.

Moreover, PV panel layout affects the power loss due to snow. In the experiments, the average power loss of the horizontal layout was 14% lower than the average power loss of the vertical layout. Hence, a proper layout can reduce the negative effects of nonuniform snow accretion on PV power production. One of the main objectives of this study was to provide a practical tool for investigating the impacts of snow/ice on the electrical characteristics of a PV array. The proposed model forms the basis for addressing the operation of large PV arrays, in order to more precisely determine the influence of snow/ice on the energy production of PV systems.

- 3) Since the power generated by the PV modules depends on environmental conditions, an MPPT controller is required to ensure that the highest possible power is generated. Partial shading conditions, where parts of the PV array experience different irradiances, hinder efficient MPPT and lead to suboptimal performance. Nonetheless, the portion of the energy that could be collected in these conditions is decided by the MPPT technique of the power electronic interface. The conventional MPPT algorithms, such as P&O, are successful in tracking the maximum power under uniform insolation where only one maximum power point exists in the  $P-V$  curve. However, in partial shading condition, where there are multiple maximum power points in the  $P-V$  curve, the conventional algorithms are unsuccessful in identifying the global maximum power point. Tracking the true peak of a PV system under partial shading condition has clear advantages and optimizes the power production. The previous global MPPT methods mostly present complicated algorithms, or are dependent on complex models of PV array and extra equipment (such as sensors and monitoring cells). Although the modeling and additional sensors could increase the speed of controllers, they become system dependent and imply limited application. In fact, implementing a working shade-tolerant MPPT for real operating condition is not a simple task. For instance, PV systems are normally subjected to dynamic variation of irradiance intensity during daytime, which causes significant oscillations in PV power and loss of energy generation. This research project proposed a high performance shade-tolerant MPPT technique based on average current-mode control. The current-mode control with the P&O algorithm track the maximum power point of the uniformly irradiated PV array. Simple innovations are implemented to the MPPT control to enable it for partial shading

condition. Useful features from the  $I$ - $V$  curves of PV array are derived to track the global maximum power point at a great speed. It was shown that instead of scanning the voltage in a  $P$ - $V$  curve under partial shading condition, it is more beneficial to work on a  $I$ - $V$  characteristic. The idea behind using the  $I$ - $V$  characteristics is to significantly reduce the search space, to make the algorithm independent of shading conditions and PV array configuration, and to inherently recognize the occurrence of partial shading condition. The proposed technique successfully tracks the global maximum power point under different partial shading conditions in less than 30 ms. It also achieves a dynamic efficiency and a steady-state efficiency of approximately 99% and 99.6%, respectively.

## 6.2 Research Perspectives

Based on the research work in this thesis, several recommendations for future studies are presented here:

- Developing a PV model with reduced simulation time for large-scale PV arrays
- Verifying the effects of shading on large-scale PV farms
- Proper design and arrangement of PV arrays and power electronic interfaces to minimize the effects of shading
- Verification of an optimum tilt angle in cold climate regions to reduce the snow loss
- A study on the energy losses of different PV array configurations due to different snow accumulation patterns for a proper selection of PV system configuration and power electronic interface
- Proper selection of PV module technology in snowy climates
- Verifying the appropriateness of the bifacial PV modules as a candidate for cold regions
- Lifetime evaluation of PV modules and PV inverters in cold regions
- Stability analysis of a grid-connected PV system considering the dynamics of the MPPT controller
- Implementing the proposed STMPPT technique in this thesis for single-stage PV inverters



# APPENDICES

---

## Appendix A Interface Circuits

---

### A.1 Analog to Digital Conversion

A current sensor and a voltage sensor from LabVolt were inserted to measure current and voltage at PV terminal. The sensors convert a high-level current and a high-level voltage into two low-level (0 to  $\pm 10$  V) output signals, electrically isolated from the high-level signal source. This allows the output signals to be used in control circuits as current or voltage feedback signals. The HCPL-7840 isolation amplifier is the main component of the sensors to provide a proper isolation. The bandwidth of this amplifier is 100 kHz, hence, it does not adversely affect the response speed of the overall circuit with the switching frequency of 20 kHz.

Accurate measurements are essential for the MPPT control. A proper Analog to Digital Converter (ADC) is necessary for accurate measurements. One of the most important specifications of an ADC is the resolution. The resolution is reflected on the length of the register in which the measured value is stored. The TMS320F28335 ADC module is a 12-bit converter which is sufficient for the MPPT controller.

In most cases, ADCs also require an interface circuit to DSP. The choice of the interface circuit is a challenging task in the experimental implementation. It is necessary to decide on an architecture of an interface which depends on the specifications of the system under study as well as control objectives. For the experiments conducted, a three-stage ADC interface circuit featuring a level translation, a filter, and a protection circuit was designed.

A level shifting is required to adapt the sensor output voltage to the ADC input range. The output of the current sensor and the voltage sensor in the experiments is a voltage between 0 V and 10 V. However, the allowable analog input range of the DSP ADC is between 0 V and 3 V. Therefore, it is required to develop interface circuits that convert voltage signals to levels acceptable for the low-voltage ADC.

Moreover, before the ADC input, the signal is processed with an electronic low-pass filter to remove all frequencies above the Nyquist frequency (one-half the sampling rate). This is done to prevent aliasing during sampling, and is correspondingly called

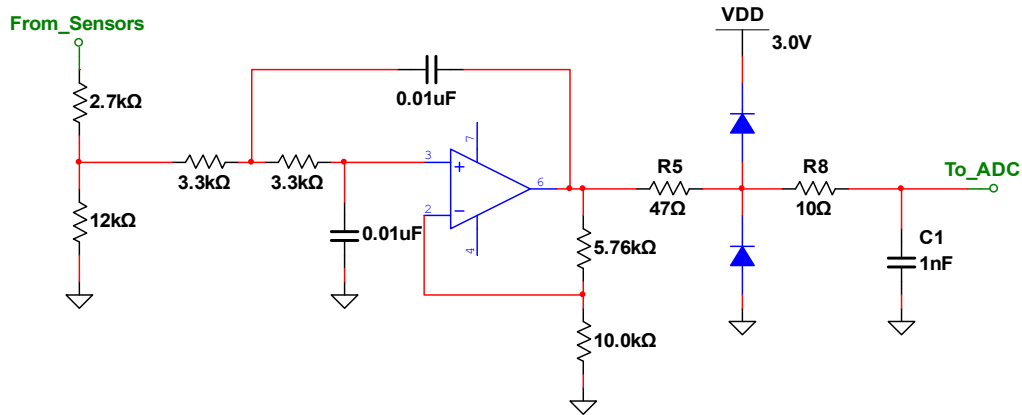


Figure A.1 Analog interface circuit for DSP ADC.

an *antialiasing filter*. Figure A.1 shows the circuit schematic of the ADC interface circuit designed for the experiments. The sensors output voltage is reduced by a resistive divider. Then, the signal passes through a 2-pole Butterworth filter which is designed to remove the frequency components above one-half of the sampling rate. The sampling rate in the experiments is 20 kHz which is equal to the switching frequency, and therefore, the cut-off frequency of the filter is 10 kHz. At the final stage, a protection circuit is added.

## A.2 PWM Signal

The enhanced pulse width modulator (ePWM) peripheral of DSP is a key element in controlling many of the power electronic systems found in commercial and industrial equipment. These systems include digital motor control, switch mode power supply control, PV systems, and other forms of power conversion. The ePWM peripheral performs a digital-to-analog (DAC) function, where the duty cycle is proportional to the DAC analog value; it is sometimes referred to as a Power DAC.

To control the PV system in the experiments via the boost converter, the duty cycle of the switching device is produced by the ePWM peripheral. Two main properties of the PWM signal need to be verified: its frequency, which should be 20 kHz, and the function that updates the duty-cycle of the PWM signal. However, the ePWM output voltage is 0

V or 3.3 V which is not suitable for driving the switching devices. Furthermore, the DSP needs to be isolated from the power stage.

Insulated gate bipolar transistor (IGBT) is the power switching device that is used in power conversion stage in the experimental setup. The IGBT is a voltage controlled device, which gives it the ability to turn on and off quickly. The IGBTs that are used in Lab-Volt Chopper/Inverter have an internal driver with the input signal range of 0 V and 5 V. Therefore, a driver circuit was designed to connect the PWM signal of DSP to the IGBT switch, as shown in Figure A.2. A high-pass filter is considered at the first stage. Then, the buffer circuit is used to limit the current drawn from the DSP pins. Finally, the 6N139 High Speed Optocoupler is used for isolation purpose and driving the switch with 0 V and 5 V.

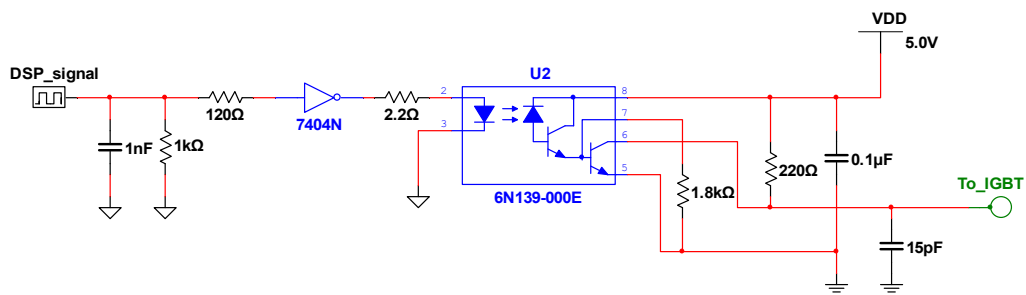


Figure A.2 IGBT driver circuit.

---

## Appendix B MPPT Software Development on DSP

---

In this section, the software implementation will be presented in greater detail for P&O MPPT algorithm. This will entail a look at the general structure of the MPPT algorithm, ADC code, and timing code to ensure everything operates in a controlled manner.

### B.1 Timing Code

The CPU-Timer0 of the DSP is used to set the MPPT controller frequency. The timer interrupt frequency determines how often the duty cycle of the PWM signal is updated. We verified the timer interrupt frequency to be working correctly at 40 Hz or every 25 ms. The selection of this frequency depends on the time-constant of the specific PV system. In fact, the PV system should reach a steady-state operation before another MPPT cycle begins.

The timing code is critical as it determines the update frequency of the MPPT. It must also ensure that the code does not overrun and cause unpredictable behavior. The interrupt code is shown below.

```
interrupt void cpu_timer0_isr(void)
{
    Timing_Code = 1;
    PieCtrlRegs.PIEACK.all = PIEACK_GROUP1;
}
```

When the interrupt is called an integer called *Timing\_Code* is set to one, then the interrupt flag is cleared allowing the interrupt request to be executed and exited quickly. Inside the main function there is a continuous *while* loop in which the following code is running.

```

while(1)
{
    if (Timing_Code == 1)
    {
        GpioDataRegs.GPBTOGGLE.bit.GPIO35 = 1;

        ADC_Update();
        MPPT_Control();

        GpioDataRegs.GPBTOGGLE.bit.GPIO35 = 1;

        Timing_Code = 0;
    }
}

```

Every time the interrupt sets the variable called *Timing\_Code* to one, it allows the functions *ADC\_Update()* and *MPPT\_Control()* to be executed, and once these functions have completed, *Timing\_Code* is set to zero. The *ADC\_Update()* function reads the PV current and voltage measurements from the ADC channels. Thereafter, these measurements are used in the *MPPT\_Control()* function to perform the P&O MPPT algorithm. There are two additional lines of code which toggle the GPIO pin 35. These are used for testing and allowing the code execution time to be monitored on an oscilloscope. As a result of these lines, a square wave pulse is produced and the pulse width gives an indication of the code execution time of the functions *ADC\_Update()* and *MPPT\_Control()*.

## B.2 ADC Code

The ADC sampling is triggered by the PWM on every first event with a sampling rate of 20 kHz. The ADC sampling code can be seen below inside the function *ADC\_Update()*.

```

void ADC_Update(void)
{
    Uint16 numberOfSamples = 64;
    ADC0_Sum = 0;
    ADC1_Sum = 0;

    for (i=0; i<numberOfSamples; i++)
    {
        while (AdcRegs.ADCST.bit.INT_SEQ1== 0) {} // Waits for interrupt
        ADCA0 = AdcRegs.ADCRESULT0>>4;
        ADCA1 = AdcRegs.ADCRESULT1>>4;
        ADC0_Sum += (ADCA0 * (3.0/4096));
        ADC1_Sum += (ADCA1 * (3.0/4096));
    }

    ADC_A0 = ADC0_Sum/numberOfSamples;
    ADC_A1 = ADC1_Sum /numberOfSamples;

    Voltage = (ADC_A0 / IP_Volt_Const);
    Current = (ADC_A1 / IP_Amp_Const);

    New_PW_In = (Voltage * Current);
}

```

These lines consist of a *for* loop which uses the integer *i* as a counter and *numberOfSamples* as the count value. In fact, at the end of each MPPT cycle, 64 voltage and current measurements are averaged to ensure the accuracy of the ADC. Inside the *for* loop, the program will wait until the next PWM trigger is received. This initiates the ADC Start of Conversion (SOC) channel number 0. Once ADC channel 0 is finished, it initiates channel 1.

The samples are added to the *ADCx\_Sum* variable. An accumulated value of 64 measurements is built up of the total samples every time the *for* loop is executed. Therefore, the sum in *ADCx\_Sum* is divided by *numberOfSamples*. To convert

the measurements to real world voltages and currents, they are divided by constant values which are calculated based on the ADC interface circuitry.

### B.3 P&O MPPT Algorithm

After the ADC measurements, the MPPT algorithm is executed in *MPPT\_Control()* function. This function creates a controlled duty cycle for the boost converter to achieve MPPT of the PV array. The C code of the P&O MPPT technique can be seen below to show how these algorithms work generally.

```
void MPPT_Control(void) {
    if (New_PW_In > Old_PW_In) {
        if (Voltage > Old_Voltage)
        {
            Duty_Cycle -= stepsize;
        }
        else
        {
            Duty_Cycle += stepsize;
        }
    }
    else {
        if (IP_Volt > Old_IP_Volt)
        {
            Duty_Cycle += stepsize;
        }
        else
        {
            Duty_Cycle -= stepsize;
        }
    }

    if (Duty_Cycle < lowerlimit) {
        Duty_Cycle = lowerlimit;
    }
    if (Duty_Cycle > upperlimit) {
        Duty_Cycle = upperlimit;
    }
    EPwm1Regs.CMPB = Duty_Cycle;

    Old_Voltage = Voltage;
    Old_PW_In = New_PW_In;
}
```

The P&O MPPT control is a rather simple algorithm. Simple *if* and *else* statements determine which direction the algorithm takes, which is dependent on the sampled ADC data. The result of these steps either increases or decreases the PWM duty cycle with a predefined step-size. These lines of code would control the IGBT switch along with the ePWM peripheral of DSP. This is accomplished by updating the Compare Register (EPwm1Regs.CMPB) of the ePWM peripheral.

## REFERENCES

- [1] IEA. (2018). Snapshot of global photovoltaic markets. *Report IEA PVPS T1-33*. [Online]. Available: <http://www.iea-pvps.org/>
- [2] European Photovoltaic Industrial Association. (2013). Global market outlook for photovoltaics 2013-2017. [Online]. Available: <http://www.epia.org/>
- [3] R. W. Andrews, A. Pollard, and J. M. Pearce, "The effects of snowfall on solar photovoltaic performance," *Sol. Energ.*, vol. 92, pp. 84-97, 2013.
- [4] IEA. (2016). Energy policies of IEA countries: Canada 2015 review. *Int. Energy Agency, Paris, France*. [Online]. Available: <https://www.iea.org>
- [5] CanSIA. Roadmap 2020: powering Canada's future with solar electricity. *Canadian Solar Industries Association*. [Online]. Available: [www.cansia.ca](http://www.cansia.ca)
- [6] K. Ogimoto, I. Kaizuka, Y. Ueda, and T. Oozeki, "A good fit: Japan's solar power program and prospects for the new power system," *IEEE Power Energy Mag.*, vol. 11, no. 2, pp. 65-74, Apr. 2013.
- [7] S. Shongwe and M. Hanif, "Comparative analysis of different single-diode PV modeling methods," *IEEE J. Photovolt.*, vol. 5, no. 3, pp. 938-946, May. 2015.
- [8] P. Maffezzoni, L. Codecasa, and D. D'Amore, "Modeling and simulation of a hybrid photovoltaic module equipped with a heat-recovery system," *IEEE Trans. Ind. Electron.*, vol. 56, no. 11, pp. 4311-4318, Nov. 2009.
- [9] A. Mellit, M. Benghamem, and S. A. Kalogirou, "Modeling and simulation of a stand-alone photovoltaic system using an adaptive artificial neural network: Proposition for a new sizing procedure," *Renewable Energy*, vol. 32, no. 2, pp. 285-313, Feb. 2007.
- [10] P. E. Kakosimos, A. G. Kladas, and S. N. Manias, "Fast photovoltaic-system voltage- or current oriented MPPT employing a predictive digital current-controlled converter," *IEEE Trans. Ind. Electron.*, vol. 60, no. 12, pp. 5673-5685, Dec. 2012.
- [11] M. A. Vitorino, M. Beltrao de Rossiter Correa, C. B. Jacobina, and A. M. N. Lima, "An effective induction motor control for photovoltaic pumping," *IEEE Trans. Ind. Electron.*, vol. 58, no. 4, pp. 1162-1170, Apr. 2011.
- [12] M. Amirabadi, A. Balakrishnan, H. A. Toliyat, and W. C. Alexander, "High-frequency ac-link PV inverter," *IEEE Trans. Ind. Electron.*, vol. 61, no. 1, pp. 281-291, Jan. 2014.
- [13] E. I. Batzelis, G. E. Kampitsis, S. A. Papathanassiou, and S. N. Manias, "Direct MPP calculation in terms of the single-diode PV model parameters," *IEEE Trans. Energy Convers.*, vol. 30, no. 1, pp. 226-236, Mar. 2015.
- [14] Y. A. Mahmoud, W. Xiao, and H. H. Zeineldin, "A parameterization approach for enhancing PV model accuracy," *IEEE Trans. Ind. Electron.*, vol. 60, no. 12, pp. 5708-5716, Dec. 2013.
- [15] B. C. Babu and S. Gurjar, "A novel simplified two-diode model of photovoltaic (PV) module," *IEEE J. Photovolt.*, vol. 4, no. 4, pp. 1156- 1161, Jul. 2014.
- [16] M. G. Villalva, J. R. Gazoli, and E. R. Filho, "Comprehensive approach to modeling and simulation of photovoltaic arrays," *IEEE Trans. Power Electron.*, vol. 24, no. 5, pp. 1189-1208, May. 2009.

- [17] A. Molina-Garcia, J. Guerrero-Pérez, M. C. Bueso, M. Kessler, and E. Gómez-Lázaro, "A new solar module modeling for PV applications based on a symmetrized and shifted Gompertz model," *IEEE Trans. Energy Convers.*, vol. 30, no. 1, pp. 51-59, Mar. 2015.
- [18] Y. Mahmoud and E. F. El-Saadany, "A photovoltaic model with reduced computational time," *IEEE Trans. Ind. Electron.*, vol. 62, no. 6, pp. 3534-3544, Jun. 2015.
- [19] Y. Chen, X. Wang, D. Li, R. Hong, and H. Shen, "Parameters extraction from commercial solar cells I–V characteristics and shunt analysis," *Appl. Energy*, vol. 88, no. 6, pp. 2239-2244, 2011.
- [20] A. Labouret and M. Vilozz, *Solar photovoltaic energy*. London, United Kingdom: The Institution of Engineering and Technology, 2010.
- [21] M. Donovan, B. Bourne, and J. Roche, "Efficiency VS. irradiance characterization of PV modules requires angle-of-incidence and spectral corrections," presented at the 35th IEEE Photovolt. Specialists Conf. (PVSC), Hawaii, 20-25 June 2010.
- [22] K. Kawajiri, T. Oozeki, and Y. Genchi, "Effect of temperature on PV potential in the world," *Environ. Sci. Technol.*, vol. 45, no. 20, pp. 9030–9035, 2011.
- [23] D. C. Jordan, J. H. Wohlgemuth, and S. R. Kurtz, "Technology and climate trends in PV module degradation," in *Eur. PV Solar Energy Conf.*, Sep. 2012, pp. 3118–3124.
- [24] A. Sangwongwanich, Y. Yang, D. Sera, and F. Blaabjerg, "Lifetime evaluation of grid-connected PV inverters considering panel degradation rates and installation sites," *IEEE Trans. Power Electron.*, vol. 33, no. 2, pp. 1225-1236, Feb. 2018.
- [25] B. Marion, R. Schaefer, H. Caine, and G. Sanchez, "Measured and modeled photovoltaic system energy losses from snow for Colorado and Wisconsin locations," *Sol. Energ.*, vol. 97, pp. 112-121, 2013.
- [26] C. Rahmann, V. Vittal, J. Ascui, and J. Haas, "Mitigation control against partial shading effects in largescale PV power plants," *IEEE Trans. Sustain. Energy*, vol. 7, no. 1, pp. 173-180, Jan. 2016.
- [27] A. Luque and S. Hegedus, *The physics of the solar cell*, Second ed. (Handbook of Photovoltaic Science and Engineering). Chichester: John Wiley & Sons, 2011.
- [28] S. Salivahanan, N. Suresh Kumar, and A. Vallavaraj, *Semiconductor diodes*, Second ed. (Electronic Devices and Circuits). New Delhi, Tata McGraw-Hill, 2008.
- [29] N. Tanaka. (2010). Technology Roadmap — Solar Photovoltaic Energy. *Photovoltaic Power Syst. Programme, IEA, Paris, France*. [Online]. Available: <https://www.iea.org>
- [30] A. Chatterjee, A. Keyhani, and D. Kapoor, "Identification of photovoltaic source models," *IEEE Trans. Energy Convers.*, vol. 26, no. 3, pp. 883-889, Jun. 2011.
- [31] D. Sera, R. Teodorescu, and P. Rodriguez, "PV panel model based on datasheet values," in *IEEE Int. Symp. Ind. Electron.*, 2007, pp. 2392-2396.
- [32] V. Scarpa, S. Buso, and G. Spiazzi, "Low-complexity MPPT technique exploiting the PV module MPP locus characterization," *IEEE Trans. Ind. Electron.*, vol. 56, no. 5, pp. 1531-1538, May. 2009.
- [33] J. J. Soon and K.-S. Low, "Optimizing photovoltaic model parameters for simulation," presented at the IEEE International Symposium on Industrial Electronics, 2012.
- [34] D. Dondi, A. Bertacchini, D. Brunelli, L. Larcher, and L. Benini, "Modeling and optimization of a solar energy harvester system for self-powered wireless sensor networks," *IEEE Trans. Ind. Electron.*, vol. 55, no. 7, pp. 2759-2766, Jul. 2008.

- [35] R. Kadri, J.-P. Gaubert, and G. Champenois, "An improved maximum power point tracking for photovoltaic grid-connected inverter based on voltage-oriented control," *IEEE Trans. Ind. Electron.*, vol. 58, no. 1, pp. 66-75, Jan. 2011.
- [36] A. Yazdani *et al.*, "Modeling guidelines and a benchmark for power system simulation studies of three-phase single-stage photovoltaic systems," *IEEE Trans. Power Del.*, vol. 26, no. 2, pp. 1247-1264, Apr. 2011.
- [37] F. Adamo, F. Attivissimo, and M. Spadavecchia, "A tool for Photovoltaic panels modeling and testing," in *IEEE Instrumentation and Measurement Technology Conference*, 2010.
- [38] F. Adamo, F. Attivissimo, A. Di Nisio, and M. Spadavecchia, "Characterization and testing of a tool for photovoltaic panel modeling," *IEEE Transactions Instrum. Meas.*, vol. 60, no. 5, pp. 1613-1622, May. 2011.
- [39] F. Attivissimo, A. Di Nisio, M. Savino, and M. Spadavecchia, "Uncertainty analysis in photovoltaic cell parameter estimation," *IEEE Trans. Instrum. Meas.*, vol. 61, no. 5, pp. 1334-1342, May. 2012.
- [40] Y. Mahmoud, W. Xiao, and H. H. Zeineldin, "A parameterization approach for enhancing PV model accuracy," *IEEE Trans. Ind. Electron.*, vol. 60, no. 12, pp. 5708-5716, Dec. 2013.
- [41] M. Hejri and H. Mokhtari, "On the comprehensive parametrization of the photovoltaic cells and modules," *IEEE J. Photovolt.*, vol. 7, no. 1, pp. 250-258, Jan. 2017.
- [42] W. De Soto, S. A. Klein, and W. A. Beckman, "Improvement and validation of a model for photovoltaic array performance," *Sol. Energy*, vol. 80, no. 1, pp. 78-88, Jan. 2006.
- [43] R.K.Varma S.A.Rahman, andT.Vanderheide,"",vol.8,no.3,pp.217-229, 2014., "Generalized model of a photovoltaic panel," *IET Renew. Power Gener.*, vol. 8, no. 3, pp. 217-229, Apr. 2014.
- [44] M. Hejri, H. Mokhtari, M. R. Azizian, M. Ghandhari, and L. Soder, "On the parameter extraction of a five-parameter double-diode model of photovoltaic cells and modules," *IEEE J. Photovolt.*, vol. 4, no. 3, pp. 915-923, May 2014.
- [45] M. G. Villalva, J. R. Gazoli, and E. R. Filho, "Comprehensive approach to modeling and simulation of photovoltaic arrays," *IEEE Trans. Power Electron.*, vol. 24, no. 5, pp. 1189-1208, 2009.
- [46] Y. Mahmoud, W. Xiao, and H. H. Zeineldin, "A simple approach to modeling and simulation of photovoltaic modules," *IEEE Trans. Sustain. Energy*, vol. 3, no. 1, pp. 185-186, Jan. 2012.
- [47] B. C. Babu and S. Gurjar, "A novel simplified two-diode model of photovoltaic (PV) module," *IEEE J. Photovolt.*, vol. 4, no. 4, pp. 1156-1161, Jul. 2014.
- [48] C. Carrero, D. Ramirez, J. Rodriguez, and C. A. Platero, "Accurate and fast convergence method for parameter estimation of PV generators based on three main points of the I-V curve," *Renew. Energy*, vol. 36, no. 11, pp. 2972-2977, Nov. 2011.
- [49] F. Ghani, M. Duke, and J. Carson, "Numerical calculation of series and shunt resistances and diode quality factor of a photovoltaic cell using the Lambert W-function," *Sol. Energy*, vol. 91, pp. 422-431, May 2013.
- [50] A. Orioli and A. Di Gangi, "A procedure to calculate the five-parameter model of crystalline silicon photovoltaic modules on the basis of the tabular performance data," *Appl. Energy*, vol. 102, pp. 1160-1177, Feb. 2013.

- [51] A. A. Elbaset, H. Ali, and M. Abd-El Sattar, "Novel seven-parameter model for photovoltaic modules," *Sol. Energy Mater. Sol. Cells*, vol. 130, pp. 442–455, Nov. 2014.
- [52] A. Chatterjee, A. Keyhani, and D. Kapoor, "Identification of photovoltaic source models," *IEEE Trans. Energy Convers.*, vol. 26, no. 3, pp. 883–889, Sep. 2011.
- [53] T. Ikegami, T. Maezono, F. Nakanishi, Y. Yamagata, and K. Ebihara, "Estimation of equivalent circuit parameters of PV module and its application to optimal operation of PV system," *Sol. Energy Mater. Sol. Cells*, vol. 67, pp. 389–395, Mar. 2001.
- [54] M. Haouari-Merbah, M. Belhamel, I. Tobías, and J. M. Ruiz, "Extraction and analysis of solar cell parameters from the illuminated current–voltage curve," *Sol. Energy Mater. Sol. Cells*, vol. 87, pp. 225–233, May 2005.
- [55] A. Ortiz-Conde, F. García Sánchez, and J. Muci, "New method to extract the model parameters of solar cells from the explicit analytic solutions of their illuminated I-V characteristics," *Sol. Energy Mater. Sol. Cells*, vol. 90, no. 3, pp. 352–361, Feb. 2006.
- [56] L. H. I. Lim, Z. Ye, J. Ye, D. Yang, and H. Du, "A linear identification of diode models from single I-V characteristics of PV panels," *IEEE Trans. Ind. Electron.*, vol. 62, no. 7, pp. 4181–4193, Jul. 2015.
- [57] M. Zagrouba, A. Sellami, M. Bouaïcha, and M. Ksouri, "Identification of PV solar cells and modules parameters using the genetic algorithms: Application to maximum power extraction," *Sol. Energy*, vol. 84, no. 5, pp. 860–866, May 2010.
- [58] H. Fathabadi, "Novel neural-analytical method for determining silicon/plastic solar cells and modules characteristics," *Energy Convers. Manage.*, vol. 76, pp. 253–259, Dec. 2013.
- [59] M. R. AlRashidi, M. F. AlHajri, K. M. El-Naggar, and A. K. Al-Othman, "A new estimation approach for determining the I–V characteristics of solar cells," *Sol. Energy*, vol. 85, no. 7, pp. 1543–1550, Jul. 2011.
- [60] J. J. Soon and K.-S. Low, "Photovoltaic model identification using particle swarm optimization with inverse barrier constraint," *IEEE Trans. Power Electron.*, vol. 27, no. 9, pp. 3975–3983, Sep. 2012.
- [61] K. Ishaque and Z. Salam, "An improved modeling method to determine the model parameters of photovoltaic (PV) modules using differential evolution (DE)," *Sol. Energy*, vol. 85, no. 9, pp. 2349–2359, Sep. 2011.
- [62] A. Askarzadeh and A. Rezazadeh, "Extraction of maximum power point in solar cells using bird mating optimizer-based parameters identification approach," *Sol. Energy*, vol. 90, pp. 123–133, Apr. 2013.
- [63] K. E. Hemsas O. Hachana, G. M. Tina, and C. Ventura, "Comparison of different metaheuristic algorithms for parameter identification of photovoltaic cell/module," *J. Renew. Sustain. Energy*, vol. 5, no. 5, Sep. 2013, article no. 053122., "Comparison of different metaheuristic algorithms for parameter identification of photovoltaic cell/module," *J. Renew. Sustain. Energy*, vol. 5, no. 5, Sep. 2013.
- [64] E. I. Batzelis and S. A. Papathanassiou, "A method for the analytical extraction of the single-diode PV model parameters," *IEEE Trans. Sustain. Energy*, vol. 7, no. 2, pp. 504–512, Apr. 2016.
- [65] E. Cuce, P. M. Cuce, and T. Bali, "An experimental analysis of illumination intensity and temperature dependency of photovoltaic cell parameters," *Appl. Energy*, vol. 111, pp. 374–382, 2013.

- [66] F. Ghani, G. Rosengarten, M. Duke, and J. Carson, "On the influence of temperature on crystalline silicon solar cell characterisation parameters," *Sol. Energy*, vol. 112, pp. 437–445, 2015.
- [67] F. Khan, S. Singh, and M. Husain, "Effect of illumination intensity on cell parameters of a silicon solar cell," *Sol. Energy Mater. Sol. Cells*, vol. 94, no. 9, pp. 1473–1476, 2010.
- [68] M. Averbukh, S. Lineykin, and A. Kuperman, "Obtaining small photovoltaic array operational curves for arbitrary cell temperatures and solar irradiation densities from standard conditions data," *Progr. Photovolt. Res. Appl.*, vol. 21, pp. 1016–1024, 2013.
- [69] V. Lo Brano, A. Orioli, and G. Ciulla, "On the experimental validation of an improved five-parameter model for silicon photovoltaic modules," *Sol. Energ. Mat. Sol. Cells*, vol. 105, no. 2012, pp. 27–39, 2012.
- [70] S. Lineykin, M. Averbukh, and A. Kuperman, "Issues in modeling amorphous silicon photovoltaic modules by single-diode equivalent circuit," *IEEE Trans. Ind. Electron.*, vol. 61, no. 12, pp. 6785–6793, Dec. 2014.
- [71] C. W. Hansen. (2015). Parameter estimation for single diode models of photovoltaic modules. *Sandia National Laboratories, Albuquerque, New Mexico and Livermore, California*. [Online]. Available: <http://prod.sandia.gov/techlib/access-control.cgi/2015/152065.pdf>
- [72] F. Ratzel, *Die Schneedecke besonders in deutschen Gebirgen*. J. Engelhorn, 1889.
- [73] F. Sauberer, *Versuche über spektrale messungen der strahlungseigenschaften von schnee und eismit photoelementen*. Met. Z., 1938.
- [74] R. V. Dunkle and J. T. Bevans, "An approximate analysis of the solar reflectance and transmittance of a snow cover," *J. Meteorology* vol. 13, pp. 212–216, 1956.
- [75] J. H. G. Glendinning and E. M. Morris, "Incorporation of spectral and directional radiative transfer in a snow model," *Hydrol. Process*, vol. 13, no. 12-13, pp. 1761–1772, 1999.
- [76] B. L. Brench, "Snow-covering effects on the power output of solar photovoltaic arrays," The U.S. Department of Energy, Massachusetts Institute of Technology, 1979, [Online]. Available: <https://www.osti.gov/>.
- [77] E. Usher, G. Jeana, and Howell G., "The use of photovoltaics in a northern climate," *Solar Energy Materials and Solar Cells*, vol. 34, no. 1-4, pp. 73-81, 1994.
- [78] M. M. D. Ross, "Snow and ice accumulation on photovoltaic arrays: an assessment of the TN conseil passive melting technology," Energy Diversification Research Laboratory, CANMET, Natural Resources Canada, Varennes, Canada, 1995, vol. EDRL 95-68 (TR) [Online]. Available: <http://www.rerinfo.ca/>.
- [79] G. Becker, B. Schiebelsberger, W. Weber, C. Vodermayr, M. Zehner, and G. Kummerle, "An approach to the impact of snow on the yield of grid connected PV systems," Bavarian Association for the Promotion of Solar Energy, Munich, Germany, 2006, [Online]. Available: <https://www.sev-bayern.de/>.
- [80] T. Townsend and L. Powers, "Photovoltaics and snow: an update from two winters of measurements in the sierra," in *37th IEEE Photovoltaic Specialists Conference (PVSC)*, Seattle, WA, 2011, pp. 3231-3236.
- [81] D. L. King, W. E. Boyson, and J. A. Kratochvil. (2004). Photovoltaic array performance model. *Sandia National Laboratories, Albuquerque, New Mexico*. [Online]. Available: <http://prod.sandia.gov/techlib/access-control.cgi/2004/043535.pdf>

- [82] Rob W. Andrews, Andrew Pollard, and Joshua M. Pearce, "Improved parametric empirical determination of module short circuit current for modelling and optimization of solar photovoltaic systems," *Solar Energy*, vol. 86, no. 9, pp. 2240-2254, 2012.
- [83] Rob W. Andrews and Joshua M. Pearce, "The effect of spectral albedo on amorphous silicon and crystalline silicon solar photovoltaic device performance," *Solar Energy*, vol. 91, pp. 233-241, 2013.
- [84] M. P. Brennan, A. L. Abramase, R. W. Andrews, and J. M. Pearce, "Effects of spectral albedo on solar photovoltaic devices," *Sol. Energ. Mater. Sol. Cells*, vol. 124, pp. 111-116, 2014.
- [85] A. G. Husu, M. F. Stan, C. Cobianu, N. Fidel, and O. Nedelcu, "An inedited solution to increase the energy efficiency of photovoltaic panels for regions with snow," in *13th International Conference on Engineering of Modern Electric Systems (EMES)*, Oradea, 2015: IEEE.
- [86] N. Heidari, J. Gwamuri, T. Townsend, and J. M. Pearce, "Impact of snow and ground interference on photovoltaic electric system performance," *IEEE J. Photovolt.*, vol. 5, no. 6, pp. 1680 - 1685, 2015.
- [87] B. P. Jelle, "The challenge of removing snow downfall on photovoltaic solar cell roofs in order to maximize solar energy efficiency—Research opportunities for the future," *Energ. Buildings*, vol. 67, pp. 334-351, 2013.
- [88] Y. H. Liu, S. C. Huang, J. W. Huang, and W. C. Liang, "A particle swarm optimization-based maximum power point tracking algorithm for PV systems operating under partially shaded conditions," *IEEE Trans. Energy Convers.*, vol. 27, no. 4, pp. 1027-1035, Dec. 2012.
- [89] F. Paz and M. Ordonez, "High-performance solar MPPT using switching ripple identification based on a lock-in amplifier," *IEEE Trans. Ind. Electron.*, vol. 63, no. 6, pp. 3595 - 3604, Jun. 2016.
- [90] E. Koutroulis, K. Kalaitzakis, and N. C. Voulgaris, "Development of a microcontroller-based photovoltaic maximum power point tracking control system," *IEEE Trans. Power Electron.*, vol. 16, no. 1, pp. 46-54, Jan. 2001.
- [91] R. Gules, J. D. P. Pacheco, H. L. Hey, and J. Imhoff, "A maximum power point tracking system with parallel connection for PV stand-alone applications," *IEEE Trans. Ind. Electron.*, vol. 55, no. 7, pp. 2674-2683, Jul. 2008.
- [92] S. B. Kjaer, "Evaluation of the hill climbing and the incremental conductance maximum power point trackers for photovoltaic power systems," *IEEE Trans. Energy Convers.*, vol. 27, no. 4, pp. 922-929, Dec. 2012.
- [93] A. K. Abdelsalam, A. M. Massoud, S. Ahmed, and P. Enjeti, "High-performance adaptive perturb and observe MPPT technique for photovoltaic-based microgrids," *IEEE Trans. Power Electron.*, vol. 26, no. 4, pp. 1010-1021, Apr. 2011.
- [94] F. Liu, S. Duan, F. Liu, B. Liu, and Y. Kang, "A variable step size INC MPPT method for PV systems," *IEEE Trans. Ind. Electron*, vol. 55, no. 7, pp. 2622-2628, Jul. 2008.
- [95] Q. Mei, M. Shan, L. Liu, and J. M. Guerrero, "A novel improved variable step-size incremental-resistance MPPT method for PV systems," *IEEE Trans. Ind. Electron*, vol. 58, no. 6, pp. 2427-2434, Jun. 2011.
- [96] M. A. Elgendy, B. Zahawi, and D. J. Atkinson, "Assessment of the incremental conductance maximum power point tracking algorithm," *IEEE Trans. Sustain. Energy*,

vol. 4, no. 1, pp. 108-117, Jan. 2013.

- [97] T. K. Soon and M. Saad, "Modified incremental conductance algorithm for photovoltaic system under partial shading conditions and load variation," *IEEE Trans. Ind. Electron.*, vol. 61, no. 10, pp. 5384-5392, Oct. 2014.
- [98] M. Miyatake, M. Veerachary, F. Toriumi, N. Fujii, and H. Ko, "Maximum power point tracking of multiple photovoltaic arrays: A PSO approach," *IEEE Trans. Aerosp. Electron. Syst.*, vol. 47, no. 1, pp. 367-380, Jan. 2011.
- [99] K. L. Lian, J. H. Jhang, and I. S. Tian, "A maximum power point tracking method based on perturb-and-observe combined with particle swarm optimization," *IEEE J. Photovoltaics*, vol. 4, no. 2, pp. 626-633, Mar. 2014.
- [100] M. Seyedmahmoudian *et al.*, "Simulation and hardware implementation of new maximum power point tracking technique for partially shaded PV system using hybrid DEPSO method," *IEEE Trans. Sustain. Energy*, vol. 6, no. 3, pp. 850-862, Jul. 2015.
- [101] H. Renaudineau *et al.*, "A PSO-based global MPPT technique for distributed PV power generation," *IEEE Trans. Ind. Electron.*, vol. 62, no. 2, pp. 1047-1058, Feb. 2015.
- [102] K. Sundareswaran, P. Sankar, P. S. R. Nayak, S. P. Simon, and S. Palani, "Enhanced energy output from a PV system under partial shaded conditions through artificial bee colony," *IEEE Trans. Sustain. Energy*, vol. 6, no. 1, pp. 198-209, Jan. 2015.
- [103] S. Mohanty, B. Subudhi, and P. K. Ray, "A new MPPT design using grey wolf optimization technique for photovoltaic system under partial shading conditions," *IEEE Trans. Sustain. Energy*, vol. 7, no. 1, pp. 181-188, Jan. 2016.
- [104] S. Lyden and M. E. Haque, "A simulated annealing global maximum power point tracking approach for PV modules under partial shading conditions," *IEEE Trans. Power Electron.*, vol. 31, no. 6, pp. 4171-4181, Jun. 2016.
- [105] C. Manickam, G. P. Raman, G. R. Raman, S. I. Ganesan, and N. Chilakapati, "Fireworks enriched P&O algorithm for GMPPT and detection of partial shading in PV systems," *IEEE Trans. Power Electron.*, vol. 32, no. 6, pp. 4432-4443, Jun. 2017.
- [106] C. Huang, L. Wang, R. S. C. Yeung, Z. Zhang, H. S. H. Chung, and A. Bensoussan, "A prediction model-guided Jaya algorithm for the PV system maximum power point tracking," *IEEE Trans. Ind. Electron.*, vol. 9, no. 1, pp. 45-55, Jan. 2018.
- [107] K. S. Tey and S. Mekhilef, "Modified incremental conductance algorithm for photovoltaic system under partial shading conditions and load variation," *IEEE Trans. Ind. Electron.*, vol. 61, no. 10, pp. 5384-5392, Oct. 2014.
- [108] H. Patel and V. Agarwal, "Maximum power point tracking scheme for PV systems operating under partially shaded conditions," *IEEE Trans. Ind. Electron.*, vol. 55, no. 4, pp. 1689-1698, Apr. 2008.
- [109] K. Chen, S. Tian, Y. Cheng, and L. Bai, "An improved MPPT controller for photovoltaic system under partial shading condition," *IEEE Trans. Sustain. Energy*, vol. 5, no. 3, pp. 978-985, Jul. 2014.
- [110] A. Ramyar, H. Iman-Eini, and S. Farhangi, "Global maximum power point tracking method for photovoltaic arrays under partial shading conditions," *IEEE Trans. Ind. Electron.*, vol. 64, no. 4, pp. 2855-2864, Apr. 2017.
- [111] M. A. Ghasemi, H. M. Foroushani, and M. Parniani, "Partial shading detection and smooth maximum power point tracking of PV arrays under PSC," *IEEE Trans. Power Electron.*, vol. 31, no. 9, pp. 6281-6292, Sep. 2016.

- [112] D. Vinnikov, R. Kosenko, A. Chub, and E. Liivik, "Shade-tolerant photovoltaic microinverter with time adaptive seamless P-V curve sweep MPPT," presented at the Power Electronics and Applications (EPE'17 ECCE Europe), Warsaw, Poland, Sep. 2017.
- [113] X. Li, H. Wen, Y. Hu, L. Jiang, and W. Xiao, "Modified beta algorithm for GMPPT and partial shading detection in photovoltaic systems," *IEEE Trans. Power Electron.*, vol. 33, no. 3, pp. 2172-2186, Mar. 2018.
- [114] A. M. S. Furtado, F. Bradaschia, M. C. Cavalcanti, and L. R. Limongi, "A reduced voltage range global maximum power point tracking algorithm for photovoltaic systems under partial shading conditions," *IEEE Trans. Ind. Electron.*, vol. 65, no. 4, pp. 3252-3262, Apr. 2018.
- [115] A. Kouchaki, H. Iman-Eini, and B. Asaei, "A new maximum power point tracking strategy for PV arrays under uniform and non-uniform insolation conditions," *Solar Energy*, vol. 91, pp. 221-232, May 2013.
- [116] S. M. R. Kazmi, H. Goto, O. Ichinokura, and H. J. Guo, "An improved and very efficient MPPT controller for PV systems subjected to rapidly varying atmospheric conditions and partial shading," in *AUPEC 2009*, Adelaide, SA, Australia, 27-30 Sept. 2009.
- [117] J. Ahmed and Z. Salam, "An improved method to predict the position of maximum power point during partial shading for PV arrays," *IEEE Trans. Ind. Informat.*, vol. 11, no. 6, pp. 1378-1387, Dec. 2015.
- [118] J. A. Duffie and W. A. Beckman, *Solar engineering of thermal processes*. New York: John Wiley and Sons, 2013.
- [119] I. Reda and A. Andreas. (2008). Solar position algorithm for solar radiation applications. *NREL Report No. TP-560-34302*, Golden, Colorado.
- [120] G. M. Masters, *Renewable and efficient electric power systems*. Hoboken, New Jersey: John Wiley & Sons, 2013.
- [121] <http://www.sandia.gov/pv>.
- [122] N. H. Reich *et al.*, "Weak light performance and spectral response of different solar cell types," in *20th EU PVSEC*, Barcelona, Spain, 2005.
- [123] O. Järvinen and M. Leppäranta, "Solar radiation transfer in the surface snow layer in Dronning Maud Land, Antarctica," *Polar Science*, vol. 7, no. 1, pp. 1-17, Mar. 2013.
- [124] S. G. Warren, "Optical properties of snow," *Rev. Geophys. Space Phys.*, vol. 20, no. 1, pp. 67-89, 1982.
- [125] M. Gergely, M. Schneebeli, and K. Roth, "Snow characterization by optical properties," in *International Snow Science Workshop*, Davos, Swiss, 2009.
- [126] D. K. Perovich, "Light reflection and transmission by a temperate snow cover," *J. Glaciology*, vol. 53, no. 181, pp. 201-210, 2007.
- [127] A. A. Kokhanovsky and P. E. Zege, "Scattering optics of snow," *Appl. Optics*, vol. 43, no. 7, pp. 1589-1602, 2004.
- [128] F. Domine *et al.*, "Snow physics as relevant to snow photochemistry," *Atmos. Chem. Phys.*, vol. 8, no. 2, pp. 171-208, 2008.
- [129] K. Ishaque, Z. Salam, and H. Taheri, "Simple, fast and accurate two-diode model for photovoltaic modules," *Sol. Energ. Mater. Sol. Cells*, vol. 95, pp. 586-594, 2011.
- [130] S. Chih-Tang, R. N. Noyce, and W. Shockley, "Carrier generation and recombination in

- P-N junctions and P-N junction characteristics," in *Proceedings of the IRE*, Sep. 1957, vol. 45, no. 9, pp. 1228-1243.
- [131] C. Rahmann, V. Vittal, J. Ascui, and J. Haas, "Mitigation control against partial shading effects in large-scale PV power plants," *IEEE Trans. Sustain. Energy*, vol. 7, no. 1, pp. 173-180, Jan. 2016.
- [132] S. Lee. (2014). Practical feedback loop analysis for current-mode boost converter. *Texas Instruments*, [Online]. Available: <http://www.ti.com/lit/an/slva636/slva636.pdf>.
- [133] S. K. Kollimalla and M. K. Mishra, "A novel adaptive P&O MPPT algorithm considering sudden changes in the irradiance," *IEEE Trans. Energy Convers.*, vol. 29, no. 3, pp. 602-610, Sep. 2014.
- [134] Q. Z. Zhu, X. Zhang, S. Li, C. Liu, and H. Ni, "Research and test of power-loop-based dynamic multi-peak MPPT algorithm," *IEEE Trans. Ind. Electron.*, vol. 63, no. 12, pp. 7349-7359, Dec. 2016.
- [135] M. Alonso and F. Chenlo, "Testing microinverters according to EN 50530," in *29th EU PVSEC*, Amsterdam, The Netherlands, 2014.
- [136] *Overall efficiency of grid connected photovoltaic inverters, EN 50530*, 2010.